CARBON AND MERCURY ACCUMULATION IN LAKE SEDIMENTS OF RAPIDLY THAWING DISCONTINUOUS PERMAFROST PEATLANDS (NORTHWEST TERRITORIES, CANADA)

Rachael Ehimen Abulu

A thesis submitted to the Faculty of Graduate Studies in partial fulfillment of the requirements for the degree of Master of Science

Graduate Program in Geography

York University

Toronto, Ontario, Canada

January 2024

ABSTRACT

This research uses a paleolimnological approach to address gaps in our understanding of lakes as potential sinks for carbon and mercury released from thawing discontinuous permafrost peatlands. Sediment cores were collected from 14 small lakes in the southern Northwest Territories, and core chronologies and sediment accumulation rates established using ^{210}Pb radioisotopes. Most lakes exhibited increases in mercury concentrations independent of organic carbon. Atomic C/N ratios indicated that the proportion of organic carbon from algal sources has also increased. The low sediment focussing factor (< 1.0) observed in the majority of the lakes suggests that small, hydrologically connected shallow lakes act as flow-through systems, which may promote the downstream transport of sediment (and associated carbon and mercury) through sub-arctic watersheds draining thawing permafrost peatlands, rather than acting primarily as carbon and mercury sinks.

ACKNOWLEDGEMENTS

My graduate program has been an unbelievable journey and not one I would forget in a while. First and foremost, I would like to thank my supervisor, Professor Jennifer B. Korosi, for her guidance, unwavering academic and moral support, which I deeply appreciated when I was having doubts and going through health challenges. You played a major role in my master's degree completion and through your mentorship, I gained valuable knowledge and field experience in the field of paleolimnology, which I developed genuine interest for. Through your support, I was able to excel not only academically but also improve my presentation skills as I had the opportunity to present preliminary findings of my research in national conferences.

I would also like to thank the scholarly faculty of my committee, Professor Kathy Young for her insightful feedback and support. This section would not be complete without appreciating Professor Josh Thienpont for assisting me with figuring out my codes and lab work, it was a great experience being your Teaching Assistant and also gaining laboratory and analytical skills from you. To Kristen Coleman, you were one of the first people I connected with, and I appreciate your friendship and also thank you for the academic and field support as the cores and data I analyzed were part of your research work. I would also like to appreciate the LPRG lab group and Jackson the lab technician for all their support, you all became like family to me.

Special thanks to my family for the moral and emotional support, especially during my surgery and academic journey. To my support system of friends: Lord Emmanuel, Ria and Prateeksha, we pushed each other and genuinely wanted each other to succeed, from the night classes, mock presentations and group discussions; I can't wait to see all we achieve in the future. In conclusion, I would like to thank all those who contributed to this thesis in various ways. Your support and encouragement have been instrumental in my academic journey.

TABLE OF CONTENTS

LIST OF TABLES

LIST OF FIGURES

1.0 INTRODUCTION

1.1 Background

Permafrost, defined as ground that remains frozen for two or more consecutive years, is thawing rapidly across the circumpolar North. The circumpolar North has warmed at rates of up to 3-4 times greater than the global average (Rantanen et al., 2022), which has led to the acceleration of permafrost thaw. In regions with excess ground ice, permafrost thaw takes the form of thermokarst, where melting ground ice causes the ground surface above to collapse (Olefeldt et al., 2016; Kokelj and Jorgensen, 2013). In discontinuous permafrost peatlands, wetland thermokarst is often the dominant form of thermokarst (Olefeldt et al. 2016). Wetland thermokarst involves peatland collapse, with the conversion of forested peat plateaus into treeless wetlands through the development of thermokarst bogs and fens (Figure 1.1).

Figure 1.1: Wetland thermokarst involves land subsidence followed by conversion of forested peat plateaus into wetlands. Image shows drunken (drowned) trees near the Scotty Creek Research Station (Dehcho region, NWT), which is a visual indication that wetland thermokarst is occurring on the landscape. Photo taken in 2018 by Joshua Thienpont (York University).

Permafrost contains globally significant stores of carbon and mercury that can be remobilized by permafrost thaw (Selin, 2009; Schuur et al., 2015; Schuster et al., 2018; Turetsky et al., 2020; Chételat et al., 2022). This can happen through the release of mercury and carbon that had been locked in permafrost for thousands of years (Vonk et al., 2015, Schuster et al., 2018, Schuur et al., 2015; Chételat et al., 2022), and as a result of enhanced hydrological connectivity of watersheds following permafrost thaw (Beilman and Robinson, 2003; Quinton et al., 2009; Quinton et al., 2011; Connon et al., 2014). In subarctic Canada, permafrost peatland degradation has significantly increased the hydrological connectivity of watersheds, resulting in higher stream flow and altered biogeochemical fluxes from land to water (Connon et al., 2014; Chasmer and Hopkinson, 2017; Olefeldt et al., 2021).

It has been predicted that there will be an increase in the export of dissolved organic carbon and mercury to downstream waterbodies as the hydrological connectivity of the watershed increases, altering water quality and aquatic biogeochemical processes (Coleman et al., 2015; Wauthy et al., 2018). Small lakes are abundant across boreal peatlands and are known hotspots of biogeochemical cycling (Landers et al., 1998; Heathcote et al., 2015). Biogeochemical processes in small lakes are also highly responsive to climate change (Lattaud et al., 2021). Lake sediments serve as potential sinks for carbon and mercury released from thawing permafrost, contributing to global carbon sequestration, and providing a storage mechanism for inorganic mercury (Guillemette et al., 2017; Stopford and Goldwater, 1975; Selin, 2009; Gopikrishna et al., 2020). Interest in the potential role of lakes in the burial of organic carbon and mercury at a global scale has increased significantly over the past century (Anderson et al., 2013; Chmiel et al., 2015; Heathcote et al., 2015; Gordon et al., 2016); however, knowledge on the role lake sediments play in controlling the fate of carbon and mercury released from thawing permafrost peatlands is still

limited, and there remains high uncertainty when predicting aquatic carbon response to permafrost thaw (Walvoord and Striegl, 2021).

Lake sediment cores can be used to examine how ecosystems have changed over time (the field of paleolimnology), including quantifying carbon and mercury burial rates over time (Engstrom, 1984; Brännvall et al., 1997; Hermanns and Biester, 2013). Paleolimnology reconstructs environmental change over centuries to millennia using physical, chemical, and biological proxy data stored in lake sediment cores. Paleolimnology has made, and continues to make, significant contributions to our understanding of thermokarst landscapes and their responses to climate change (Bouchard et al., 2016; Anderson et al., 2019; Korosi et al., 2022).

1.2 Study Rationale

Global estimates of the carbon cycle have barely considered spatiotemporal variation in lake carbon burial, while knowledge on the organic carbon storage capacity of lakes in thermokarst regions, and the mechanisms supporting sedimentation and carbon burial, is limited (Turetsky et al., 2020; Manasypov et al., 2022). There is also limited knowledge on the impacts of thermokarst processes on mercury cycling, especially in permafrost peatlands where soil mercury concentrations are high and saturated conditions in thawing peatlands may favor methylation (Selin, 2009; Chételat et al., 2022). A recent study provided evidence that shallow lakes in permafrost peatlands may be critical sinks for methylmercury, reducing transport of methylmercury to the drainage outlets (Thompson et al., 2023). This, combined with evidence that climate change and permafrost thaw may lead to increased dissolved organic carbon transport to lakes in thermokarst regions, highlighted the importance of understanding the fate of carbon and mercury transported to shallow lakes in permafrost peatlands. My MSc research addresses this

knowledge gap by quantifying carbon and mercury burial in sediment cores from 14 shallow lakes within or near the Scotty Creek Research Station in the Dehcho region of the Northwest Territories. The Scotty Creek Research Station is an internationally recognized field site for long-term ecohydrological and biogeochemical research, and has undergone extensive permafrost thaw-induced land cover changes since the 1970's (Quinton et al., 2019).

1.3 Research Objectives and Questions

My MSc research objectives are to:

1) Quantify the flux rates of carbon and mercury to lake sediments over the post-industrial period (since ~1850) in rapidly thawing discontinuous permafrost peatlands in 14 lakes at or near the Scotty Creek Research Station.
2) Document spatiotemporal patterns in the burial of total mercury and organic carbon, as well as carbon sources, as assessed by the elemental ratio of organic carbon to nitrogen.
3) Qualitatively assess temporal associations between mercury and organic carbon burial and lake physical characteristics or hydrological connectivity.

The objectives listed above will help me to answer the following questions:

1) Is there an association between organic carbon, mercury, and C:N, or do they change independently of one another?
2) How have carbon and mercury concentrations and flux rates changed over time?
3) Is there a relationship between the prevalence of thermokarst bogs and fens on lake shorelines (an indicator of hydrological connectivity) and carbon and mercury burial in lake sediments?

2.0 LITERATURE REVIEW

2.1 Overview

Lakes occupy ~2% of the Earth's surface (Lattaud et al., 2021) and receive matter and energy from both the surrounding watershed and the atmosphere (Tranvik et al., 2018). Shallow lakes are hotspots of biogeochemical cycling (Landers et al., 1998; Heathcote et al., 2015) and are highly sensitive to the ecological and hydrological impacts of climate change (Meerhoff et al., 2007; Williamson et al., 2009; Lattaud et al., 2021). Awareness of the need to better integrate lakes and other inland waters into global models for the biogeochemical cycling of carbon has been growing, as lakes are active sites for the transport, transformation, storage, and burial of terrestrial carbon (Cole et al., 2007; Tranvik et al., 2009; Tranvik et al., 2018). Lakes also influence the global cycling of mercury (Selin, 2009; Chételat et al., 2022), a pollutant of global concern in Arctic and subarctic lakes and rivers (Lockhart et al., 2005).

Arctic temperatures warmed 3-4 times faster than the global average between 1971 and 2021 (AMAP, 2021; Rantanen et al., 2022), with further increases in temperature up to 4-7ºC predicted over the 21st century (Post et al., 2019). Warming temperatures are accelerating glacial melt, coastal erosion, and permafrost thaw (Jorgenson et al., 2010; Quinton et al., 2011; Turetsky et al., 2020). Thaw-induced landscape changes in the Arctic and subarctic will alter mercury and carbon biogeochemical cycling in the environment through multiple pathways (Schuur et al., 2015; Schuster et al., 2018; Turetsky et al., 2020; Chételat et al., 2022). Of particular concern is the potential for permafrost thaw to lead to remobilization of carbon and mercury previously frozen in the permafrost over thousands of years (Vonk et al., 2015; Obrist et al., 2017).

2.2 Permafrost Thaw

Permafrost refers to soil or other ground that remains frozen for two or more consecutive years. Approximately 25% of the landmass of the Northern Hemisphere is underlain with permafrost (Zhang et al., 1999). Permafrost landscapes are classified based on the extent of the land that is underlain by permafrost. The continuous permafrost zone has 90-100% of the land underlain by permafrost; the extensive discontinuous permafrost zone has 50-90% permafrost coverage; the sporadic discontinuous permafrost has 10-50% permafrost coverage; and isolated permafrost has <10% permafrost coverage (Brown et al., 1997). Rapid loss of permafrost has been observed in recent decades across the circumpolar North in response to anthropogenic climate change (Olefeldt et al., 2016; Biskaborn et al., 2019; Smith et al., 2022). Factors such as permafrost extent, topography and ground ice content influence how permafrost thaw manifests, as well as the hydrological and biogeochemical responsiveness of the watershed to thaw (O'Neill et al., 2019; Vonk et al., 2019; Tank et al., 2020).

Ground ice content within the permafrost acts as the primary determinant of whether permafrost thaw occurs gradually or abruptly (Kokelj and Jorgensen, 2013). In areas of ice-rich permafrost, an abrupt form of permafrost thaw called thermokarst occurs, where melting ground ice causes the ground surface to collapse (Kokelj and Jorgensen, 2013). There are three main types of thermokarst, categorized based on where and how they form (Kokelj and Jorgensen, 2013). Hillslope thermokarst landforms occur due to a combination of land subsidence followed by lateral soil transport. Lake thermokarst describes the processes of thermokarst lake basin development mediated by the melting of ground ice, including lake formation, expansion, and eventual drainage (Kokelj and Jorgenson, 2013; Grosse et al., 2013; Bouchard et al., 2016). Wetland thermokarst is

characterized by the conversion of boreal forest or tundra dry shrub into thermokarst bogs and fens (Jorgenson et al., 2008; Kokelj and Jorgenson, 2013, Olefeldt et al., 2016). The extent of ground ice content exhibits spatial heterogeneity across the circumpolar North (Zhang et al., 1999; O'Neill et al., 2019).

Discontinuous permafrost peatlands at the southern limit of permafrost are particularly susceptible to permafrost thaw due to the relatively shallow depth (<10m) of permafrost in this region (Quinton et al., 2009), as well as the spatial fragmentation of the peatlands that exposes them to lateral heat transfer from non-permafrost bodies and heat conduction from the ground surface, requiring less energy to thaw at freezing temperature (Quinton et al., 2009; Chasmer et al., 2011; Kurylyk et al., 2016; Devoie et al., 2019). Rapid climate warming and accelerated permafrost thaw are projected to lead to the further disappearance of permafrost in most parts of the southern discontinuous permafrost zone over the next 50 years (Delisle, 2007; Schaefer et al., 2011; Schuster et al., 2011; Lawrence et al., 2012). Permafrost thaw in southern discontinuous permafrost peatlands mainly occurs in the form of wetland thermokarst (Jorgenson et al., 2008; Quinton et al., 2011; Quinton et al., 2019).

2.2.1 Permafrost thaw in southern discontinuous permafrost peatlands

Peatlands cover 19% of the northern circumpolar permafrost zones (Tarnocai et al., 2009; Jones et al., 2010). At the southern limit of permafrost, permafrost is restricted to peat plateaus and palsas because of the thermal properties of peat (Brown, 1970; Burn and Smith, 1988; Heginbottom et al., 1995). Peat plateaus and palsas are mounds that are raised 1-2 m above the ground due to the presence of ground ice (Zoltai, 1993; 1975; 2011). Peat plateaus cover between 30 and 70% of peatlands within the discontinuous permafrost zone (Kremenetski et al., 2003;

Baltzer et al., 2014; Gibson et al., 2018). Palsas, also known as frost mounds or large hill-bogs, are small circular to elongated mounds that have many similarities with peat plateaus but are smaller in lateral extents and often occupy a smaller fraction of larger peatlands (Olefeldt et al., 2021). Because of this, they are less likely than peat plateaus to have a large influence on overall peatland surface hydrology and runoff patterns (Olefeldt et al., 2021).

Southern permafrost peatlands are characterised by a mosaic of permafrost peat plateaus and palsas, as well as permafrost-free thermokarst bogs, fens, lakes, and ponds. (Connon et al., 2014; Olefeldt et al., 2016). In North America, black spruce (*Picea mariana*) is the most common type of woody vegetation found on peat plateaus and palsas (Quinton et al., 2011), which is able to grow as a result of the relatively drier soils compared to the surrounding wetland landscape. Thermokarst flat bogs are circular depressions formed by the thawing and settlement of ice-rich soils (Jorgenson et al., 2008; Sannel and Kuhry, 2008). Channel fens are long, linear depressions that occur on flat to gently sloping terrain where discharge of groundwater to surface springs causes the rapid collapse of ice-rich lowland deposits (Jorgenson et al., 2008). Drunken forests are an indicator of recent wetland thermokarst occurrence (Osterkamp et al., 2000; Finger et al., 2016; Korosi et al., 2022).

Permafrost peat plateaus, channel fens, and thermokarst bogs have specific hydrological functions that collectively influence how water and chemical constituents move across the discontinuous permafrost peatland landscape. Thermokarst bogs store water until it evaporates or percolates into the groundwater; channel fens convey water to the drainage outlet; and permafrost peat plateaus act as run-off generators (Quinton et al., 2009). Degradation of permafrost peatlands has significantly increased the hydrological connectivity of watersheds in the discontinuous

permafrost zone, resulting in higher stream flows and altered biogeochemical fluxes from land to water (Connon et al., 2014; Chasmer and Hopkinson, 2017; Olefeldt et al., 2021).

2.3 Implications of Permafrost Thaw for Water Quality

Permafrost thaw has significant implications for surface water quality through associated changes in water storage and movement across the landscape (Vonk et al., 2015; Olefeldt et al., 2021). In particular, permafrost contains globally significant stores of carbon and mercury that are being rapidly mobilized as a result of permafrost thaw (Selin, 2009; Schuur et al., 2015; Schuster et al., 2018; Turetsky et al., 2020; Chételat et al., 2022). This can happen through the release of previously frozen mercury and carbon and through enhanced hydrological connectivity of watersheds caused by thaw (Rydberg et al., 2010; Olefeldt and Roulet, 2012; Coleman et al., 2015; Korosi et al., 2015; Gordon et al., 2016). As permafrost thaws, carbon and mercury that have been locked in the soil for thousands of years becomes liberated (Obrist et al., 2017), while enhanced hydrological connectivity alters the movement and processing of carbon and mercury through the landscape to the drainage outlets (Fouché et al., 2020; Turetsky et al, 2020; Olefeldt et al., 2021). Significant increase in lake dissolved organic carbon (DOC) concentrations have been predicted in surface waters draining thermokarst landscapes because of permafrost thaw (Wauthy et al., 2018), and demonstrated in field data (Olefeldt et al., 2014). Lake DOC is an important control on light penetration, thermal regime, and lake metabolism (Vonk et al., 2015).

2.4 Biogeochemical Cycling of Carbon in Lakes

Permafrost thaw could enhance global climate warming by 0.13–0.27 °C by 2100 through the permafrost carbon feedback system (Schuur et al., 2015). Approximately 1,000±150 petagrams

(PgC) of carbon is contained in the top 3 metres of active layer and permafrost peatland soils, which could be liberated by permafrost thaw (Turetsky et al., 2020). Some of the liberated organic carbon will be broken down by microbial decomposition, resulting in the release of carbon dioxide (CO_2) and methane (CH_4) into the atmosphere as part of a positive feedback loop that would enhance global warming, causing more thawing of the permafrost, more release of previously stored carbon, and more production of greenhouse gases from thawed permafrost (Schuur et al., 2009; Schädel et al., 2014, Schuur et al. 2015; Turetsky et al., 2020; Voigt et al., 2020; Heslop et al., 2020).

Since the 1950s, there has been increased permafrost-induced land-cover change which has resulted in increased mobilization of terrestrial carbon previously sequestered in permafrost (Houghton, 2003; Heslop et al., 2020). Much of the carbon released from thawing permafrost will end up in lakes, where it can be processed, transported, and/or stored (Cole et al., 2007; Tranvik et al., 2009; Tranvik et al., 2018). Thermokarst landforms resulting from abrupt permafrost thaw have a significant influence on the downstream movement of remobilized carbon into lakes, rivers, and oceans, affecting the global carbon cycle (Schuur et al., 2015; Anthony et al., 2014). Carbon can be released in the form of dissolved organic carbon (DOC), dissolved inorganic carbon (DIC), particulate organic carbon (POC), or gaseous carbon (CO_2 or CH_4) (Vonk et al., 2015; Schaphoff et al., 2013; Burke et al., 2012; Schuur et al., 2011; Zhuang et al., 2006). DOC has been identified as the largest source of carbon input in boreal lakes (Cole et al., 2007; Tranvik et al., 2009). Recent studies in boreal and Arctic regions have observed an increased export of dissolved organic matter and DOC concentrations from terrestrial catchments to lakes and rivers, including from thawing permafrost (Monteith et al., 2007; Garmo et al., 2014; de Wit et al., 2016; Räike et al., 2016; Wauthy et al., 2018).

Carbon in aquatic systems can be mineralized to CO_2 and CH_4, transported through hydrological networks (Battin et al., 2009); or buried in lake sediments (Vonk et al., 2013; Schädel et al., 2016; Serikova et al., 2018). Lakes are active sites for mineralization of DOC to CO_2 and CH_4 (Schädel et al, 2016). CO_2 and CH_4 levels in lakes are controlled by internal biogeochemical processes such as organic matter decomposition, methanogenesis, respiration, primary production, and methane oxidation, as well as external inputs from the catchment (Cole et al., 2007). In-lake respiration is the main source of CO_2 emissions from lakes (Del Giorgio et al., 1999; Jansson et al., 2000). Mineralization of CO_2 also occurs via photochemical reactions acting on DOC (Salonen and Vahatalo, 1994; Graneli et al., 1996; Tranvik et al., 2009), with CO_2 then emitted into the atmosphere from supersaturated lakes (Sobek et al., 2003; Sobek et al., 2005).

Precipitation-induced runoff may significantly impact CO_2 and CH_4 emissions in lakes due to increased inputs of allochthonous (i.e. external or terrestrial) organic matter (Rantakari and Kortelainen, 2005; Ojala et al., 2011; Vachon and del Giorgio, 2014). CO_2 supersaturation occurs as a result of high input of allochtonous organic carbon, as respiration dominates over primary production due to light limitation (Tranvik et al., 2009). The global CO_2 emissions from lakes have been estimated to reach as high as 0.53 Pg C yr-1 (Downing et al., 2006), and these emissions play a substantial role in regional carbon budgets, particularly in Arctic regions (Kling et al., 1991). Anoxic (absence of oxygen) conditions in lakes favor the conversion of organic carbon to CH_4 by methanotrophic bacteria, which is a more potent greenhouse gas than CO_2 (Bastviken et al., 2004; Bastviken et al., 2008). The global CH_4 emitted from lakes is estimated to be between 6 and 36 TgC (Cole et al., 2007).

Lakes are part of broader hydrological networks, and some of the carbon transported to lakes from thawing permafrost will continue to be transported downstream through this network (Cole et al., 2007). There is limited knowledge about the mechanical controls and processing of organic carbon flowing through subarctic and Arctic watersheds (Mann et al., 2012; Wickland et al., 2012), but this is critical to resolve, as the ultimate fate of organic carbon transported downstream would be ending up in the ocean. Studies suggest that an average of 34 Tg C yr^{-1} of dissolved organic carbon (DOC) and 6 Tg C yr^{-1} of particulate organic carbon (POC) is transported to the Arctic Ocean (Holmes et al., 2012; McGuire et al., 2009). Furthermore, increasing temperatures can result in increased freshwater discharge (Savelieva et al., 2000; Semiletov et al., 2000; Peterson et al., 2002), which has been documented to increase organic carbon transport through fluvial systems into the ocean (Guo et al., 2004; van Dongen et al., 2008; Vonk et al., 2010a; Gustafsson et al., 2011).

Lake sediments are an important sink in the global carbon cycle (Dean and Gorham, 1998; Vonk et al., 2015). Factors such as landscape characteristics (Walter Anthony et al., 2014) and lake shape (e.g. small and deep vs. large and shallow; Ferland et al., 2012) strongly affect burial efficiencies in boreal lakes. Carbon storage rates in lakes commonly increase with lake productivity and are inversely proportional to lake size (Mulholland and Elwood, 1982; Paterson et al., 1998; Kortelainen et al., 2004; Cole et al., 2007). Consequently, the small and shallow boreal lakes that are abundant across permafrost peatlands may represent a critical sink for carbon released from thawing permafrost peatland soils. Studies quantifying carbon burial rates, and drivers of spatial variation in carbon burial, are limited, but may be on the order of 14 g C m^{-2} y^{-1} (Dean and Gorham, 1998). Studies have also documented increases in total organic carbon burial

rate in lakes over the past 100 years from 0.05 Pg C $year^{-1}$ to 0.12 Pg C $year^{-1}$ (Lehnherr et al., 2018; Anderson et al., 2020).

Particulate organic carbon (POC), including biological materials, is the predominant form of organic carbon in lake sediments, despite DOC being the greatest pool of carbon input in lakes (Cole et al., 2007). Flocculation is the process through which DOC can be incorporated into bulk lake sediments (Tranvik et al., 2009). Only a small fraction of sinking organic particles are thought to be sequestered in lake sediments (Guillemette et al., 2017). Still, the accumulation and burial of partially degraded organic carbon in lake sediments means that sediments have the potential to function as an effective long-term organic carbon sink (Chmiel et al., 2015). Factors such as oxygen availability, solid iron phases, type, and specific surface area of minerals as well as particle size have been suggested to control the preservation and burial efficiency of organic carbon in lakes, rivers, and oceans (Keil et al., 1997; Sobek et al., 2009; Lalonde et al., 2012; Hemingway et al., 2017; Blattmann et al., 2019).

Studies suggest that the preservation in sediments of autochthonous and allochthonous OC sinking in the water column of boreal lakes differs substantially (Guilemette et al., 2017). Sediments dominated by allochthonous inputs decay slower than sediments dominated by autochthonous material (Gudasz et al., 2012). This makes it likely that allochthonous OC will be preferentially preserved and buried in lake sediments due to the resistant nature of terrestrial compounds and delayed decomposition under anoxic conditions found in sediments. Small shallow lakes often have high light availability to support primary production (Tranvik et al., 2009), leading to high annual carbon burial rates (Downing et al., 2008).

2.5 Aquatic Biogeochemistry of Mercury

Mercury, in its elemental form Hg(0), is transported to the Arctic by long-range atmospheric deposition through various pathways such as atmospheric circulation, lakes, rivers, and oceans (Selin, 2009; Durnford et al., 2010; Gordon et al., 2016; Petrova et al., 2020; Chételat, 2022). Mercury accumulates in permafrost primarily as inorganic mercury (Hg(II)) (Mason et al., 1995; Qureshi et al., 2010; AMAP 2011; O'Driscoll et al., 2019; Chételat et al., 2022). The transport of Hg between the terrestrial and aquatic environment is influenced by organic matter, microbial activity, and light (Ariya et al., 2004; Selin, 2009; Chételat et al., 2022). Large pools of Hg have accumulated in permafrost soils (~597,000 Mg, 0-3 m depth), predominantly from vegetation uptake of Hg(0) and conversion to Hg(II) over millennia (Obrist et al., 2017; Dastoor et al., 2022; Dietz et al., 2022).

The potential for this stored mercury to be remobilized due to climate-induced permafrost thaw, and subsequently transported downstream or re-emitted to the atmosphere is a global concern due to the potential toxicity of mercury (Schlüter, 2000; Leitch, 2006; Schuster et al., 2011; Gordon et al., 2016; Schuster et al., 2018; St Pierre et al., 2018; Lim et al., 2019; Lim et al., 2020; Zolkos et al., 2020). Peatlands in northern boreal forest catchments have been found to have abundant stores of Hg(II) bonded to soil organic matter (Schuster et al. 2018). Mercury in permafrost peatland soils are of particular concern, related to the high potential for mobilization of methyl mercury (Gilmour et al., 1992; Rudd, 1995; Selin, 2009; Chételat et al., 2022).

Methyl mercury is a neurotoxin that bioaccumulates in aquatic food webs, resulting in the increased risk of mercury poisoning in humans who consume mercury-contaminated fish (Hintelmann et al., 2002; Muir et al., 2009; Gilmour et al., 2013; Bravo and Cosio, 2020; Villar et

al., 2020; Chételat et al., 2022). Mercury is more likely to be transformed into the methyl mercury form in anoxic aquatic sediments, which are common in lakes, ponds, and wetlands (Jiang et al., 2011; MacMillan et al., 2015; Yang et al., 2016; Chételat et al., 2022;). Mercury methylation is a biotic process facilitated by metabolic activity of sulfate-reducing bacteria that thrive in saturated, anoxic environments (Gilmour et al., 1998; Benoit et al., 2003; Kerin et al., 2006; Gilmour et al., 2013). Environmental factors such as temperature, pH, redox conditions, sediment structure, sulfate and DOC can affect the rate of methyl mercury production by influencing the amount of bioavailable inorganic mercury and/or the activity of methylating microbes (Mitchell et al., 2008; Selin, 2009; Lehnherr, 2014). Methylmercury production has also been measured in the water column in lakes (Eckley and Hintelmann, 2006; Eckley et al., 2005). and wetlands and lake sediments have also been reported as important environments where methylation occurs Temperate and low boreal peatlands are known sources of methyl mercury transport to downstream aquatic ecosystems (St. Louis et al., 1996; Branfireun and Roulet, 2002; Mitchell et al., 2008), and the thawing of peat plateaus and palsas has been linked to the downstream export mercury (Rydberg et al., 2010; Korosi et al., 2015; Gordon et al., 2016; Fahnestock et al., 2019). A recent study provided evidence that shallow lakes in permafrost peatlands may be critical sinks for methyl mercury, reducing the transport of methyl mercury to the drainage outlets where human risk of mercury consumption is much higher (Thompson et al., 2023).

Mercury can be transported downstream to lakes through sorption onto organic carbon (Haitzer et al., 2003; Moore et al., 2003; O'Driscoll et al., 2006; Hill et al., 2009; Rydberg et al., 2010), and thus the mercury cycle is tightly coupled to the organic carbon cycle (Yang et al., 2007; Porcal et al., 2009; Turetsky et al., 2020; Dietz et al., 2022). Organic matter is the most important component influencing the distribution and form of mercury in soils (Driscoll et al., 1995; Grigal

2003; Obrist et al. 2011). It has been suggested that an increase in organic matter transport, particularly dissolved organic carbon, may also be influencing the downstream transport and fate of mercury in Arctic rivers (Dietz et al., 2022). Elevated mercury concentrations have been documented in rivers draining permafrost landscapes (Leitch et al., 2007; Schuster et al., 2011). Concentrations of Hg(II) and methyl mercury in streams draining permafrost thaw slumps in the western Canadian Arctic have been recorded as high as 1270 ng/L for Hg(II) and 7 ng/L for methyl mercury (St. Pierre et al., 2018).

The association between mercury and organic provides a mechanism for mercury to build up in lake sediments, and sediments are also an important sink for mercury, as they are for carbon. Mercury is stable in lake sediments, and sediment cores faithfully track the history of mercury deposition in lakes (Biester et al., 2007; Selin, 2009). Variations in the source, type, and relative quantity of autochthonous versus allochthonous organic matter have been suggested to affect the delivery of mercury to aquatic systems (Jackson, 1986; Kainz et al. 2003; Sanei and Goodarzi, 2006).

2.6 Paleolimnology

Paleolimnology is a scientific discipline that reconstructs past environmental conditions in inland aquatic systems using the physical, chemical, and biological information preserved in sediment profiles (Smol, 2008). Paleolimnology most commonly uses lake sediments as natural archives, enhancing understanding of environmental changes in both lakes and their watersheds over time (Smol, 2008). Paleolimnological investigations have greatly enhanced understanding of thermokarst landscape development and thermokarst responses to climate change (Bouchard et al. 2016; Anderson et al., 2019; Korosi et al., 2022). Paleolimnological investigations have also

significantly contributed to our understanding of the temporal dynamics of carbon and mercury burial in lake sediments (Bouchard et al., 2016; Guilemette et al., 2017; Landers et al., 1998; Gordon et al., 2016; Muir et al., 2009; Lockhart et al., 2000). For example, a paleolimnological approach demonstrated that increases in organic matter in High Arctic lakes enhanced mercury accumulation in lake sediments independent of atmospheric mercury deposition patterns (Korosi et al., 2018). Paleolimnological studies have also highlighted the role of fire and wetland thermokarst in increasing terrestrial mercury transport to lakes (Rydberg et al. 2010; Korosi et al., 2015; Pelletier et al. 2022). Increase in lead and mercury in sediments have also been associated with rapid industrialization in the mid-19th century (Blais et al., 1995).

Sediment accumulation rates and age-depth models are fundamental for the application of paleolimnological techniques to document spatio-temporal trends in carbon and mercury burial in lake sediments, with factors such as sediment sources, biological processes, geological composition, and hydrodynamic regimes resulting in variable patterns of sediment deposition (Szmytkiewicz and Zalewska, 2014). To determine the accumulation rate over a century-long period, isotope methods based on changes in ^{210}Pb and 137Cs activity in sediment profiles have been employed (Appleby and Oldfield, 1978; Appleby, 1997; Baud et al., 2021). Over the last five decades, considerable efforts and coring programs were initiated globally, providing a rich collection of published data on recent lake sediment accumulation rates (Rose et al. 2011), but synthesis of spatial–temporal variability in lake sediment accumulation rates for the last 150 years is missing at a global scale (Baud et al., 2021).

2.6.1 Establishing age-depth chronologies and sediment accumulation rates

In paleolimnological investigations, the key assumption for any relative age dating is that more recent sediments overlie older sediments – known as the Law of Superposition (Barker, 2009). Radiometric methods using ^{210}Pb and ^{137}Cs are most common for establishing sediment core chronologies, which are then used to reconstruct changes in sediment accumulation rates over time (Musielak, 1985; Appleby and Oldfield, 1992; Appleby, 1997; Smol, 2009). ^{210}Pb is a naturally occurring radioisotope that has a half-life of 22.3 years. It is produced by the decay of ^{222}Rn, a member of the uranium (^{238}U) decay series ($t_{1/2}$ = 3.82 days), which is created continuously by natural processes and undergoing decay (Krisnaswamy et al., 1971; Smol, 2008).

Sedimentary ^{210}Pb activity has two components: supported ^{210}Pb, which is derived from ^{226}Ra decay *in-situ*, and unsupported ^{210}Pb (Appleby, 2001). Unsupported or excess ^{210}Pb(ex) originates from atmospheric fallout (precipitation) and is calculated by subtracting supported ^{210}Pb activity from the total ^{210}Pb activity (Smol, 2008). Unsupported ^{210}Pb activity in sediments is expected to decrease with sediment depth through decay, until it reaches background levels, unless it is disrupted by processes such as sediment mixing, input from external sources, changes in radionuclide mobility, or diagenesis (Appleby, 2001; Robbins, 1978).

There are several key assumptions that govern the use of ^{210}Pb to date sediment cores (Krisnaswamy et al., 1971):

i. the rate of atmospheric ^{210}Pb deposition has been and remains constant.
ii. Because suspended particulate matter rapidly adsorbs ^{210}Pb in water, unsupported ^{210}Pb activity in sediments is primarily due to atmospheric fallout; (however,

unsupported ^{210}Pb supplied to the lake may also include a small fraction of ^{210}Pb that was deposited on the catchment and then transported to the lake)

iii. ^{210}Pb activity in the sediments is not redistributed by post-depositional processes

iv. According to the rule of radioactive decay, ^{210}Pb decays exponentially over time.

Hydrologic processes and sediment focusing can redistribute deposits at the lake's bed, and some of the total ^{210}Pb inputs may also be lost in the outflow. Sediment focusing refers to the process by which sediments are deposited in marginal zones of a basin and then redeposited in deeper water zones (Smol, 2008) and plays an important role in lake sedimentation patterns (Hermanns and Biester, 2013).

There are three different models that can be used to calculate sediment dates from ^{210}Pb radioisotope profiles: the constant rate of supply (CRS) model, the constant initial concentration (CIC) model, and the constant flux constant sedimentation (CFCS) model. The CIC model is better suited in circumstances where there have been interruptions to sedimentation as a result of slumping or other process, and assumes that primary sedimentation rates have otherwise remained constant (Robbins, 1978; Appleby, 2001). The CFCS model assumes consistent sedimentation rates, with no interruptions or impacts (Krishnaswami et al., 1971; Bierman et al., 1998). The CRS model is most commonly used because it does not assume that sedimentation rate has remained constant over time, an assumption that is not valid for most lakes (Appleby and Oldfield, 1978). The CRS model assumes that the supply of unsupported ^{210}Pb to the sediment has remained constant, while the initial excess ^{210}Pb deposited to the sediments varies inversely with the sediment mass accumulation rate (MAR). In addition to an age-depth chronology, the CRS model also calculates changes in MAR with sediment core depth, which can then be used to determine

the burial rates of carbon, mercury, and other biogeochemical constituents in lake sediments (Hobbs et al., 2013; Engstrom and Rose, 2013).

Other isotopes that are anthropogenic in origin have also been used to determine specific periods in sedimentary sequences. Cesium-137 (^{137}Cs) isotope is commonly used to verify ^{210}Pb dates, as it is a reliable chronological marker of atmospheric bomb testing in recent lake sediments (Davis et al. 1984; Smol, 2008; Klaminder et al. 2012). ^{137}Cs was first emitted in 1945 with the dawn of the nuclear era, peaking in 1963 when global ^{137}Cs fallout from atmospheric nuclear bomb testing was at its highest level (Appleby, 2001). The 1986 Chernobyl nuclear power plant accident can also be detected using ^{137}Cs in lake sediments from northern Europe (Appleby, 2001). ^{137}Cs activity sometimes presents issues associated with post-depositional mobility, especially in organic-rich sediments, such that dating discrepancies can occur between the ^{137}Cs dates and the ^{210}Pb dates (Smol, 2008).

3.0 MATERIALS AND METHODS

3.1 Study Site Description

The Scotty Creek watershed (Northwest Territories, Canada) is located approximately 50 km south of Fort Simpson in the Northwest Territories, Canada (Figure 3.1), at the boundary between the sporadic discontinuous and the extensive discontinuous permafrost zones (Hegginbottom et al., 1995; Carpino et al., 2021). The Scotty Creek watershed drains 152 km^2 of high boreal forest with a high concentration of wetlands that formed because of the flat topography and through wetland thermokarst processes that cause the ground to subside, saturate, and transition from forest into wetland (Quinton et al., 2011; Haynes et al., 2018). The landscape is a mosaic of permafrost plateaus, channel fens, and ombrotrophic flat bogs, as well as numerous lakes and ponds (Quinton et al., 2009). Channel fens convey water and nutrients downstream, while bogs act as water storage units (Quinton et al., 2019). The Scotty Creek basin typifies the southern extent of permafrost in much of Canada (Robinson and Moore, 2000).

The Scotty Creek Research Station has been a site of long-term ecohydrological monitoring for nearly three decades (Quinton et al., 2019). It is also one of the most rapidly warming regions on Earth (Johannessen et al., 2004; Vincent et al., 2015; Haynes et al., 2018). Over the past 30 years, extensive research conducted at Scotty Creek has documented significant land cover changes resulting from accelerated permafrost thaw due to climate change (Chasmer et al., 2014; Chasmer and Hopkinson, 2017; Haynes et al., 2018; Quinton et al., 2019). Changes include the development of thermokarst landforms such as ombrotrophic flat bogs and channel fens, which make up 19% and 12% of the Scotty Creek watershed, respectively, (Chasmer et al., 2014), and increased hydrological connectivity and drainage efficiency (Connon et al., 2014).

I selected 14 small (surface area 11-244 ha), shallow (maximum depth ~1-2 m) study lakes within or near the Scotty Creek watershed (Figure 3.1). The lakes are all slightly alkaline, with high DOC (Table 3.1). The shoreline development ratio, an index that describes how close a lake is to a perfect circle, ranged from 1.02 to 1.75 (Table 3.1). Lakes with a shoreline development ratio close to 1 tend to be more circular in shape, while lakes with higher ratios have more irregular, crenulated shapes with a greater potential for littoral community development and enhanced exposure to surrounding shorelines (Coleman et al., 2023). Land classification based on airborne LiDAR and spectral data (Chasmer et al., 2014) was available for 9 of the 14 study lakes (Table 3.1). Land classification showed that the percent coverage of fens within 250 m of the lake shorelines ranged from 0%, indicating hydrological isolation, to 34% (Coleman et al., 2023). Most lakes were linked together via channel fen networks, except for SC5 and SC8 (Coleman et al., 2023).

3.2 Field Methods

Sediment cores were collected from the 14 lakes in June 2019 (Coleman et al., 2023). The lakes were accessed via helicopter and sediment cores were collected from the approximate centre of the lakes using a Uwitech^{TM} gravity corer with an internal diameter of 8.6 cm. The sediment cores were sectioned at 0.5 cm intervals into sterile Whirlpak^{TM} bags on the same day using a modified Glew (1988) extruder to avoid sediment mixing. Sediment samples were shipped back to York University where they were stored frozen until analysis.

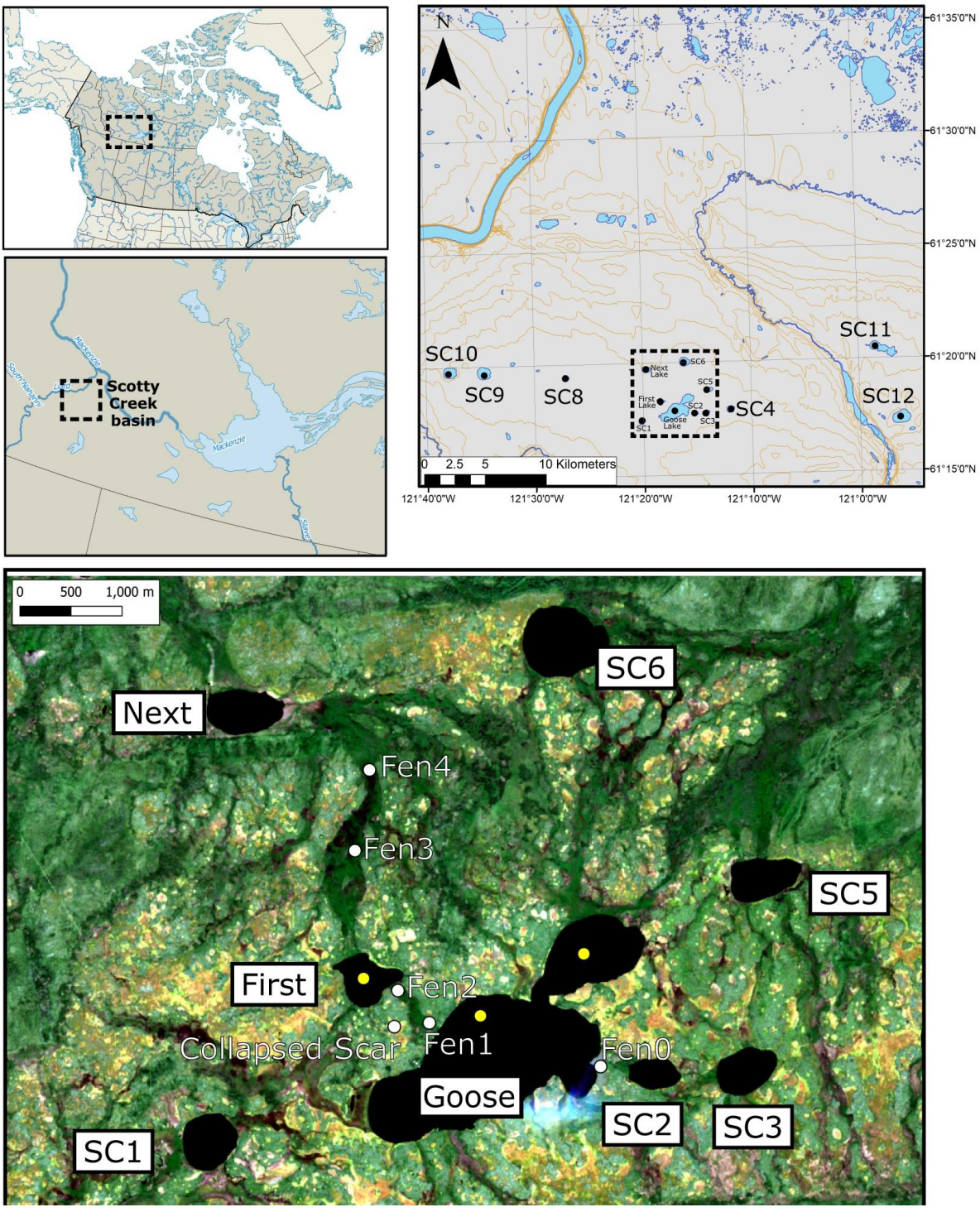

Figure 3.1 - Map of study area showing the approximate location of study area within Canada (top left) and the Taiga Plains ecozone (top right), and the locations of all study lakes in the Scotty Creek and neighbouring basins; including the hydrological connectivity (wetland thermokarst landscape) of some of the study lakes. The maps were created using ArcGIS Pro version 3.0.0.

Table 3.1: Physical characteristics and water chemistry for the 14 study lakes in the Scotty Creek and neighboring basins. (Data from Coleman et al., 2023).

Lake	Depth (m)	pH	Shoreline Development Index (DL)	Area (ha)	True Colour (TCU)	DOC (mg/L)	TN (mg/L)	Alkalinity (mg/L CaCO3)	% Bog (250m)	% Fen (250m)
Goose	1.1	8.0	1.70	244	53	23.7	1.2	50	22.9	34.1
First	0.9	8.4	1.26	17	249	21.9	1.0	43	37.7	12.9
Next	1.5	7.9	1.12	24	258	18.3	0.7	43	20.5	34.0
SC1	1.3	8.0	1.02	21	223	16.9	0.7	30	21.3	19.5
SC2	1.7	8.5	1.08	11	312	18.0	0.6	33	13.4	30.9
SC3	1.8	8.3	1.05	18	276	18.4	0.7	34	26.9	26.6
SC4	1.1	8.1	1.06	22	143	17.2	0.8	42	-	-
SC5	1.0	7.9	1.14	21	463	23.6	0.8	28	31.6	9.6
SC6	1.1	8.5	1.10	40	53	15.8	0.9	35	28.5	25.8
SC8	0.9	8.1	1.06	15	285	19.9	0.8	30	48.9	0.0
SC9	2.1	8.1	1.07	82	151	13.0	0.5	47	-	-
SC10	1.2	8.5	1.06	73	89	20.0	1.1	60	-	-
SC11	2.0	7.9	1.75	114	196	15.9	0.7	64	-	-
SC12	0.9	8.4	1.07	116	27	23.6	1.5	82	-	-
Mean	1.3	8.2	1.20	58	198	19.0	0.9	44	28.0	21.5
SD	0.4	0.2	0.20	65	122	3.3	0.3	15	10.5	11.9
Min	0.9	7.9	1.02	11	27	13.0	0.5	28	13.4	0.0
Max	2.1	8.5	1.75	244	463	23.7	1.5	82	48.9	34.1
Median	1.2	8.1	1.1	23	209.3	18.3	0.8	42.5	26.9	25.8

3.3 Laboratory Methods

3.3.1 Sediment core dating

Freeze-dried sediments were sent to the Paleoecological Environmental Assessment and Research Lab (PEARL) at Queen's University for ^{210}Pb dating by gamma spectroscopy (Appleby, 2001) using an Ortec High Purity Germanium Gamma Spectrometer (Oak Ridge, TN, USA). Certified reference materials were obtained from the International Atomic Energy Association (Vienna, Austria) for efficiency corrections. The Constant Rate of Supply (CRS) model was used to establish age-depth models based on unsupported ^{210}Pb activity, with supported ^{210}Pb assessed using ^{214}Pb (Appleby, 2001). Sediment focusing factors were calculated for each lake by dividing unsupported ^{210}Pb flux (in Bq/m^{2}yr) by the predicted ^{210}Pb flux in soils for that latitude, following

methods described in Appleby (2001). The expected regional atmospheric input was derived following Muir et al. (2009).

3.3.2 Total Mercury (THg) Analysis

Approximately 75 mg of freeze-dried, homogenized sediment per interval was weighed into nickel sample boats and analyzed for total mercury (THg) using a Direct Mercury Analyzer (Milestone DMA-80 Evo). The DMA determines THg using US-EPA method 7473, combining thermal decomposition, gold amalgamation and detection via atomic absorption spectrometry (Couillard et al., 2008). Controlled heating of the sample in an oxygenated decomposition furnace reduces elemental mercury, releasing gaseous mercury (thermal decomposition). Flowing oxygen carries the decomposition products to the gold amalgamator, which selectively traps mercury. The system is flushed with oxygen to remove other degradation products, and then the amalgamator is heated rapidly to release the mercury vapour, which is carried to the absorbance cells and measured by atomic absorption.

The sample boats were placed in the DMA autosampler wheel which automatically loaded the samples into the unit. For Quality Assurance / Quality Control (QA/QWC), every tenth sample was analyzed in triplicate. Marine Sediment Certified Reference Materials from the National Research Council of Canada (MESS-4; 0.09 ± 0.04 mg/kg) was used to monitor measurement stability and precision. Method blanks were also analyzed at the beginning and end of each analysis cycle (n=3 at the beginning and n=2 at the end), to ensure there was no excess mercury being detected in the samples.

3.3.3 Organic Carbon and Nitrogen Analysis

Approximately 30 mg of freeze dried, homogenized sediment per interval was pretreated in concentrated 12M (36%) HCl acid for 48 hours using an acid fumigator to remove inorganic carbon (Harris et al., 2001). After 48 hours, the sample vials were filled with distilled water to rinse the fumigated sediments samples and re-neutralize the sediments. The supernatant was discarded using a pipette and the sediments were transferred into centrifuge tubes, which were then filled with distilled water and centrifuged at 3000 rpm for 10 min. This step was repeated seven times in total, after which the samples were freeze-dried.

After the fumigation process, elemental carbon and nitrogen (%OC and %N) were measured using an Elementar Unicube Elemental Analyzer (EA). The Elemental analyzer measures C and N by combusting sediment samples in a furnace at a high temperature in an oxidizing atmosphere, purifying these elements into gaseous form (N_2, CO_2), and then separating out the gaseous products by chromatography before analyzing individual gases using a thermal conductivity detector (TCD). Helium was used as the carrier gas. Sulfanilamide was used as a standard to condition the instrument at the start of every day and establish a daily calibration curve. Approximately 5mg of freeze-dried sediments per interval were weighed into tin capsules to be analyzed on the EA. For Quality Assurance / Quality Control (QA/QWC), soil standard Certified Reference Material (~12.5 mg; n = 3) were analyzed before beginning measurements of actual sediment samples. Method blanks were also run at the start of the analysis cycle as an additional QA/QC procedure. At select intervals (after the 22nd actual sediment sample), additional run-in and soil standard samples (n=2; n=3 respectively) were also analyzed.

3.4 Data Analysis

The sediment accumulation rate (SAR) and sediment mass accumulation rate (MAR) was determined from the ^{210}Pb age-depth model established by the CRS method. To calculate the SAR (cm/yr), the thickness of each sediment depth interval was divided by the age of the corresponding sediment layer (Appleby & Oldfield, 1978), as expressed in (1):

$$SAR\ (cm/yr) = Z/Tz \quad (1)$$

where SAR = Sediment Accumulation Rate (cm/yr); Z = core depth (cm); Tz = age of layer at depth (yr).

Mass Accumulation rate (MAR) is required to quantify sediment flux and burial rates for carbon and mercury in lakes (Engstrom and Rose, 2013; Hobbs et al., 2013; Baud et al., 2021), measured in grams per square centimeter per year, as expressed in (2):

$$MAR\ (g/cm^2/yr) = Z * DBD / yr \quad (2)$$

where MAR = Mass accumulation rate in lake sediments; Z = depth (cm); DBD = Dry bulk density (g/cm^3); Tz = age of layer at depth (yr).

Sediment Focussing refers to the process by which sediment in lake basins is gradually redistributed to the centre or deepest part of the lake, measured as the sediment focusing factor. Sediment focusing factors (FF) will be influenced by slope and wind, and can be calculated by dividing ^{210}Pb flux (in Bq/m^2yr) by the predicted ^{210}Pb flux for that latitude (Appleby, 2001), as expressed in (3):

$$FF = {}^{210}Pb\ flux\ /80\ Bq/m^2yr \quad (3)$$

where 80 Bq/m^{2}yr is the predicted ^{210}Pb flux at Lake Laberge, YK (61.2 ºN), a similar latitude to Scotty Creek (Muir et al., 2009).

The ^{210}Pb flux was calculated as the unsupported ^{210}Pb inventory (in Bq/m^2) in the surface interval multiplied by the ^{210}Pb radioactive decay constant (λ) (Appleby, 2001), as expressed in (4):

$$^{210}Pb\ flux\ (Bq/m^2yr) = {}^{210}Pb_{ex} * \lambda \quad (4)$$

^{210}Pb$_{ex}$ = unsupported ^{210}Pb inventory (Bq/m^2) in the surface interval; λ = ^{210}Pb radioactive decay constant (0.03114 yr^{-1}).

To calculate the mercury flux rate (HgF), the total mercury (THg) concentration value was multiplied by the mass sedimentation rate (MAR), as expressed in (5), and then corrected for sediment focusing by dividing the mercury flux rate (HgF) by the focusing factor of the lake, as expressed in (6).

$$HgF\ (ng/cm^2yr) = THg * MAR \quad (5)$$

Hg = Total mercury in sediments (ng/g); MAR = Mass accumulation rate in lake sediments (in g/cm^{2}yr)

$$Corrected\ HgF\ (ng/cm^2yr) = HgF / FF \quad (6)$$

where FF = Focusing Factor.

As the sedimentation rate derived from the CRS model has errors associated with it, the mercury flux rate error was also calculated, as expressed in (7), and then corrected for sediment

focusing by dividing the mercury flux rate error (HgF_{error}) by the focusing factor of the lake, as expressed in (8).

$$HgF_{error}\ (ng/cm^2yr) = THg * MAR_{error} \quad (7)$$

where THg = Total mercury in lake sediments (ng/g); MAR_{error} = Accumulation rate error in lake sediments (in g/cm^2yr).

$$Corrected\ HgF_{error}\ (ng/cm2yr) = HgF_{error} / FF \quad (8)$$

Where FF = Focusing Factor

The percentages of carbon and nitrogen in sediment intervals were used to calculate the C/N mass ratios, which are then multiplied by 1.167 (the ratio of atomic weights of nitrogen and carbon) to yield the atomic C/N ratio (Meyers and Teranes, 2001), as expressed in (9):

$$Atomic\ C/N = (C / N) * 1.167 \quad (9)$$

where C = weight percentage of elemental carbon; N = weight percentage of elemental nitrogen; 1.167 = the ratio of atomic weights of nitrogen and carbon.

To calculate organic carbon flux rates (OCF), the weight percentage of carbon (%OC) determined from the elemental analyzer (EA) was multiplied by the MAR, as expressed in (10):

$$OCF\ (g/cm^2yr) = (\%OC) * MAR \quad (10)$$

where %OC = weight percentage of organic Carbon; MAR = Mass accumulation rate in lake sediments (g/cm^2yr).

Organic carbon flux was corrected for sediment focusing by dividing the organic carbon flux rate (OCF) by the focusing factor of the lake, as expressed in (11).

$$Corrected\ OCF\ (g/cm^2yr) = OCF / FF \quad (11)$$

where FF = Focusing Factor.

As the sedimentation rate derived from the CRS model has errors associated with it, the organic carbon flux rate error was also calculated, as expressed in (12), and then corrected for sediment focusing by dividing the organic carbon flux rate error (OCF_{error}) by the focusing factor of the lake, as expressed in (13).

$$OCF_{error}\ (g/cm^2yr) = (\%OC) * MAR_{error} \quad (12)$$

where %OC = weight percentage of organic Carbon; MAR_{error} = Accumulation rate error in lake sediments (in g/cm^2yr).

$$Corrected\ OCF_{error}\ (g/cm^2yr) = OCF_{error} / FF \quad (13)$$

where FF = Focusing Factor.

All subsequent data analyses and figure generation were performed using the gam, ggplot, riojaPlot and mgcv packages in the R software enviroment (v. 4.2.3; R Core Team, 2023). Sediment core stratigraphies were plotted using the riojaPlot package to visualize downcore changes in total mercury (THg), mercury flux rate (HgF), percentage of organic carbon (%OC), organic carbon flux rate (OCF), and atomic carbon-to-nitrogen ratio (C:N) with sediment core depth (cm). Sediment age was plotted as a secondary axis. Generalized additive models (GAM) were used to model trends in %OC, THg, and C:N with sediment core depth and to identify

statistically significant periods of change, using a gamma error distribution ($k = 5$) and restricted maximum likelihood (REML). To assess the statistical significance of the derivative (the rate of change), first derivatives and estimated simultaneous confidence intervals of the fitted GAM trends were used (Simpson, 2014). The model was fitted using the gam() function (v. 1.2.2) in the mgcv package (v.1.8-42; Wood, 2017) for R (R Core Team, 2023).

4.0 RESULTS

4.1 Goose Lake

There was a steady decline in ^{210}Pb activity from 4 cm core depth until background was reached at 18 cm (Figure 4.1). The peak in ^{137}Cs was observed at 12 cm depth. The earliest date obtained from the CRS chronology was 1927, at 14 cm depth. Sediment accumulation rate steadily increased from the bottom to the surface of the sediment core. The sediment focusing factor was 0.38 (Table 4.1).

A)

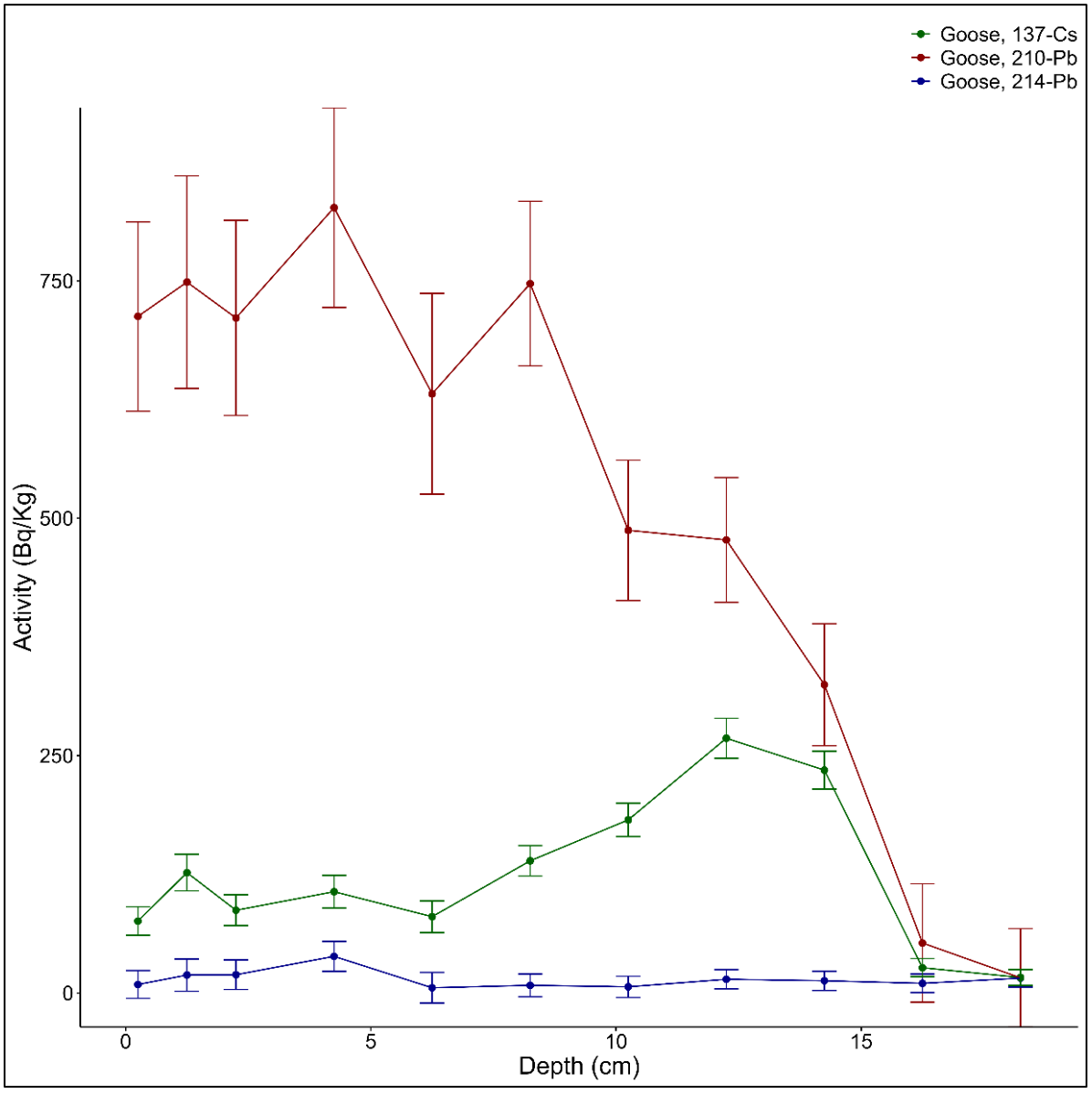

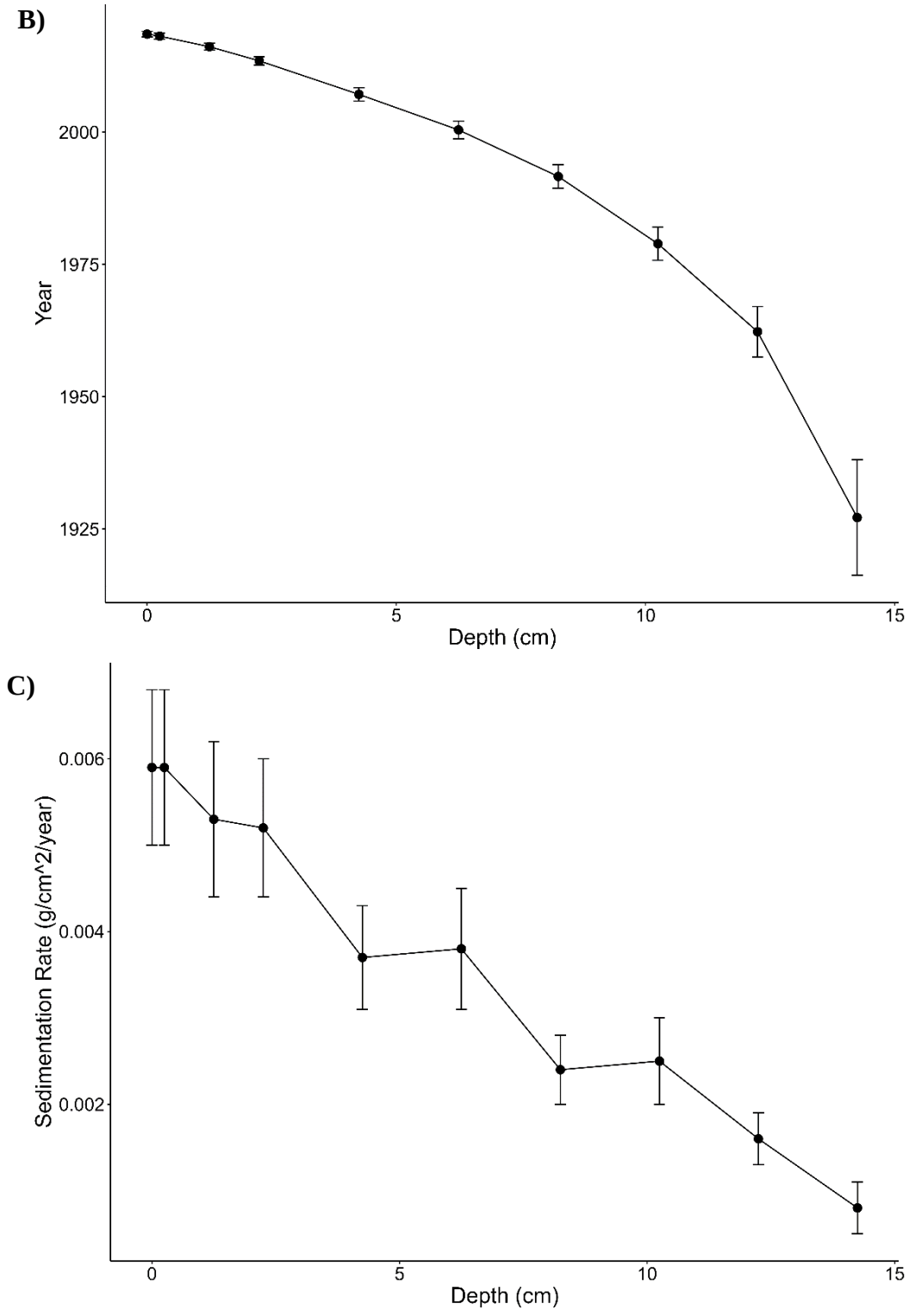

Figure 4.1: Results of ^{210}Pb dating for Goose Lake: (A) sediment depth versus activities for radioisotopes ^{210}Pb, ^{214}Pb and ^{137}Cs, (B) sediment depth versus date based on the constant rate of supply (CRS) ^{210}Pb dating model, and (C) ^{210}Pb-inferred sedimentation rate versus depth based on the CRS model. Error bars are standard error.

The total mercury (THg) concentration was relatively stable throughout the sediment core, except for a notable peak in THg of 180 ng/g at 14 cm (Figure 4.2). There was an increase in the mercury flux rate (HgF) from 6 cm (0.11 ng/cm^{2}yr) to 2 cm (0.17 ng/cm^{2}yr) (Figure 4.3). The average corrected HgF for sediment focusing over the dated portion of the core was 0.27 ± 0.05 ng/cm^{2}yr (Table 4.1). A significant linear decrease (decreasing from ~44% to ~38%) was evident for percent organic carbon (%OC) from the bottom (20 cm) to the surface of the core (Figure 4.2), while the organic carbon flux rate (OCF) increased (Figure 4.3). The average corrected OCF for sediment focusing over the dated portion of the core was 1248.9 ± 643.7 µg/cm^{2}yr (Table 4.1). There was no significant change in C:N, which ranged consistently between 13-14 (Figure 4.2).

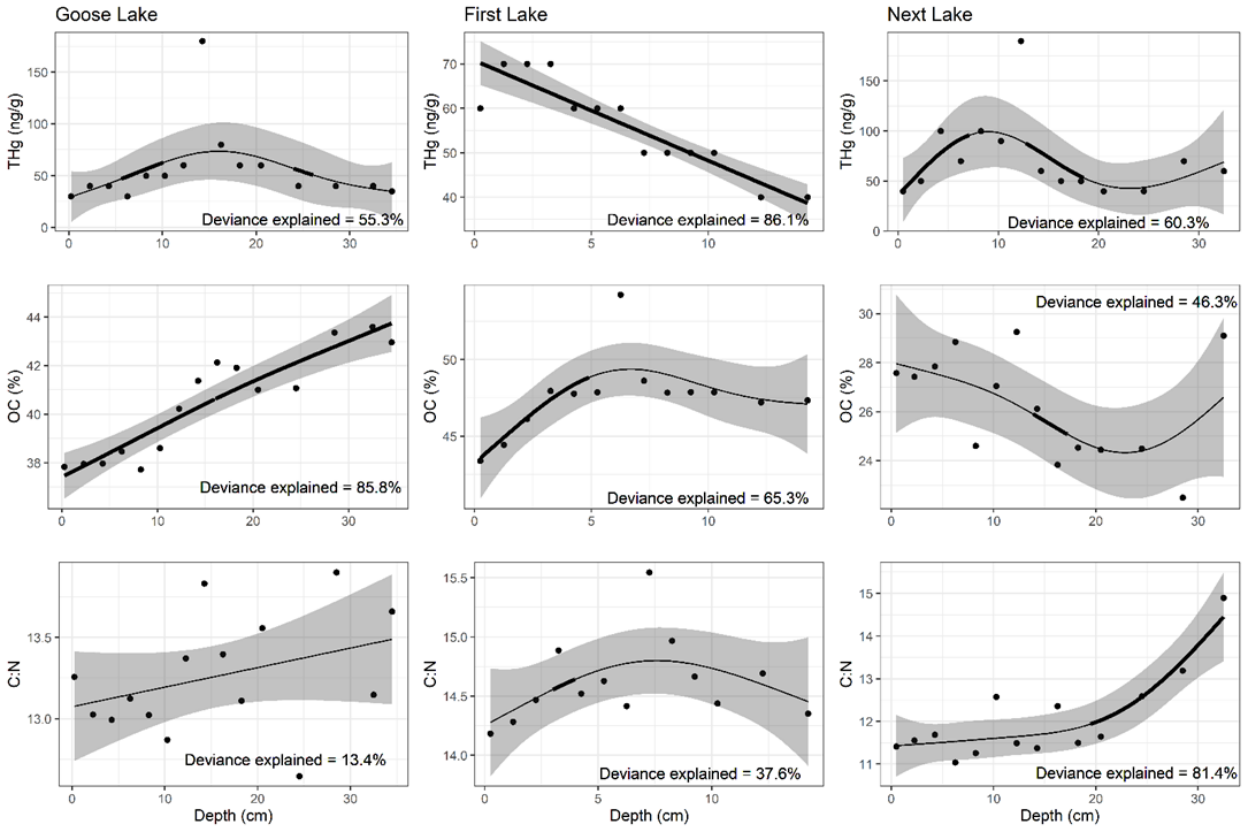

Figure 4.2: Results of the General Additive Models (GAMs) for Goose Lake, First Lake, and Next Lake, showing time series trends for total mercury (THg), the percent organic carbon content (%OC), and the atomic carbon to nitrogen ratio (C:N) plotted against sediment core depth (cm). The % of Deviance

explained from the fitted GAM model is shown. Bold portions represent areas of significant change, while grey shaded areas represent the 95% confidence intervals for the models.

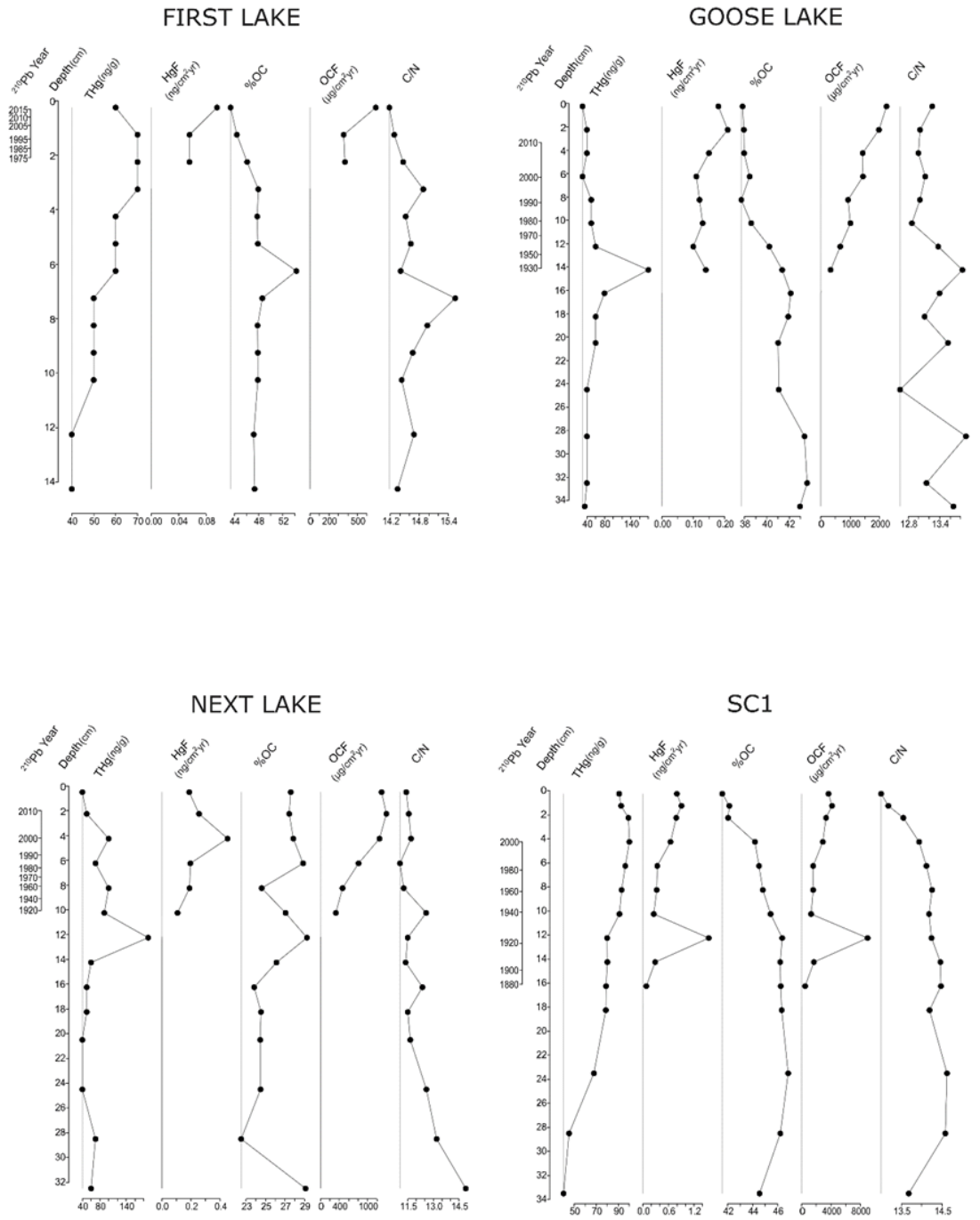

Figure 4.3: Stratigraphic profiles showing changes in total mercury (THg), mercury flux rate (HgF), % organic carbon (%OC), organic carbon flux rate (OCF), and atomic carbon to nitrogen ratio (C:N) with sediment core depth in First Lake, Goose Lake, Next Lake and SC1. The inferred dates based on the ^{210}Pb constant rate of supply model are shown on the left.

4.2 First Lake

There was a steady decline of unsupported ^{210}Pb activity from 1 cm to 6 cm, when background was reached (Figure 4.4). A peak in ^{137}Cs was observed at 1 cm depth. A CRS-based chronology could only be established for top 2 cm, incorporating the time period from ~1970 to 2018 (the year the sediment core was taken). After extrapolation, the earliest date was inferred as ~1847 (at 4.25 cm depth), although extrapolated dates should be interpreted with caution as possible changes in sedimentation rates would create uncertainties. Sedimentation rate was highest in the surface sediments (Figure 4.4). The calculated sediment focusing factor used to correct elemental flux values for sediment focusing was 0.3 (Table 4.1).

A)

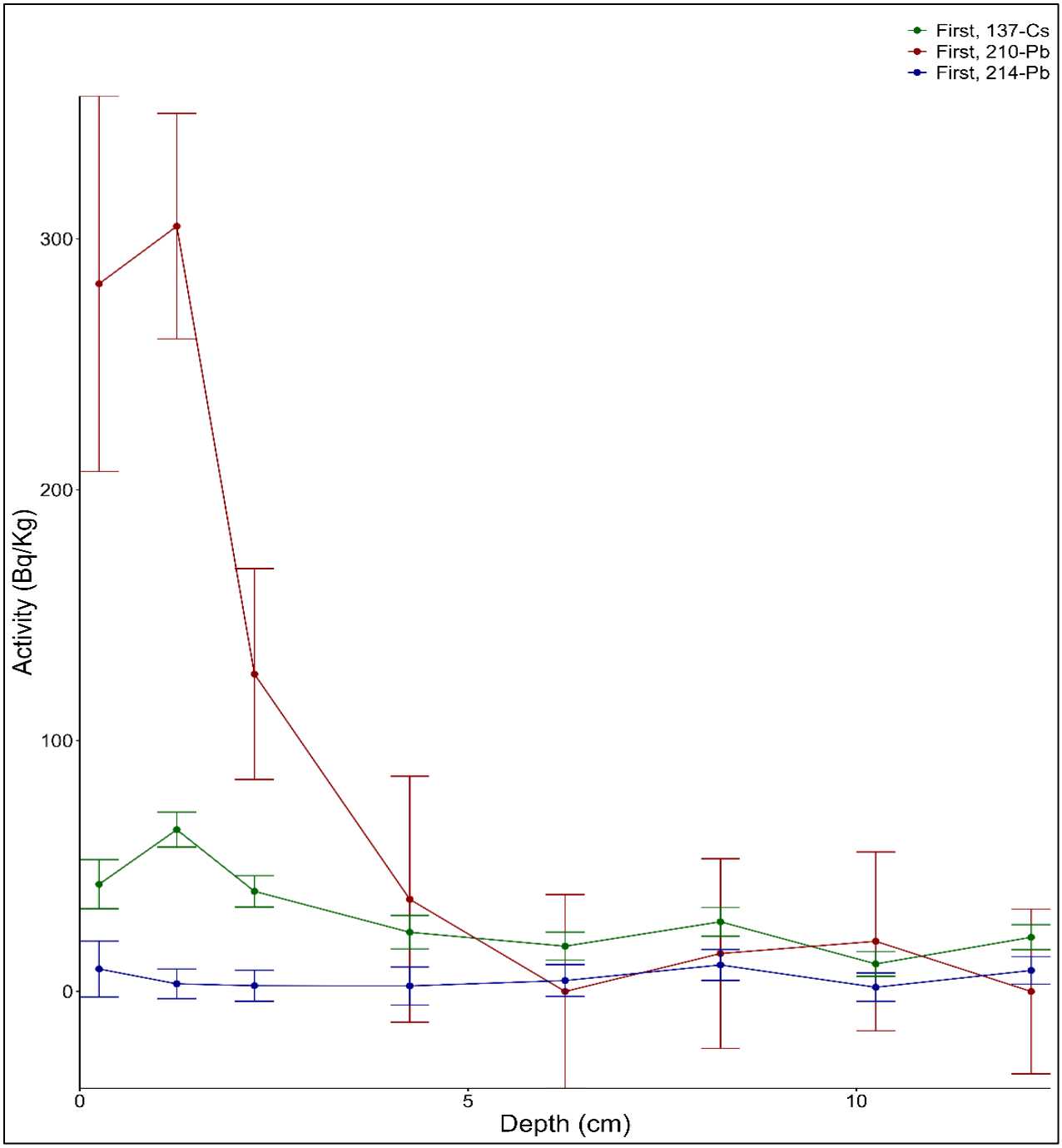
First, 137-Cs
First, 210-Pb
First, 214-Pb
Activity (Bq/Kg)
300
200
100
0
0
5
10
Depth (cm)

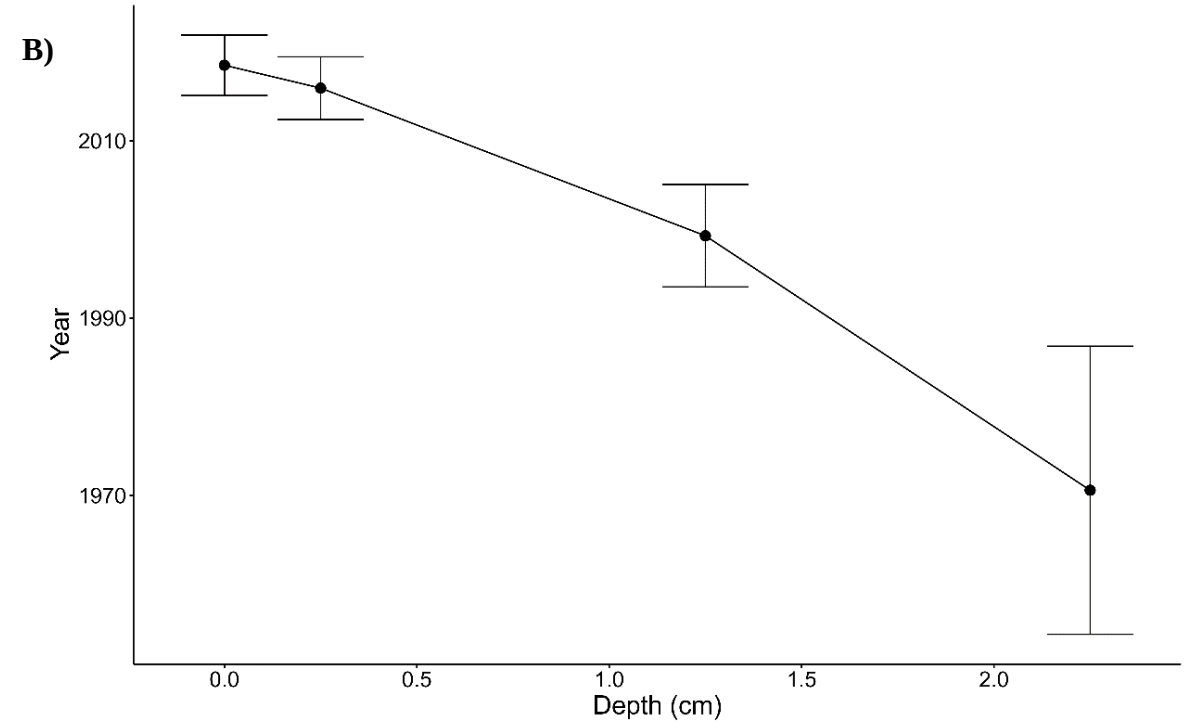

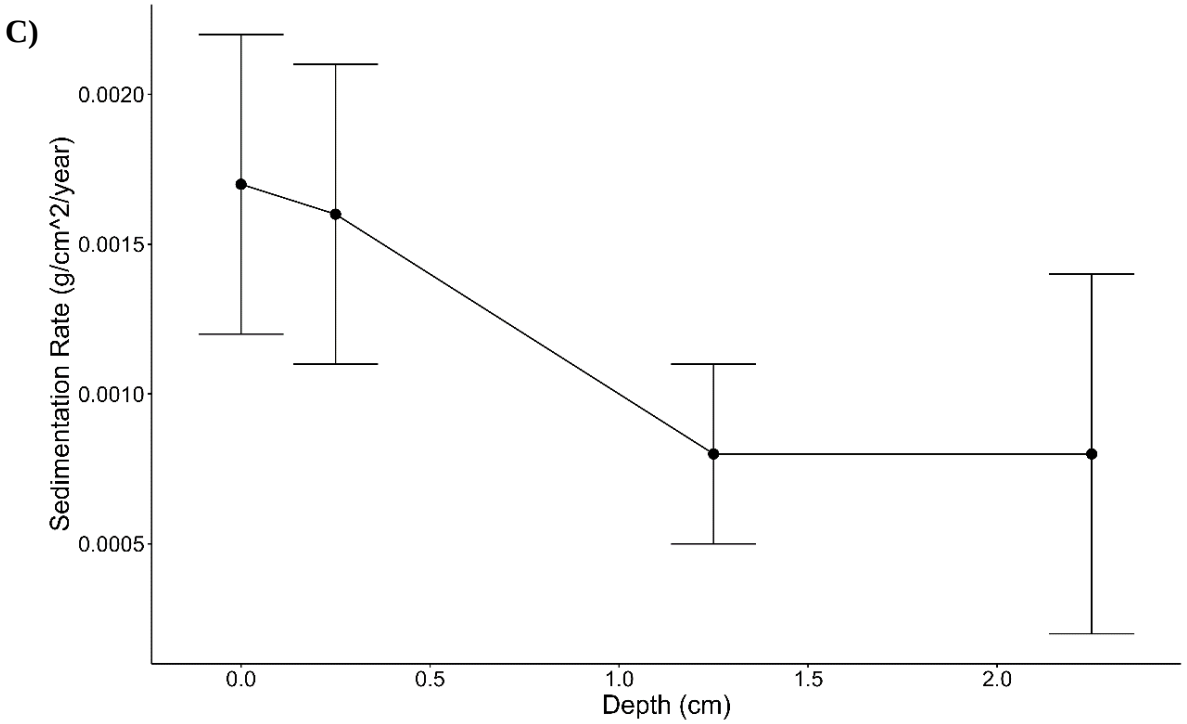

Figure 4.4: Results of ^{210}Pb dating for First Lake: (A) sediment depth versus activities for radioisotopes ^{210}Pb, ^{214}Pb and ^{137}Cs, (B) sediment depth versus date based on the constant rate of supply (CRS) ^{210}Pb dating model, and (C) ^{210}Pb-inferred sedimentation rate versus depth based on the CRS model. Error bars are standard error.

There was a significant linear increase in total mercury (THg) concentrations from the bottom (15 cm) to the surface of the core, increasing from ~60 ng/g to ~70 ng/g (Figure 4.2). An increase in mercury flux rate (HgF) was also observed in the surface sediment interval (Figure 4.3). The average HgF over the dated portion of the core, corrected for sediment focusing, was 0.7 ± 0.3 ng/cm^{2}yr (Table 4.1). There was a significant decline in organic carbon content (%OC) from 5.0 cm depth (~1860) to the core surface, although the magnitude of change was small, decreasing from ~48% to ~43% (Figure 4.2), while organic carbon flux (OCF) increased in the surface sediment interval following the same trend as HgF (Figure 4.3). The average OCF over the dated portion of the core corrected for sediment focusing was 1576.3 ± 639.4 µg/cm^{2}yr (Table 4.1). The C:N ranged consistently between 14-15, with no significant changes over time based on the GAM results (Figure 4.2).

4.3 Next Lake

The ^{210}Pb activity declined steadily with increasing core depth, with background reached at 14 cm (Figure 4.5). A peak of ^{137}Cs was observed at 9 cm. The earliest date obtained from the CRS model was 1838 (at 14.25 cm depth). Sedimentation rate increased steadily from 10.75 cm to 2.75 cm (~1915-2008), with a slight decrease recorded at 1.75 cm (~2013). The calculated sediment focusing factor used to correct elemental flux values for sediment focusing was 0.4 (Table 4.1).

A)

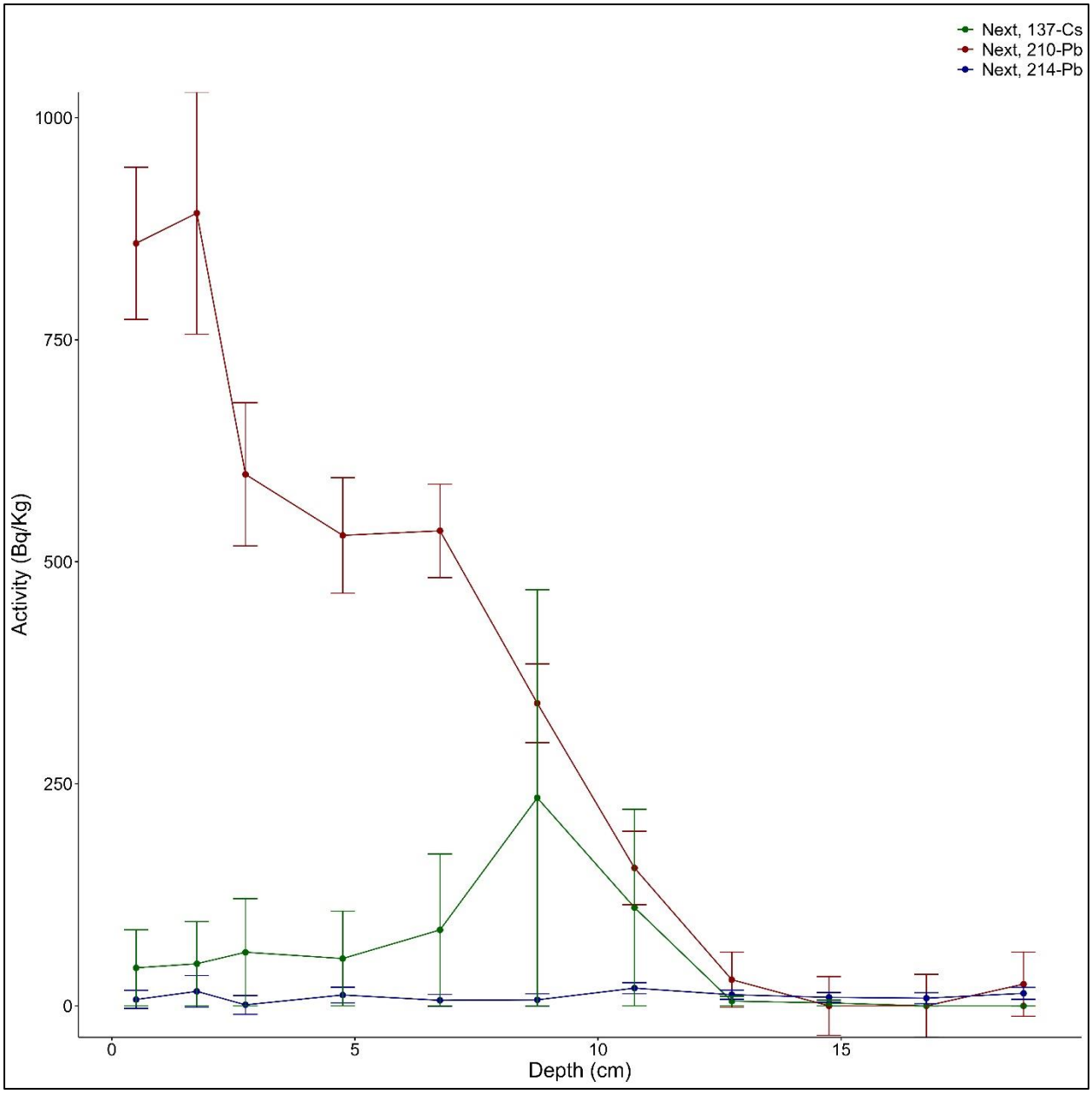
Next, 137-Cs
Next, 210-Pb
Next, 214-Pb
1000
750
500
250
0
Activity (Bq/Kg)
0
5
10
15
Depth (cm)

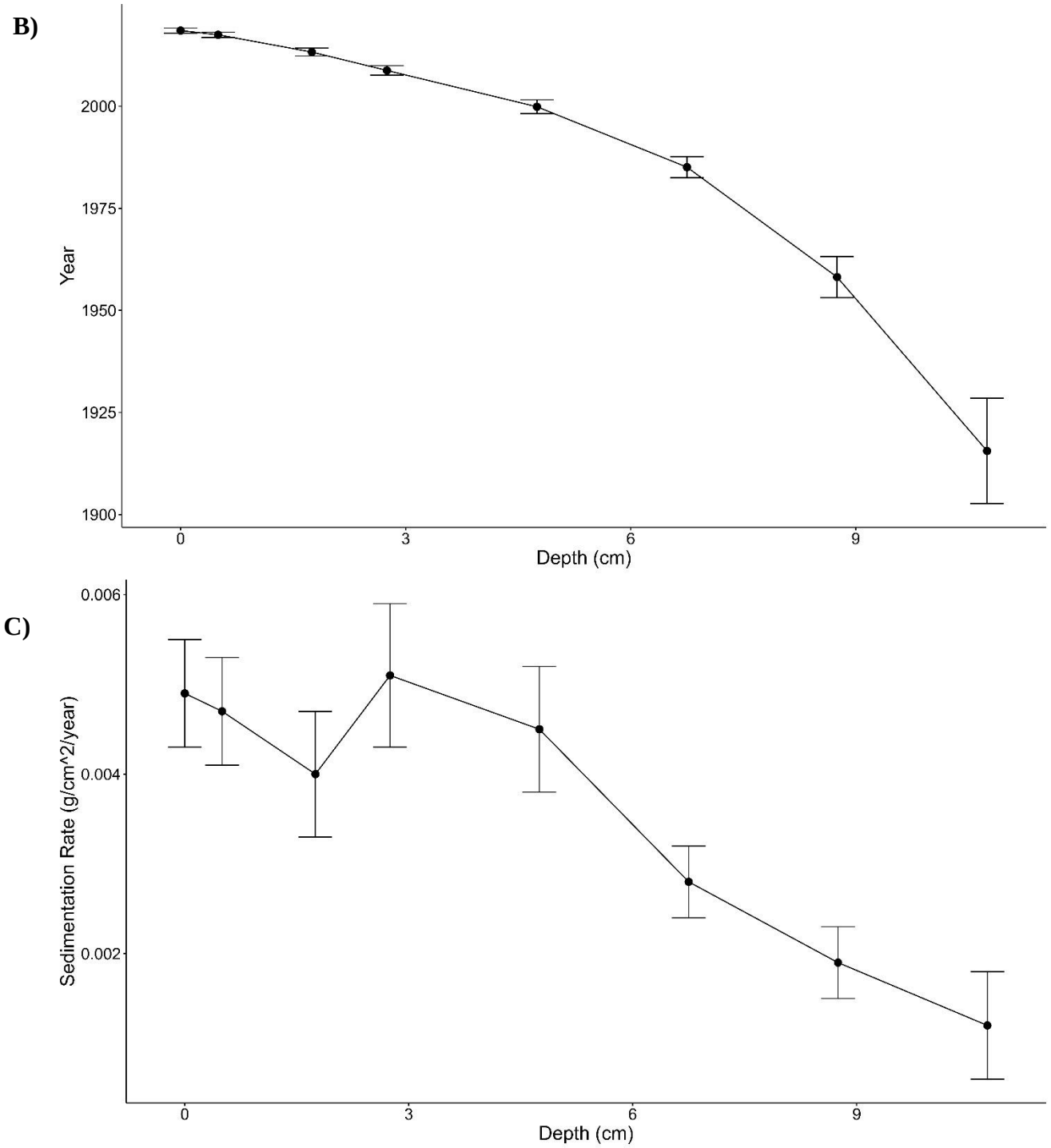

Figure 4.5: Results of ^{210}Pb dating for Next Lake: (A) sediment depth versus activities for radioisotopes ^{210}Pb, ^{214}Pb and ^{137}Cs, (B) sediment depth versus date based on the constant rate of supply (CRS) ^{210}Pb dating model, and (C) ^{210}Pb-inferred sedimentation rate versus depth based on the CRS model. Error bars are standard error.

There was a significant increase in THg from 18 cm to 12 cm (50 ng/g to 190 ng/g), followed by a significant decrease (~100 ng/g to 40 ng/g) from ~8 cm (~1960) to 0 cm (~2018) core depth (Figure 4.2). A peak in THg of 190 ng/g was observed at ~12 cm (Figure 4.2). A peak in HgF was recorded at ~4 cm depth (0.5 ng/cm^{2}yr) (Figure 4.3). The average HgF over the dated portion of the core, corrected for sediment focusing, was 0.44±0.08 ng/cm^{2}yr (Table 4.1). The %OC consistently ranged from 24-30%, with no significant changes identified by the GAM (Figure 4.2). The OCF increased from ~10 cm (324.6 µg/cm^{2}yr) to 0 cm (1296.26 µg/cm^{2}yr) core depth (Figure 4.3). The average OCF over the dated portion of the core, corrected for sediment focusing, was 2311.8 ± 1147.7 µg/cm^{2}yr (Table 4.1). There was a significant decrease in C:N content from 14.9 to 11.6 between from 32.5 and 20.5 cm (Figure 4.2).

4.4 SC-1

There was a steady decline in ^{210}Pb activity with increasing depth of the sediment profile and background was reached at 12 cm (Figure 4.6). An increase in ^{137}Cs is observed at 12 cm. The earliest date obtained from CRS chronology was ~1854 at 18.25 cm depth (Figure 4.6). There was a notable peak in sedimentation rate of 0.02 g/cm^2/yr recorded at 12 cm depth (~1920) (Figure 4.4). The calculated sediment focusing factor used to correct elemental flux values for sediment focusing was 0.05 (Table 4.1).

A)

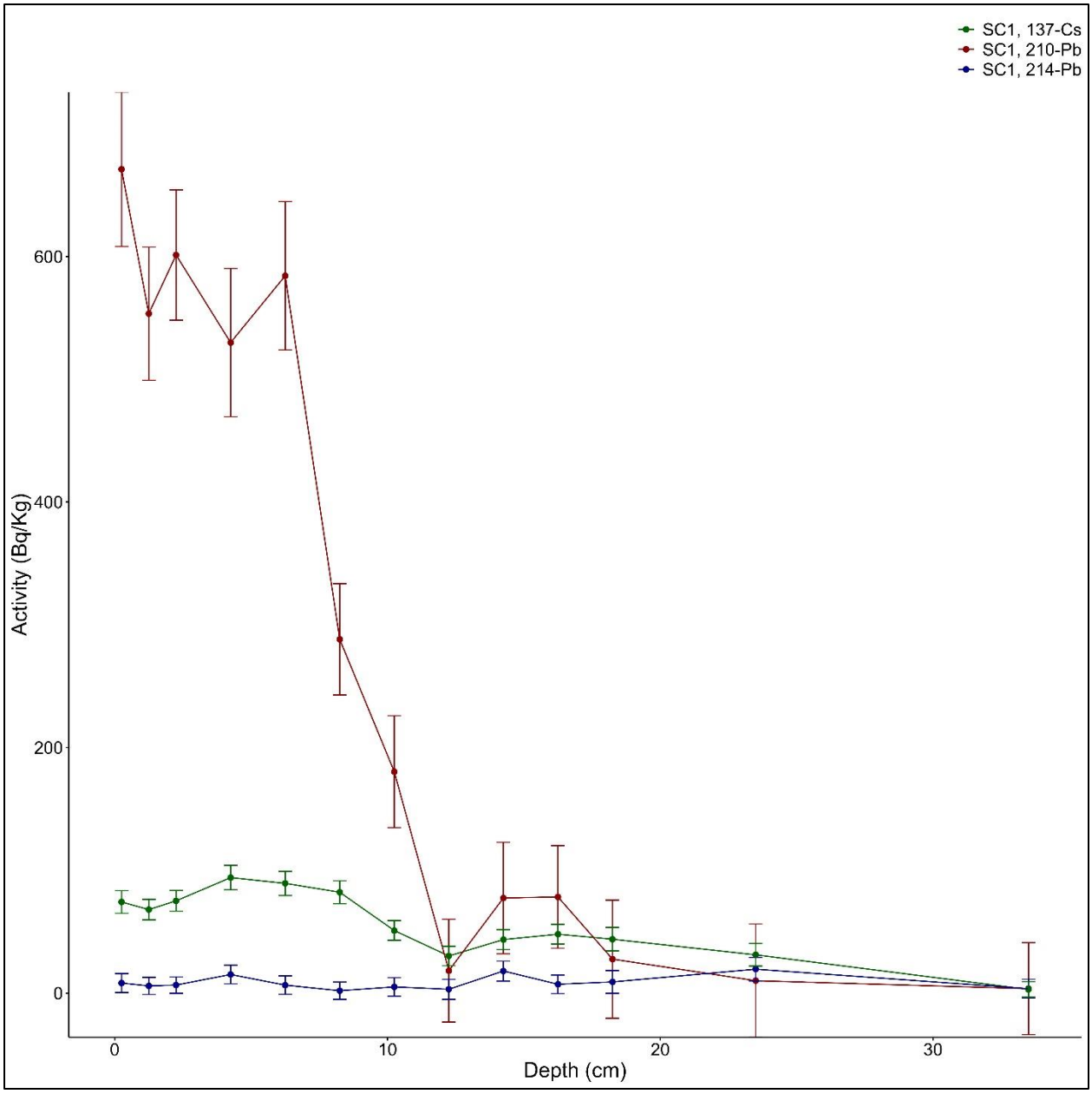
SC1, 137-Cs
SC1, 210-Pb
SC1, 214-Pb
Activity (Bq/Kg)
0
200
400
600
0
10
20
30
Depth (cm)

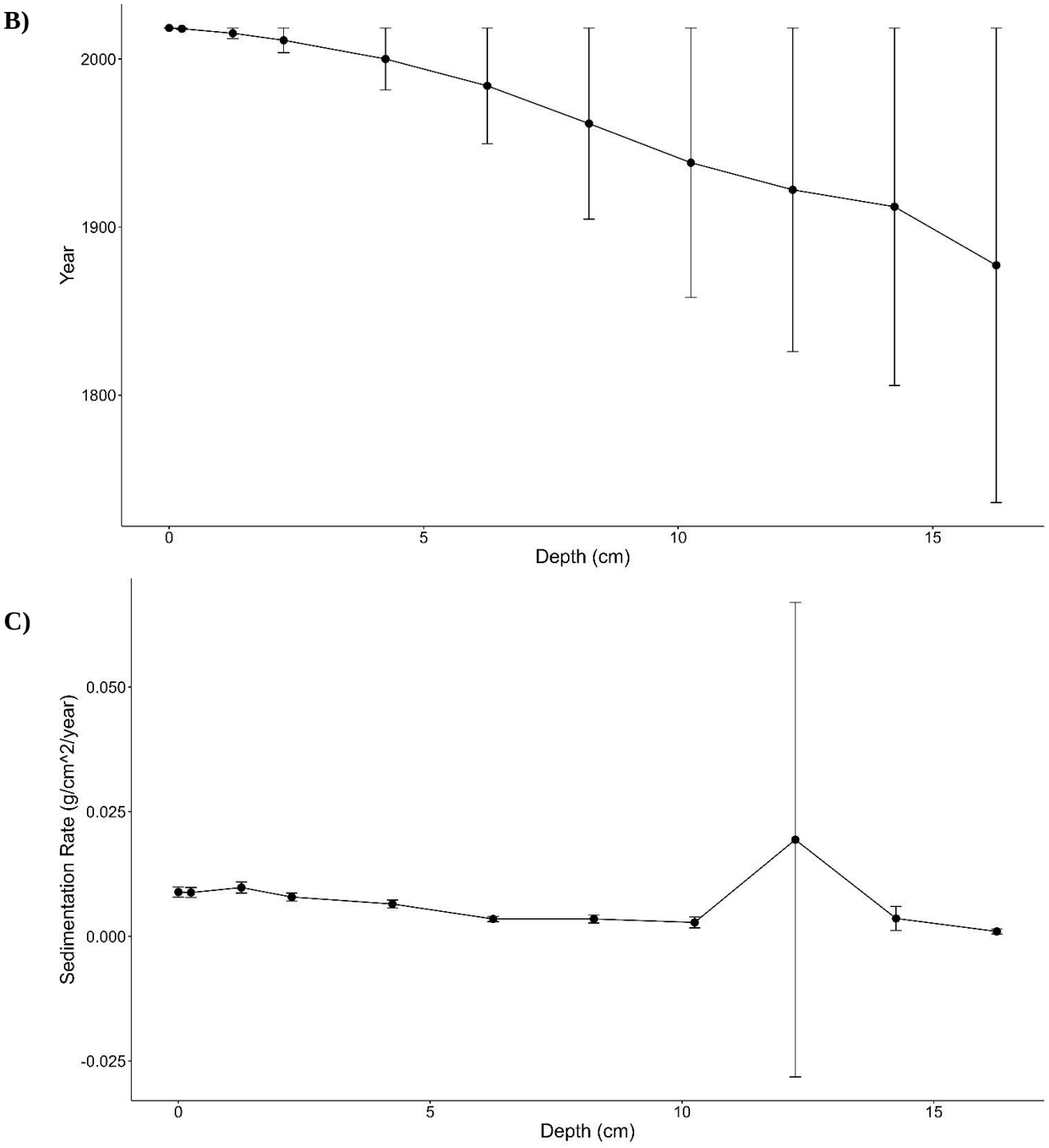

Figure 4.6: Results of ^{210}Pb dating for Lake SC-1: (A) sediment depth versus activities for radioisotopes ^{210}Pb, ^{214}Pb and ^{137}Cs, (B) sediment depth versus date based on the constant rate of supply (CRS) ^{210}Pb dating model, and (C) ^{210}Pb-inferred sedimentation rate versus depth based on the CRS model. Error bars are standard error.

A significant increase in THg concentration from 40.4 ng/g to ~ 98 ng/g was observed between 33.5 cm and 5 cm core depth (Figure 4.7). HgF increased steadily over time, and there was also a peak at ~12.5 cm depth corresponding to the peak in inferred sedimentation rate (Figure 4.3.1). The average corrected HgF for sediment focusing over the dated portion of the core was 0.81 ± 0.6 ng/cm^{2}yr (Table 4.1). There was a significant (but of small magnitude) increase in %OC from 44.5% to 46.8% between 33.5 cm to 24 cm, followed by a significant (but small magnitude) decline from 46.3% to 41.6% between 18 cm and the core surface (Figure 4.7). The OCF increased gradually from 16 cm (462.5 µg/cm^{2}yr) to the core surface (3658.16 µg/cm^{2}yr), with a peak observed at ~12.5 cm depth (8995.8 µg/cm^{2}yr) corresponding to the peak in inferred sedimentation rate and THg flux (Figure 4.3). The average corrected OCF for sediment focusing over the dated portion of the core was 58,999.4 ± 48,574.8 µg/cm^{2}yr (Table 4.1). A significant declining trend in C:N was recorded from 10 cm (14.2) to 0 cm (13.0). C:N was also lower (13.5) in the bottom sediment interval (Figure 4.7).

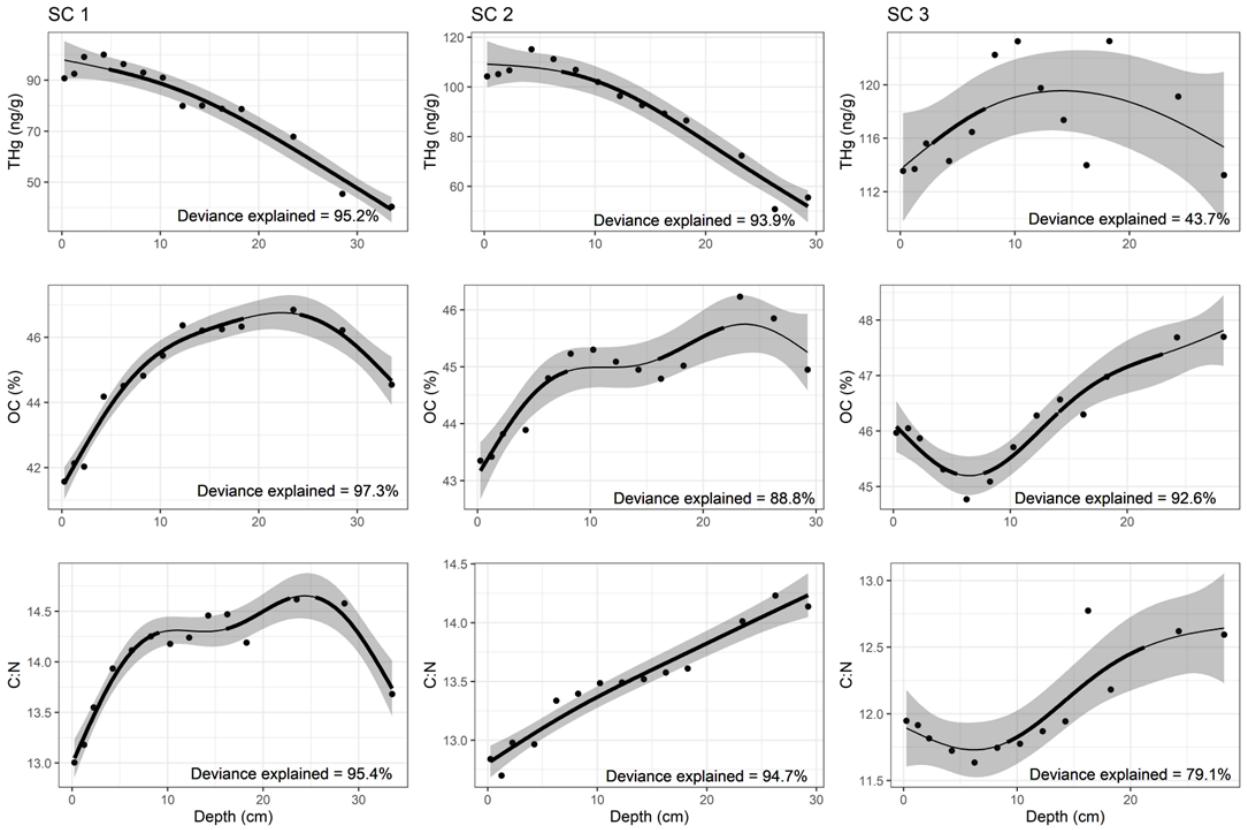

Figure 4.7: Results of the General Additive Models (GAMs) for SC1, SC2 and SC3, showing time series trends for total mercury (THg), the percent organic carbon content (%OC), and the atomic carbon to nitrogen ratio (C:N) plotted against sediment core depth (cm). The % of Deviance explained from the fitted GAM model is shown. Bold portions represent areas of significant change, while grey shaded areas represent the 95% confidence intervals for the models.

4.5 SC-2

There was a steady decline of ^{210}Pb activity with increasing depth of the sediment profile and background was reached at 10 cm depth (Figure 4.8). There was no distinct peak in ^{137}Cs. The earliest date obtained from CRS chronology is 1845, at 17.25 cm depth (Figure 4.8). Sedimentation rate generally increased towards the surface of the core, with a notable peak in sedimentation rate at 10 cm depth (~1940) (Figure 4.1.5c). The calculated sediment focusing factor used to correct elemental flux values for sediment focusing was 0.52 (Table 4.1).

A)

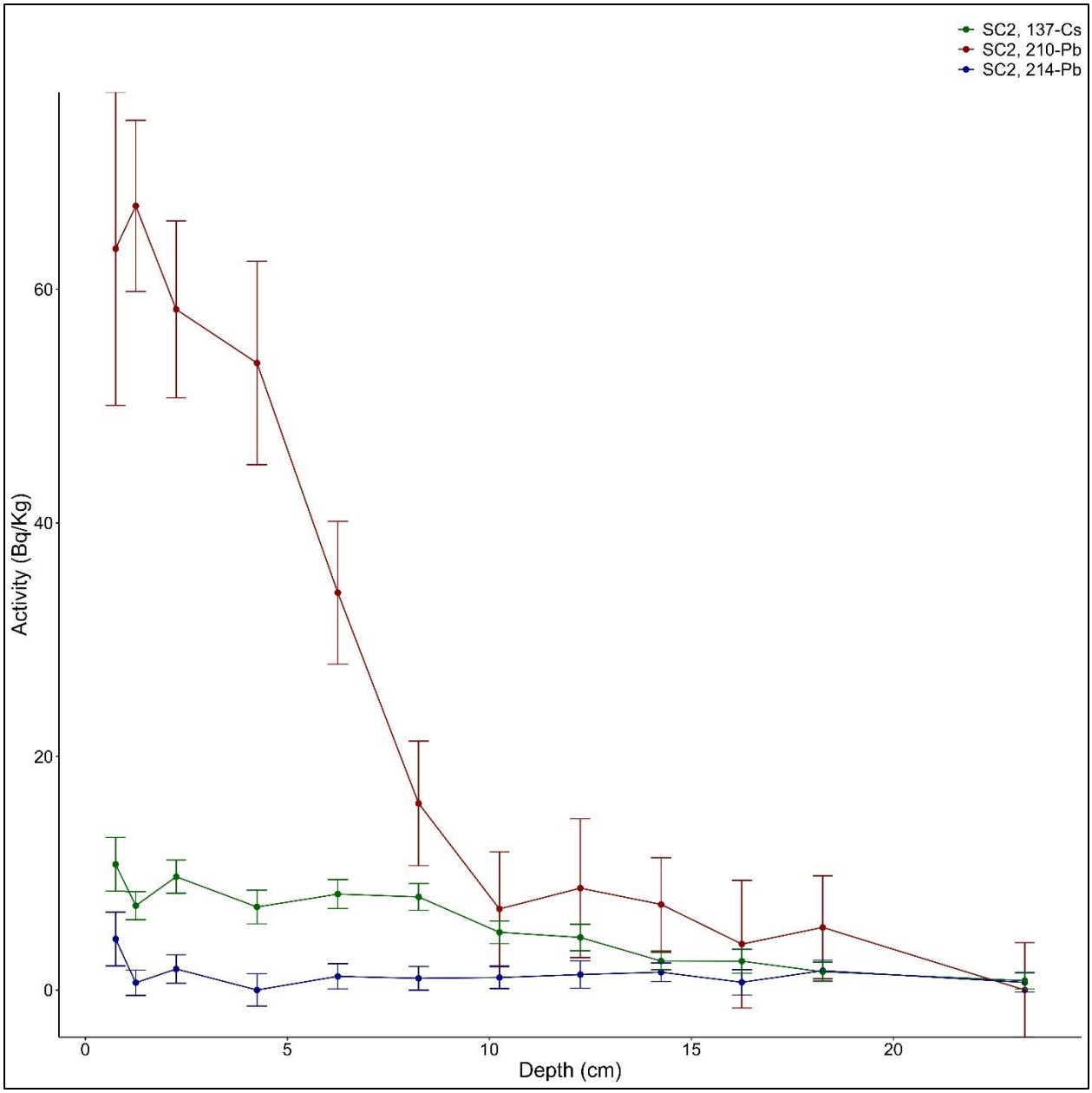
SC2, 137-Cs
SC2, 210-Pb
SC2, 214-Pb
Activity (Bq/Kg)
0
20
40
60
0
5
10
15
20
Depth (cm)

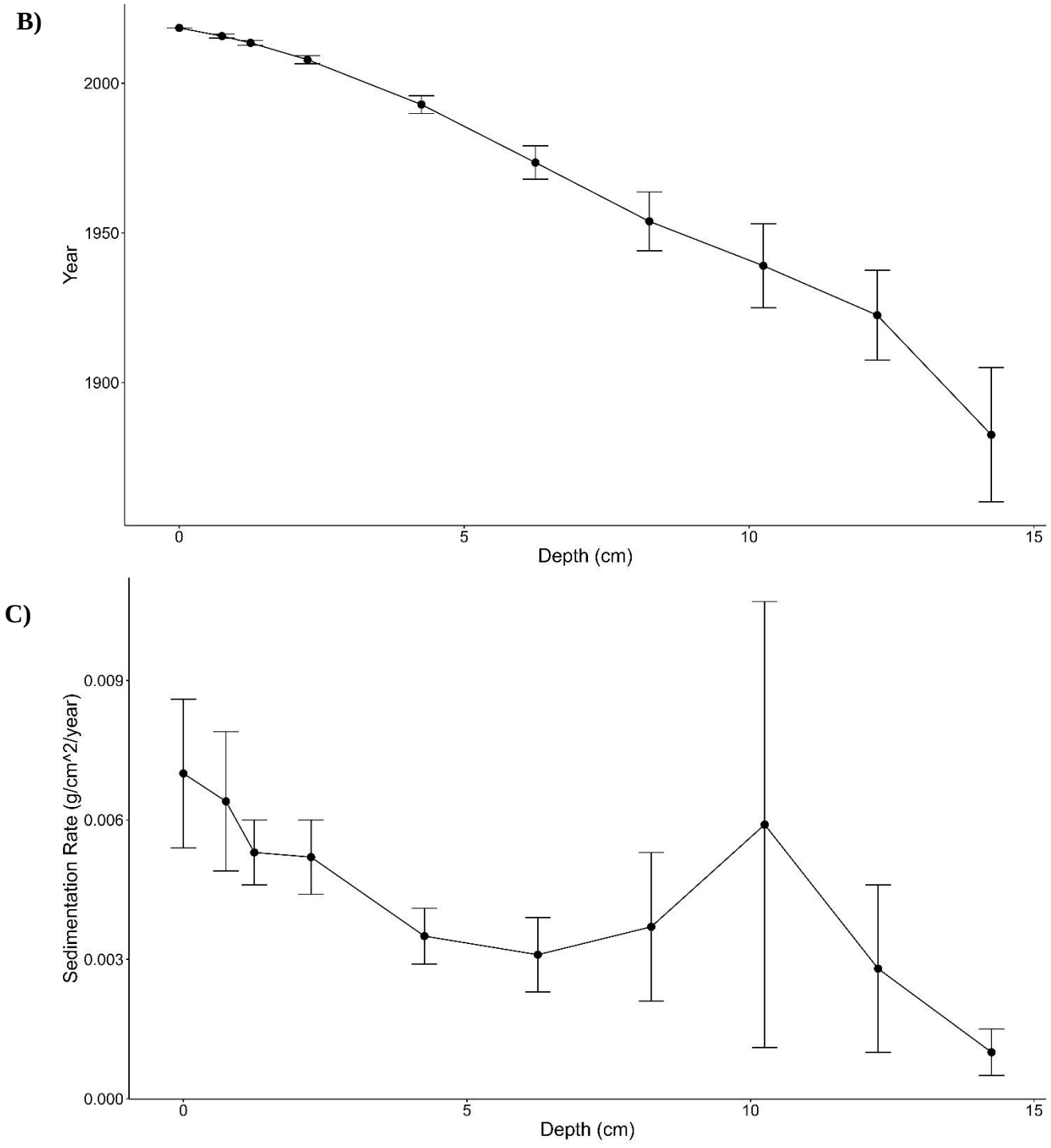

Figure 4.8: Results of ^{210}Pb dating for Lake SC-2: (A) sediment depth versus activities for radioisotopes ^{210}Pb, ^{214}Pb and ^{137}Cs, (B) sediment depth versus date based on the constant rate of supply (CRS) ^{210}Pb dating model, and (C) ^{210}Pb-inferred sedimentation rate versus depth based on the CRS model. Error bars are standard error.

A significant increase in THg was observed from 29 cm to 6 cm core depth, increasing from ~55.5 ng/g to ~ 111.2 ng/g (Figure 4.7), and HgF also increased steadily over time with a peak at 10 cm depth (~1940) corresponding to the peak in sedimentation rate (Figure 4.9). The average HgF corrected for focusing factor was 8.4 ± 2.9 ng/cm^{2}yr, which was the highest average corrected HgF recorded across all study lakes (Table 4.1). A significant but small magnitude decline in %OC was observed between 23 and 16.5 cm, decreasing from 46.2 to 44.8% (Figure 4.7). OCF followed the same trend as observed for inferred sedimentation rate and HgF (Figure 4.9). The average OCF over the dated portion of the core, corrected for sediment focusing, was 3490.9 ± 1451.4 µg/cm^{2}yr (Table 4.1). There was a significant linear decline in C:N from 14.1 to 12.8 from 29 cm to the core surface (Figure 4.7).

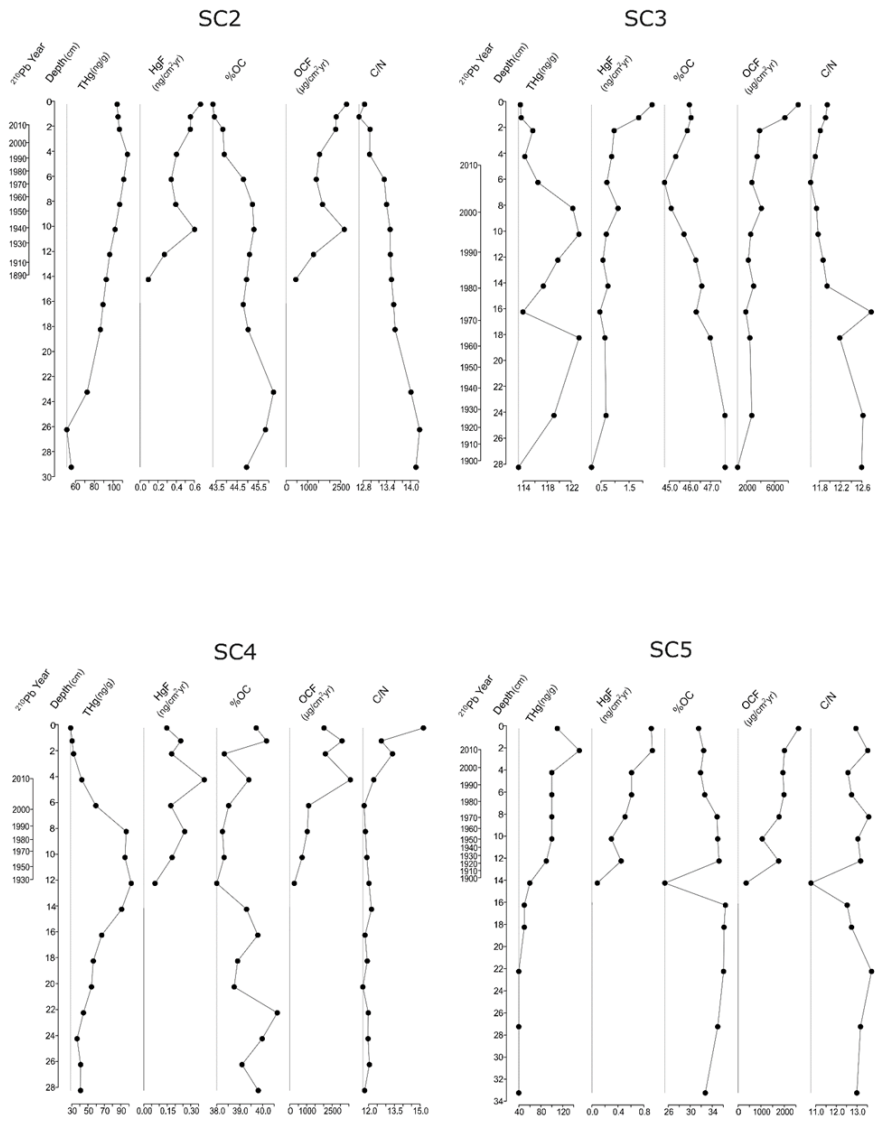

Figure 4.9: Stratigraphic profiles showing changes in total mercury (THg), mercury flux rate (HgF), % organic carbon (%OC), organic carbon flux rate (OCF), and atomic carbon to nitrogen ratio (C:N) with sediment core depth in SC2, SC3, SC4 and SC5. The inferred dates based on the ^{210}Pb constant rate of supply model are shown on the left.

4.6 SC-3

There was a general increase in ^{210}Pb activity from 25 cm to 6 cm, followed by a decline in the top 2 cm, with ^{210}Pb background reached at 24.5 cm (Figure 4.10). A peak of ^{137}Cs was observed at 21 cm depth, which dates to 1945 based on the CRS model for ^{210}Pb, and does not coincide with the 1963 background level (Figure 4.10). The earliest date obtained from CRS

chronology was ~1891, at 29.0 cm depth (Figure 4.10). There was an increase in sedimentation rate in the surface 2.0 cm (Figure 4.10). The calculated sediment focusing factor used to correct elemental flux values for sediment focusing was 0.06 (Table 4.1).

A)

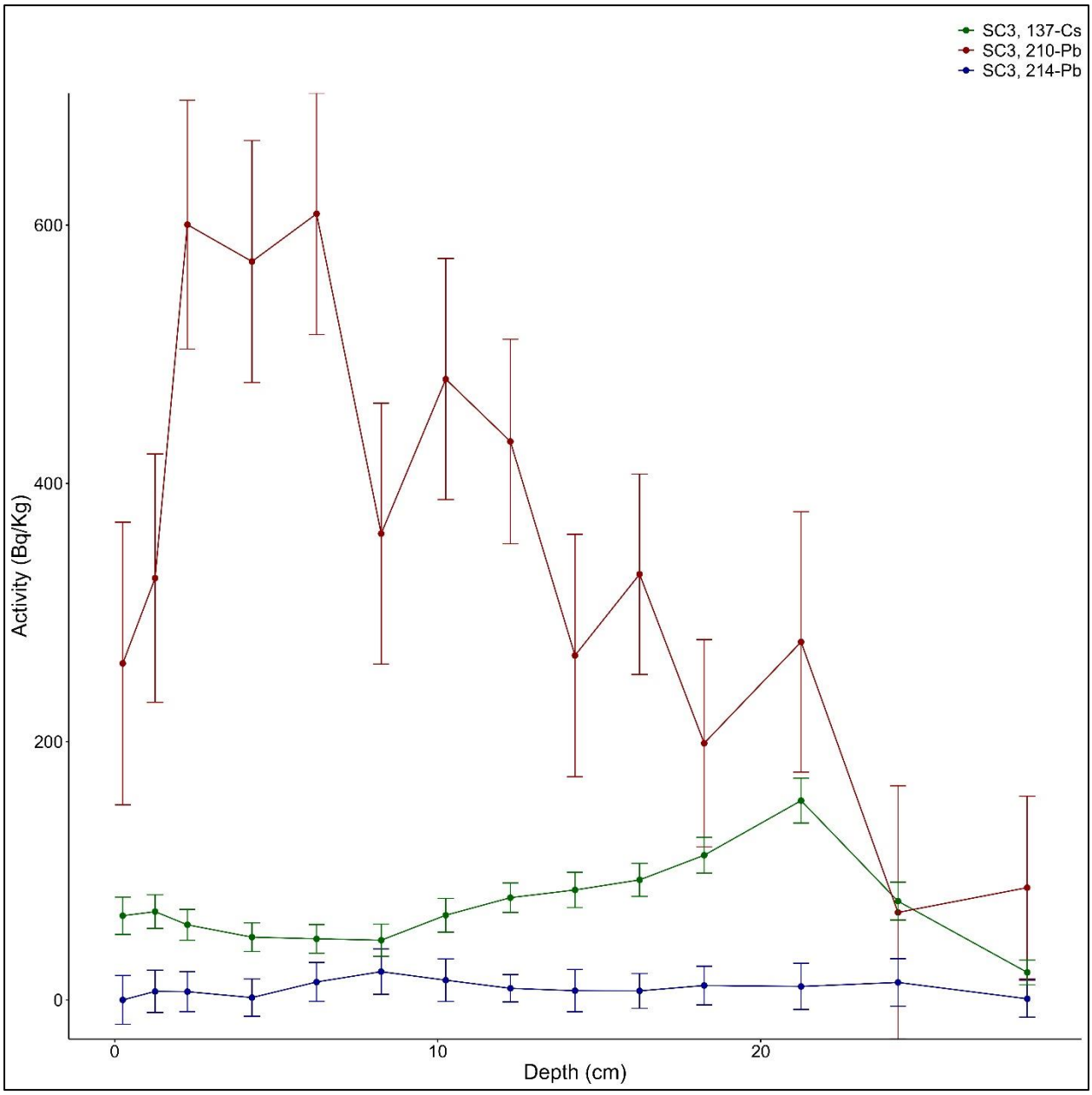

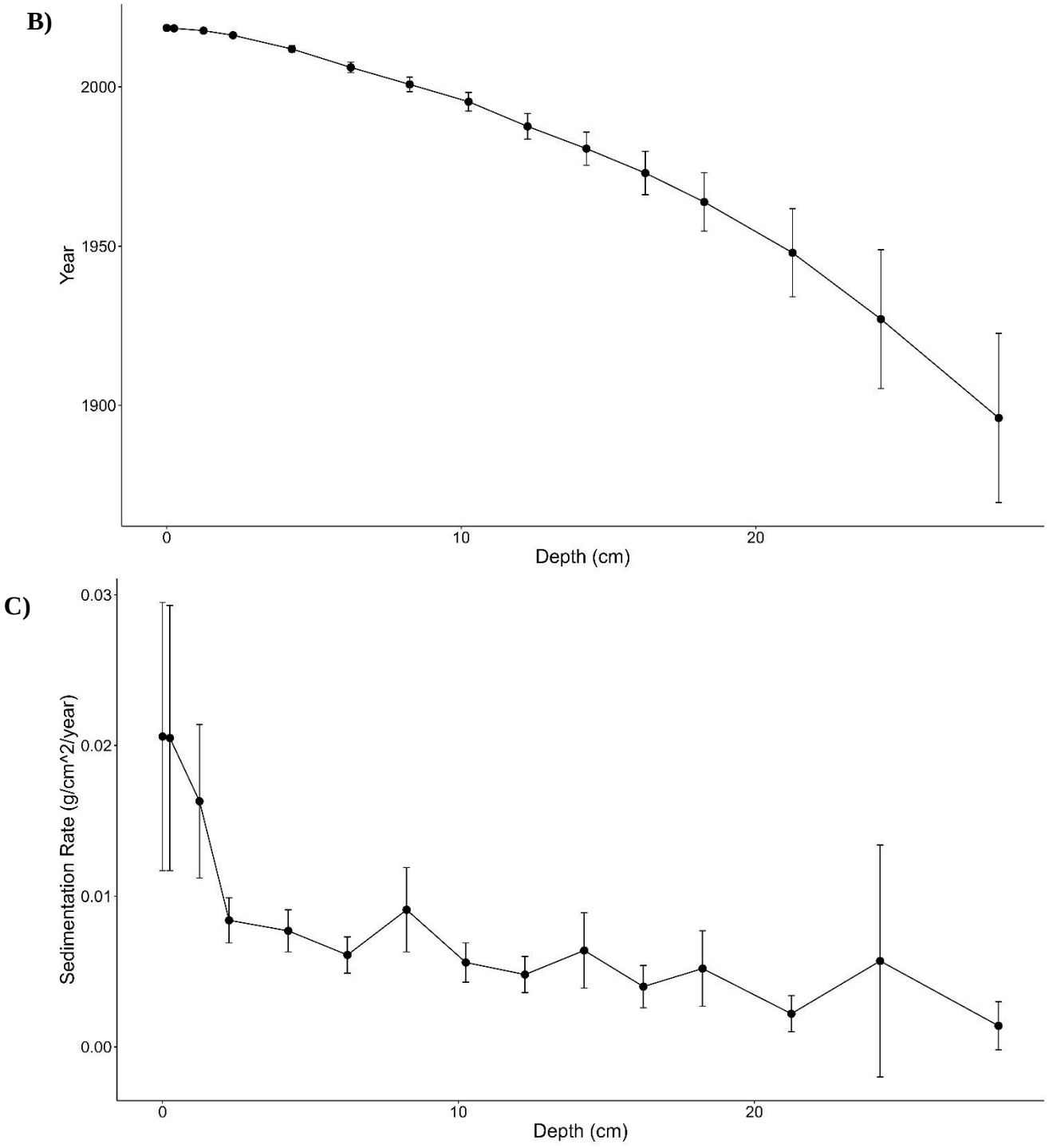

Figure 4.10: Results of ^{210}Pb dating for Lake SC-3: (A) sediment depth versus activities for radioisotopes ^{210}Pb, ^{214}Pb and ^{137}Cs, (B) sediment depth versus date based on the constant rate of supply (CRS) ^{210}Pb dating model, and (C) ^{210}Pb-inferred sedimentation rate versus depth based on the CRS model. Error bars are standard error.

THg was generally consistent over time, ranging between ~112 and ~125 ng/g (Figure 4.7). HgF increased above 2.0 cm, corresponding to the increase in inferred sedimentation rate (Figure 4.9). The average HgF over the dated portion of the core, corrected for sediment focusing, was 1.35 ± 0.52 ng/cm^{2}yr (Table 4.1). A significant (but small magnitude) decrease in %OC (47.7% to 45.1%) was observed between 24 cm and 8 cm, followed by a significant (but small) increase above 6 cm from 44.8 to 46.0% (Figure 4.7). OCF increased in the surface 2.0 cm from 7506.2 µg/cm^{2}yr to 9423.8 µg/cm^{2}yr, similar to HgF (Figure 4.9). The average OCF corrected for sediment focussing factor was 59678.0 ± 39496.5 µg/cm^{2}yr, which was the highest corrected OCF of all study lakes (Table 4.1). There was a significant decline in C:N from 21 cm (~12.3) to 9 cm (~11.8) (Figure 4.7).

4.7 SC-4

^{210}Pb activity was variable in the top 6 cm of the sediment core. A decline in ^{210}Pb activity was observed with increasing depth between 6 cm and 14.5 cm, when background was reached (Figure 4.11). The peak in ^{137}Cs was observed at 5-6 cm depth. The earliest date obtained from CRS chronology was ~1847 at 16.25 cm depth (Figure 4.11). Sedimentation rate was highest in the top 5 cm (Figure 4.11). The calculated sediment focusing factor used to correct elemental flux values for sediment focusing was 0.74 (Table 4.1).

A)

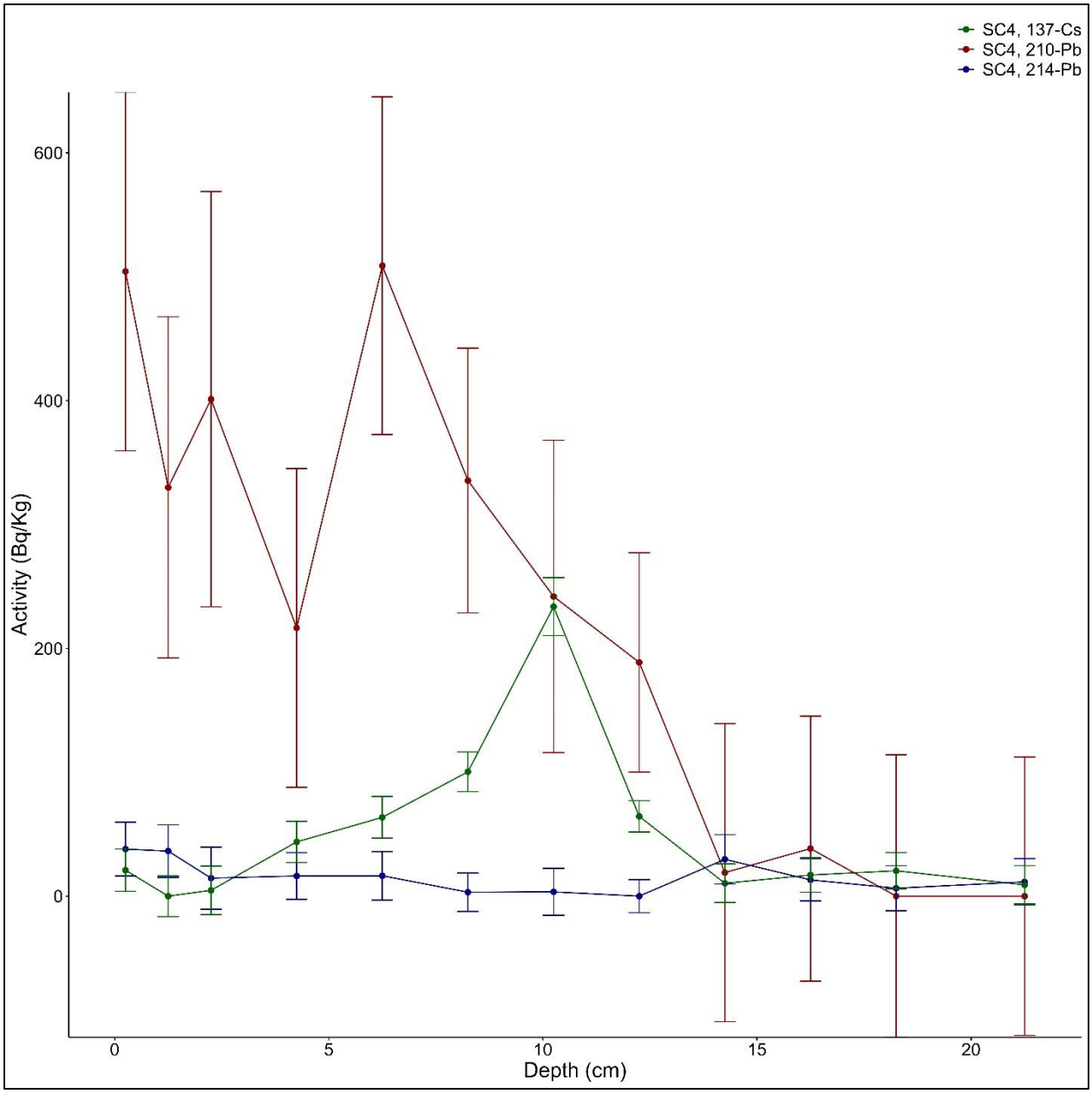
SC4, 137-Cs
SC4, 210-Pb
SC4, 214-Pb
600
400
200
0
Activity (Bq/Kg)
0
5
10
15
20
Depth (cm)

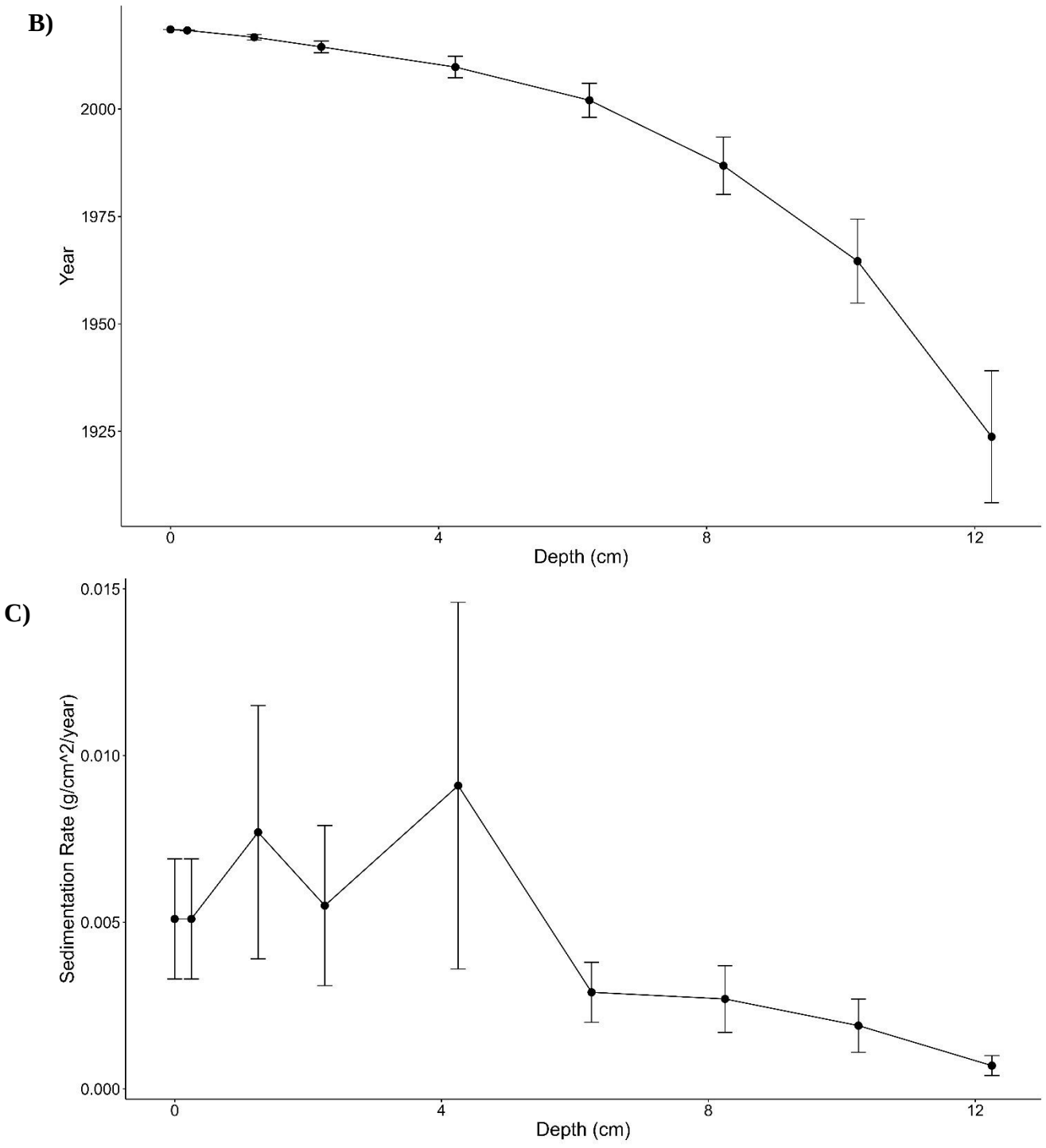

Figure 4.11: Results of ^{210}Pb dating for Lake SC-4: (A) sediment depth versus activities for radioisotopes ^{210}Pb, ^{214}Pb and ^{137}Cs, (B) sediment depth versus date based on the constant rate of supply (CRS) ^{210}Pb dating model, and (C) ^{210}Pb-inferred sedimentation rate versus depth based on the CRS model. Error bars are standard error.

There was a significant increase in THg observed from 24 cm (36.7 ng/g) to 14 cm (91.1 ng/g), followed by a significant decline in THg concentration from ~12.5 cm (102.8 ng/g) to the core surface (28.8 ng/g) (Figure 4.12). HgF increased to 4 cm and then decreased to the core surface (Figure 4.9). The average HgF corrected for sediment focusing was 0.68 ± 0.31 ng/cm^{2}yr (Table 4.1). The %OC was consistently ~38-40% over the entire core, with no changes over time (Figure 4.12). OCF followed the same trend as HgF (Figure 4.9). The average OCF corrected for sediment focusing was 2357.5 ± 1577.4 µg/cm^{2}yr (Table 4.1). C:N increased significantly from 11.8 to 15.1 in the top 8 cm (Figure 4.12).

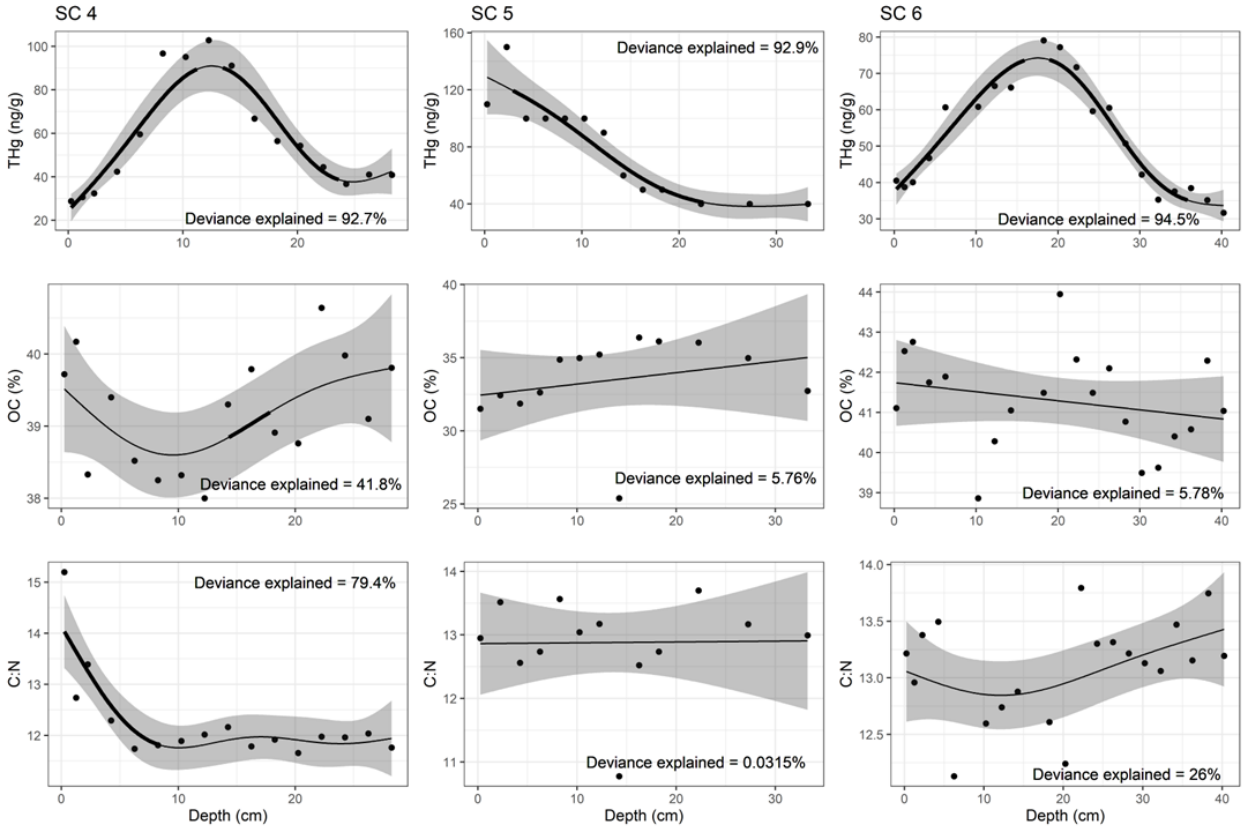

Figure 4.12: Results of the General Additive Models (GAMs) for SC4, SC5 and SC6, showing time series trends for total mercury (THg), the percent organic carbon content (%OC), and the atomic carbon to nitrogen ratio (C:N) plotted against sediment core depth (cm). The % of Deviance explained from the fitted GAM model is shown. Bold portions represent areas of significant change, while grey shaded areas represent the 95% confidence intervals for the models.

4.8 SC-5

There was a steady decline in ^{210}Pb activity observed from 1.5 cm to 16 cm, when background was reached (Figure 4.13). A peak in ^{137}Cs activity was observed at 8 cm depth (Figure 4.13). The earliest date obtained from CRS chronology was ~1845, at 17 cm depth (Figure 4.13). Sedimentation rate generally increased from the bottom to the surface of the core (Figure 4.13). The calculated sediment focusing factor used to correct elemental flux values for sediment focusing was 0.67 (Table 4.1).

A)

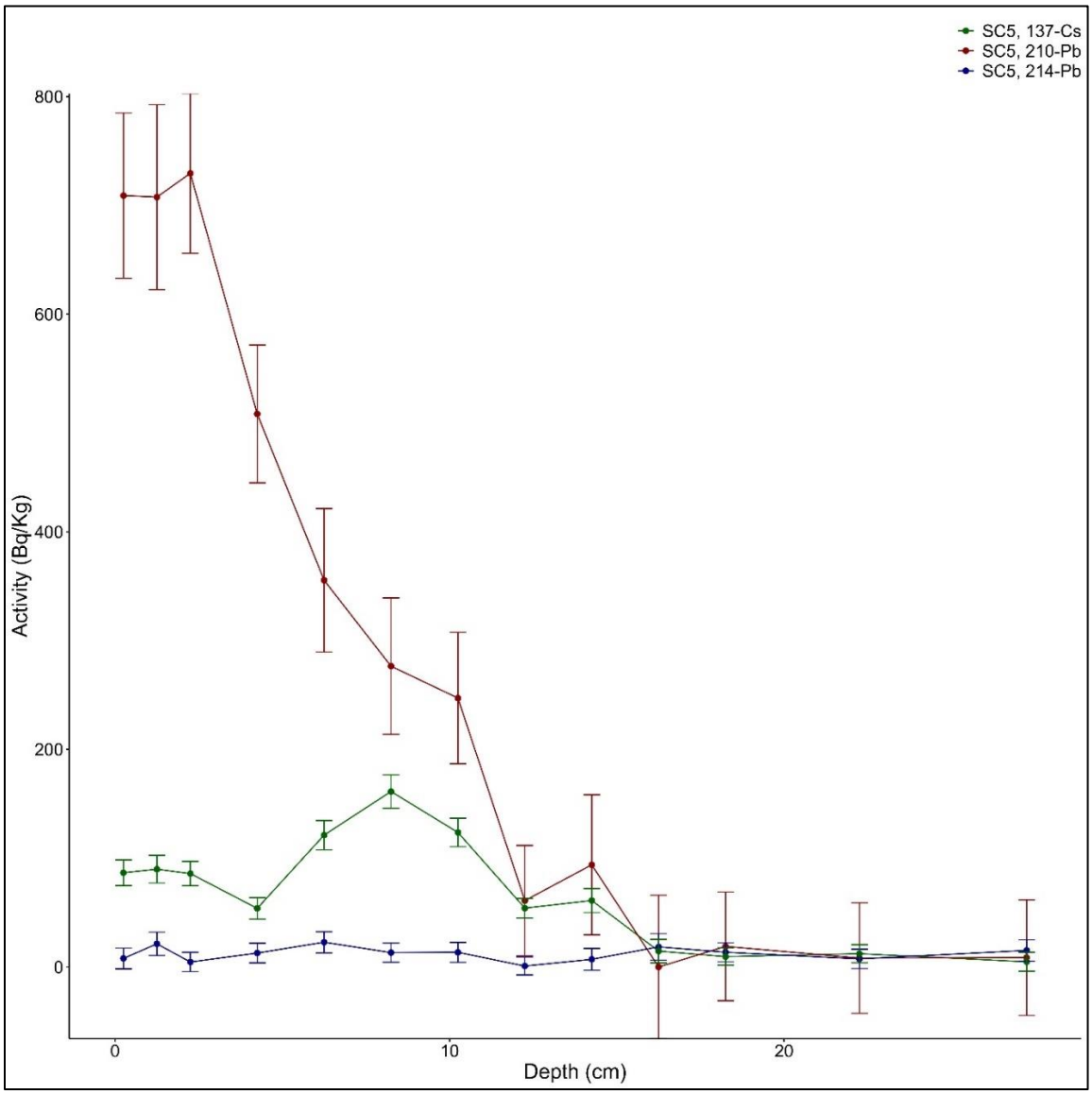

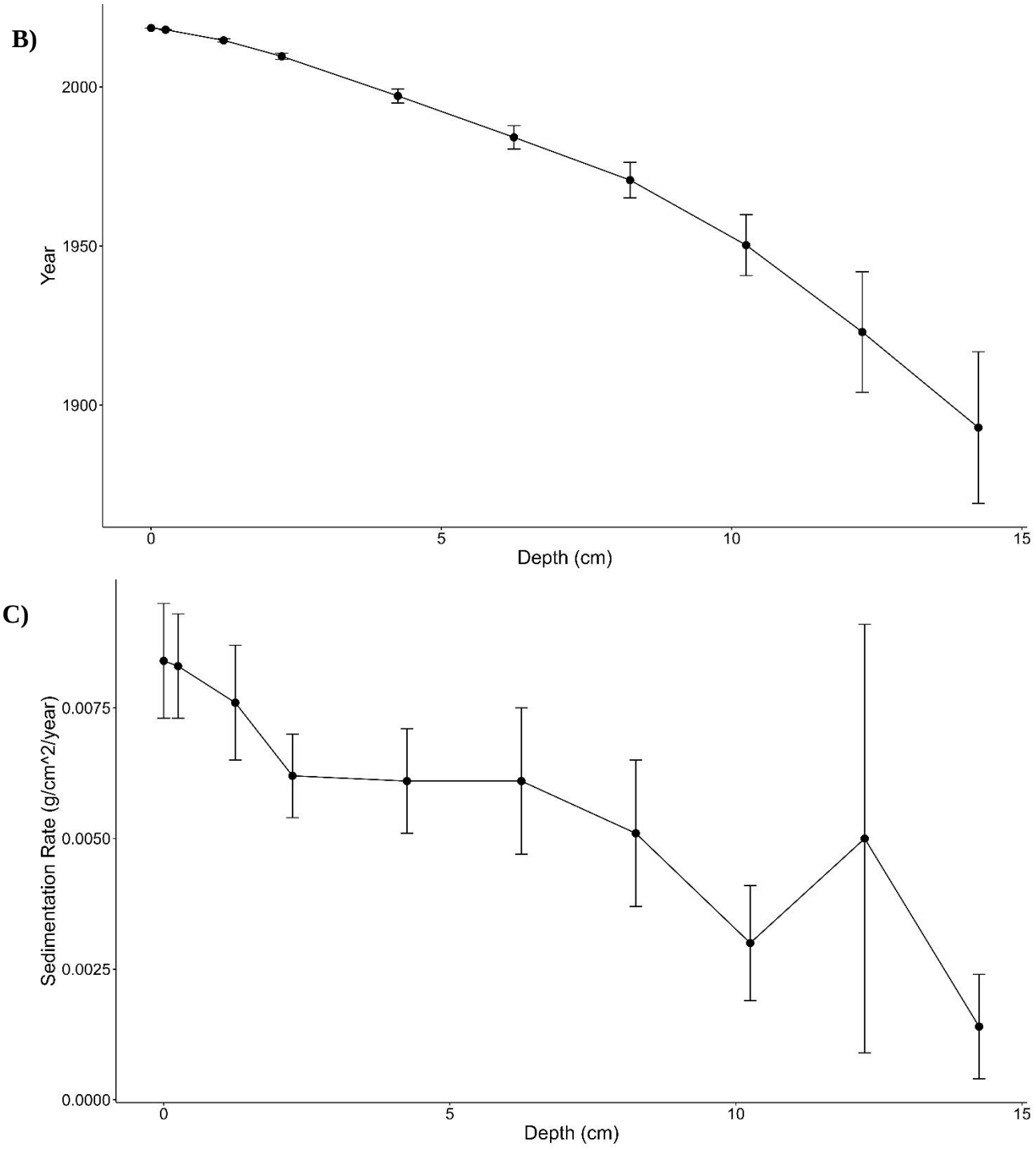

Figure 4.13: Results of ^{210}Pb dating for Lake SC-5: (A) sediment depth versus activities for radioisotopes ^{210}Pb, ^{214}Pb and ^{137}Cs, (B) sediment depth versus date based on the constant rate of supply (CRS) ^{210}Pb dating model, and (C) ^{210}Pb-inferred sedimentation rate versus depth based on the CRS model. Error bars are standard error.

There was a significant increase in THg concentration from 40 ng/g to 150 ng/g between 22.5 cm to 2.5 cm (Figure 4.12). HgF also increased steadily from 14 cm to the surface of the core (Figure 4.9). The average HgF corrected for sediment focusing factor was 0.79 ± 0.20 ng/cm^{2}yr (Table 4.1). There was no significant change in the %OC, which was consistently ~30-35% (Figure 4.12); however, there was a notable outlier at 14 cm (25.4%) (Figure 4.12). OCF increased steadily in sediment profile above 14 cm, similar to HgF (Figure 4.9). The average OCF corrected for sediment focusing was 2519.4 ± 1027.5 µg/cm^{2}yr (Table 4.1). There was no significant change in C:N, with values consistently fluctuating between 12-14 (Figure 4.12). Similar to %OC, there was a notable outlier at 14 cm, with a C:N value of 10.8 (Figure 4.12).

4.9 SC-6

The ^{210}Pb activity increased between 30 and 10 cm and decreased between 10 cm and the core surface (Figure 4.14). Background ^{210}Pb activity was reached at 30 cm (Figure 4.14). A peak in ^{137}Cs activity was observed at 18 cm depth. The earliest date obtained from CRS chronology was ~1849, at 30.5 cm core depth. Sedimentation rate decreased with depth, with the highest sedimentation rates in the top 1 cm (Figure 4.14). Sedimentation rate in SC-6 was higher than most of the other lakes, at 0.024 g/cm^2/yr (Figure 4.14). The calculated sediment focusing factor used to correct elemental flux values for sediment focusing was 0.73 (Table 4.1).

A)

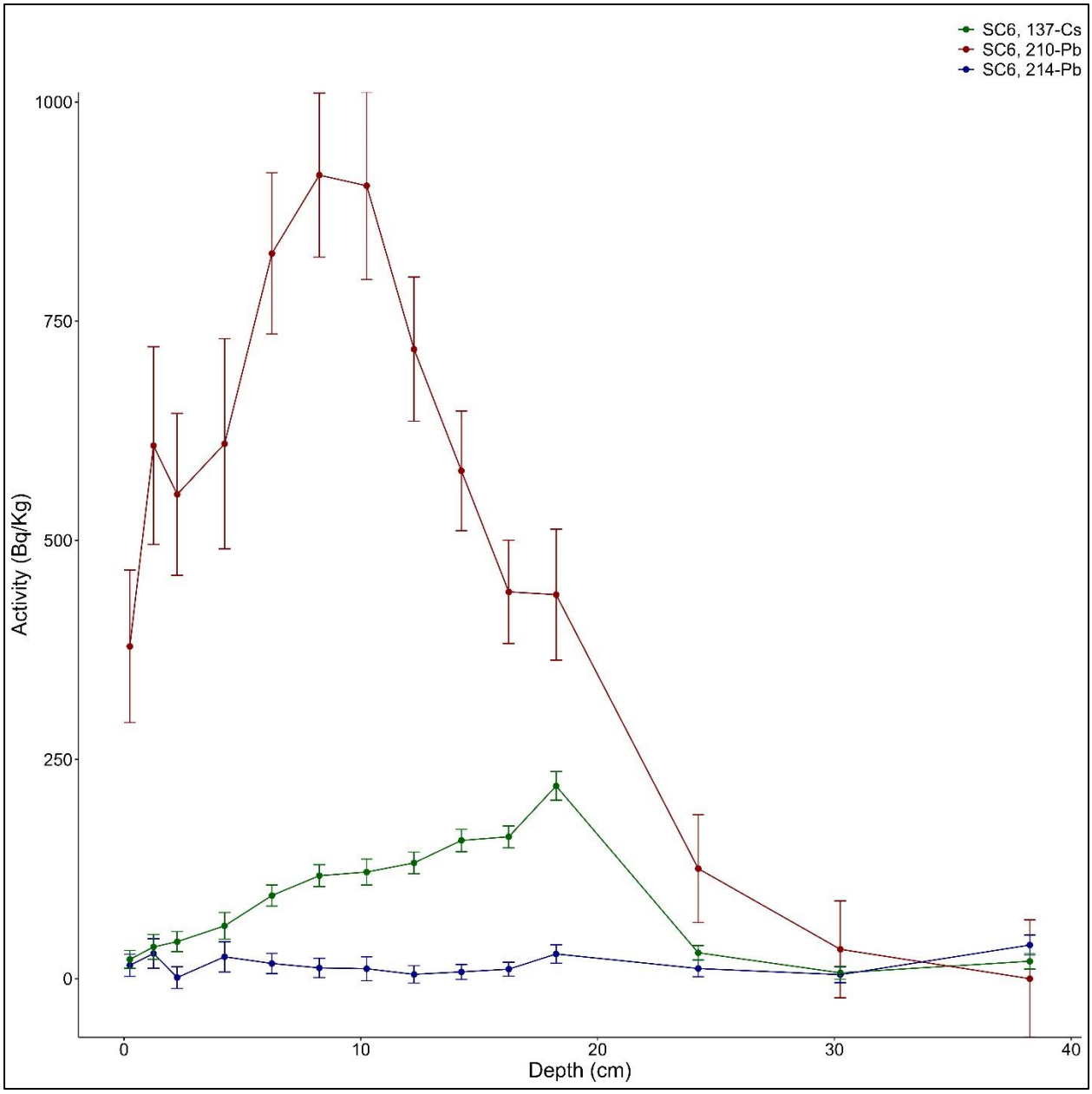
SC6, 137-Cs
SC6, 210-Pb
SC6, 214-Pb
1000
750
500
250
0
Activity (Bq/Kg)
0
10
20
30
40
Depth (cm)

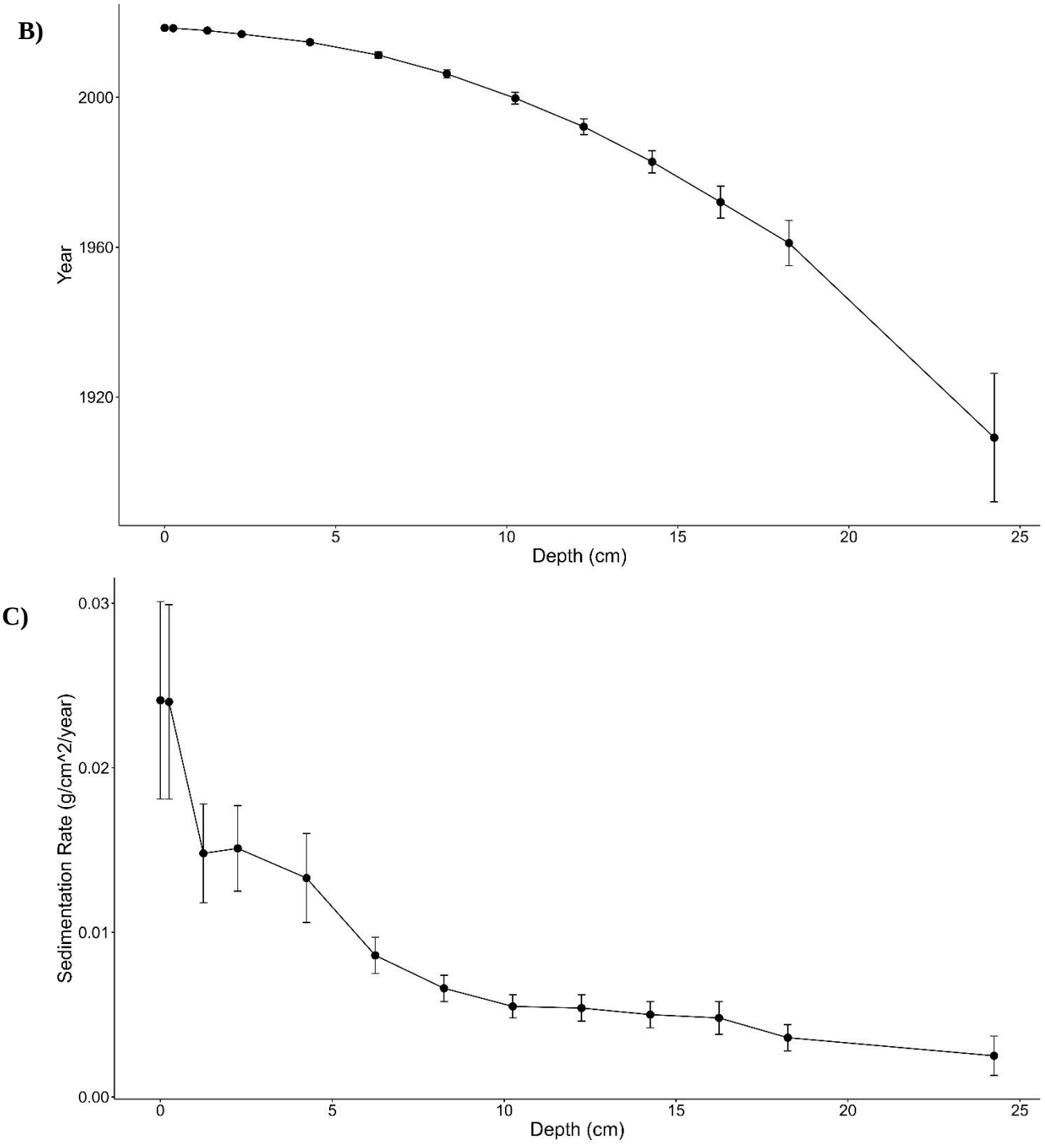

Figure 4.14: Results of ^{210}Pb dating for Lake SC-6: (A) sediment depth versus activities for radioisotopes ^{210}Pb, ^{214}Pb and ^{137}Cs, (B) sediment depth versus date based on the constant rate of supply (CRS) ^{210}Pb dating model, and (C) ^{210}Pb-inferred sedimentation rate versus depth based on the CRS model. Error bars are standard error.

There was a significant increase in THg concentration from 38.5 ng/g to 79.1 ng/g between 36.5 cm and ~18.5 cm, followed by a significant decline in THg from 66.13 ng/g to 40.5 ng/g between 14.5 cm and the core surface (Figure 4.12). HgF followed a similar trend to the inferred sedimentation rate, increasing over time with the greatest increases in the top 1.0 cm (Figure 4.15). The average HgF corrected for sediment focusing was 0.49 ± 0.09 ng/cm^{2}yr (Table 1). The %OC varied between 39-44%, with no changes over time (Figure 4.12). OCF followed a similar trend to HgF and inferred sedimentation rates (Figure 4.15). The average corrected OCF for sediment focusing over the dated portion of the core was 6032.2 ± 3865.2 µg/cm^{2}yr, which was the highest OCF rate in all the lakes (Table 4.1). The C:N fluctuated between 12.1 and 13.8, with no significant periods of change (Figure 4.12).

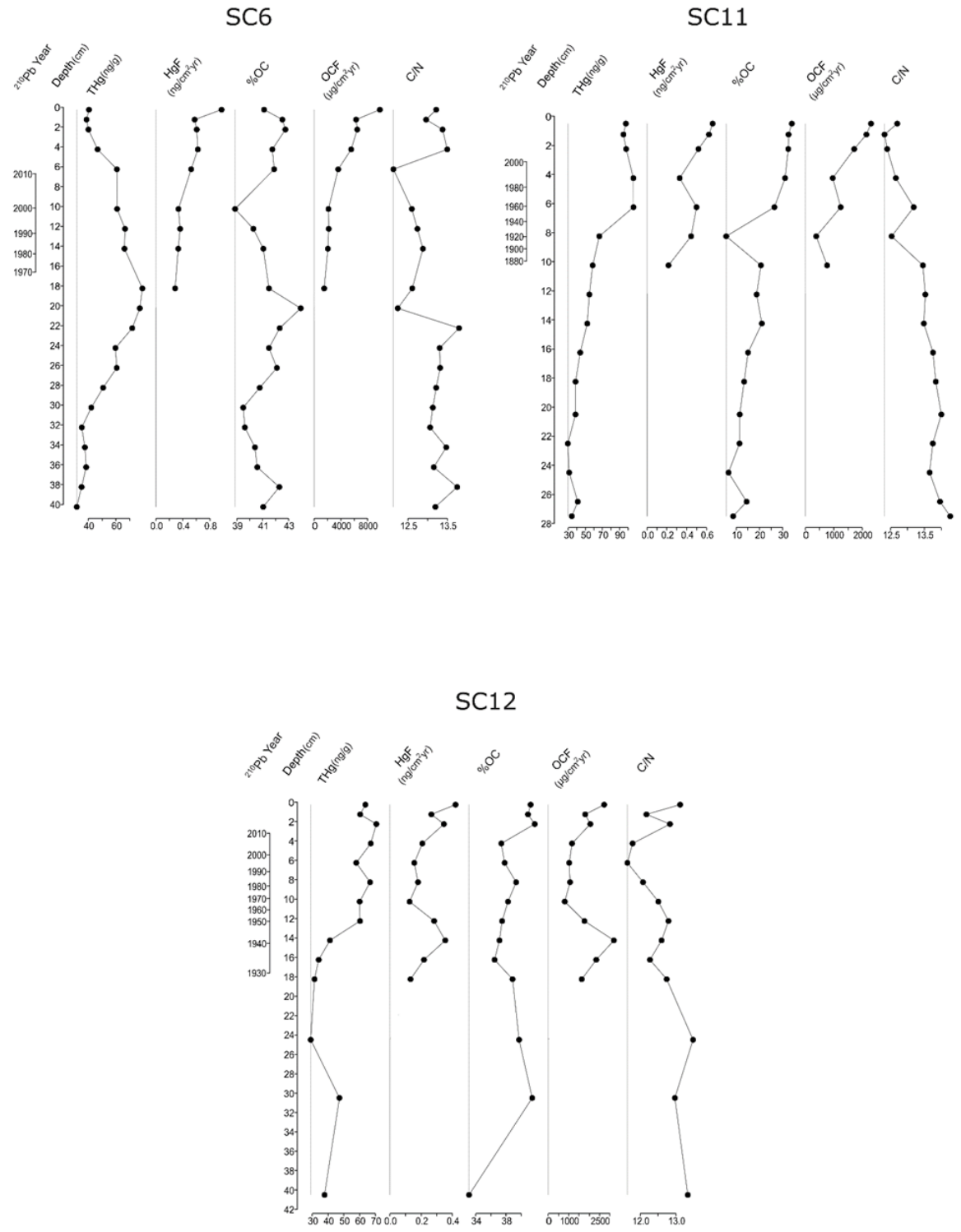

Figure 4.15: Stratigraphic profiles showing changes in total mercury (THg), mercury flux rate (HgF), % organic carbon (%OC), organic carbon flux rate (OCF), and atomic carbon to nitrogen ratio (C:N) with sediment core depth in SC6, SC11 and SC12. The inferred dates based on the ^{210}Pb constant rate of supply model are shown on the left.

4.10 SC-8

There was a steady decline in ^{210}Pb activity observed between 2 cm and 16 cm, where ^{210}Pb reached background (Figure 4.16). A peak in ^{137}Cs was observed at 8-10 cm depth (Figure 4.16). The earliest date obtained from CRS chronology was 1853, at 16.5 cm depth. There was gradual increase in sedimentation rate from 16 cm to the core surface (Figure 4.6). The calculated sediment focusing factor used to correct elemental flux values for sediment focusing was 0.81 (Table 4.1).

A)

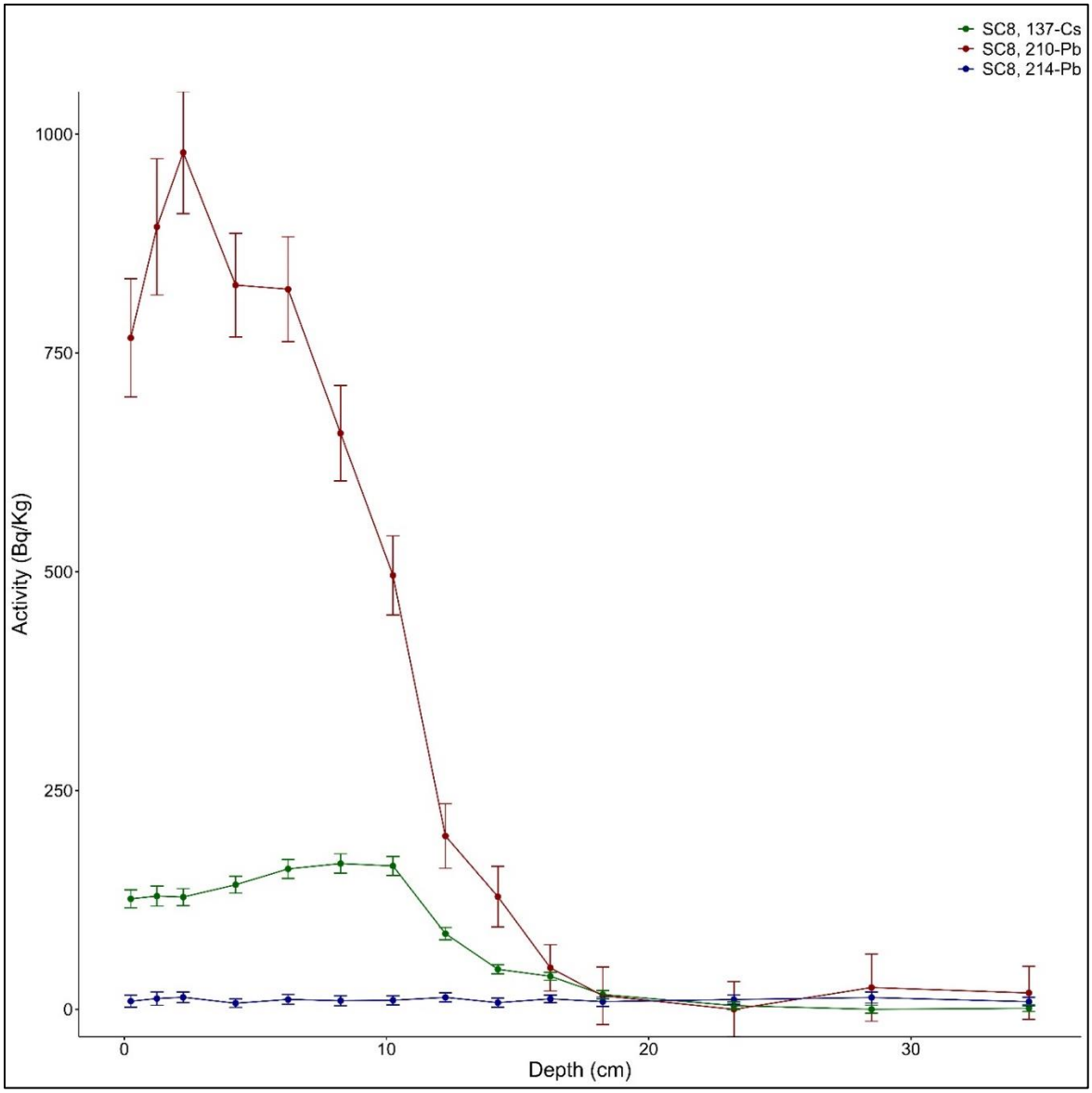

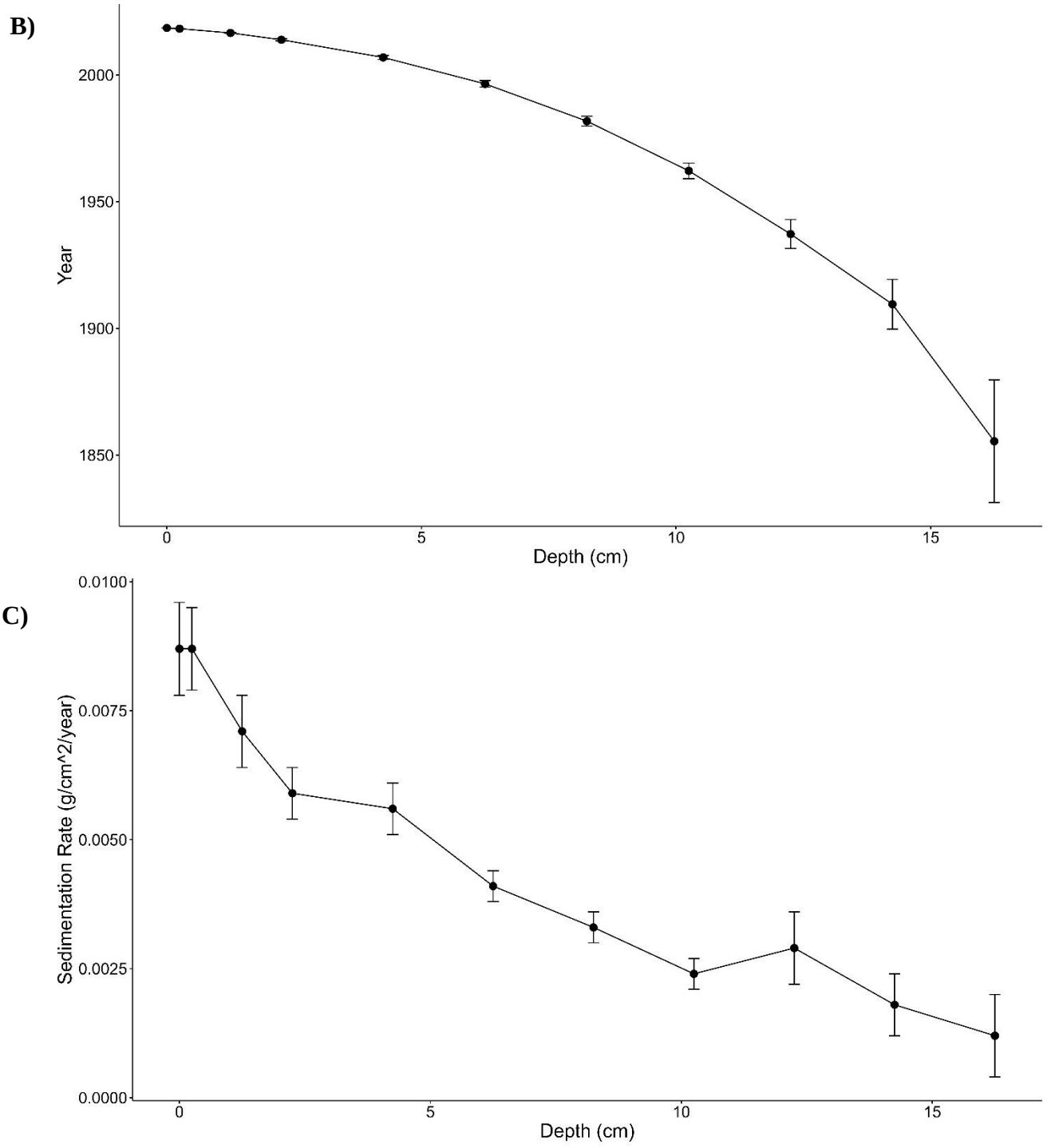

Figure 4.16: Results of ^{210}Pb dating for Lake SC-8: (A) sediment depth versus activities for radioisotopes ^{210}Pb, ^{214}Pb and ^{137}Cs, (B) sediment depth versus date based on the constant rate of supply (CRS) ^{210}Pb dating model, and (C) ^{210}Pb-inferred sedimentation rate versus depth based on the CRS model. Error bars are standard error.

There was a significant linear increase in THg from 34.5 cm to 0 cm core depth, increasing from 40 ng/g to 70 ng/g (Figure 4.17), except for a notable outlier of 10 ng/g at 6 cm (~1996) (Figure 4.17). HgF also increased from 16 to 0 cm, except for an outlier at 6 cm (Figure 4.18). The average HgF corrected for sediment focusing was 0.322 ± 0.042 ng/cm^{2}yr (Table 4.1). No significant changes in %OC were observed, and %OC ranged from ~39-43% (Figure 4.17). OCF increased steadily over time from 16 cm (494.76 µg/cm^{2}yr) to 0 cm (3555.69 µg/cm^{2}yr) (Figure 4.18). The average OCF corrected for sediment focusing was 2037.9 ± 1196.8 µg/cm^{2}yr (Table 4.1). C:N showed a significant linear decrease from 15.4 to 12.8 between 34.5 cm and 0 cm core depth (Figure 4.17).

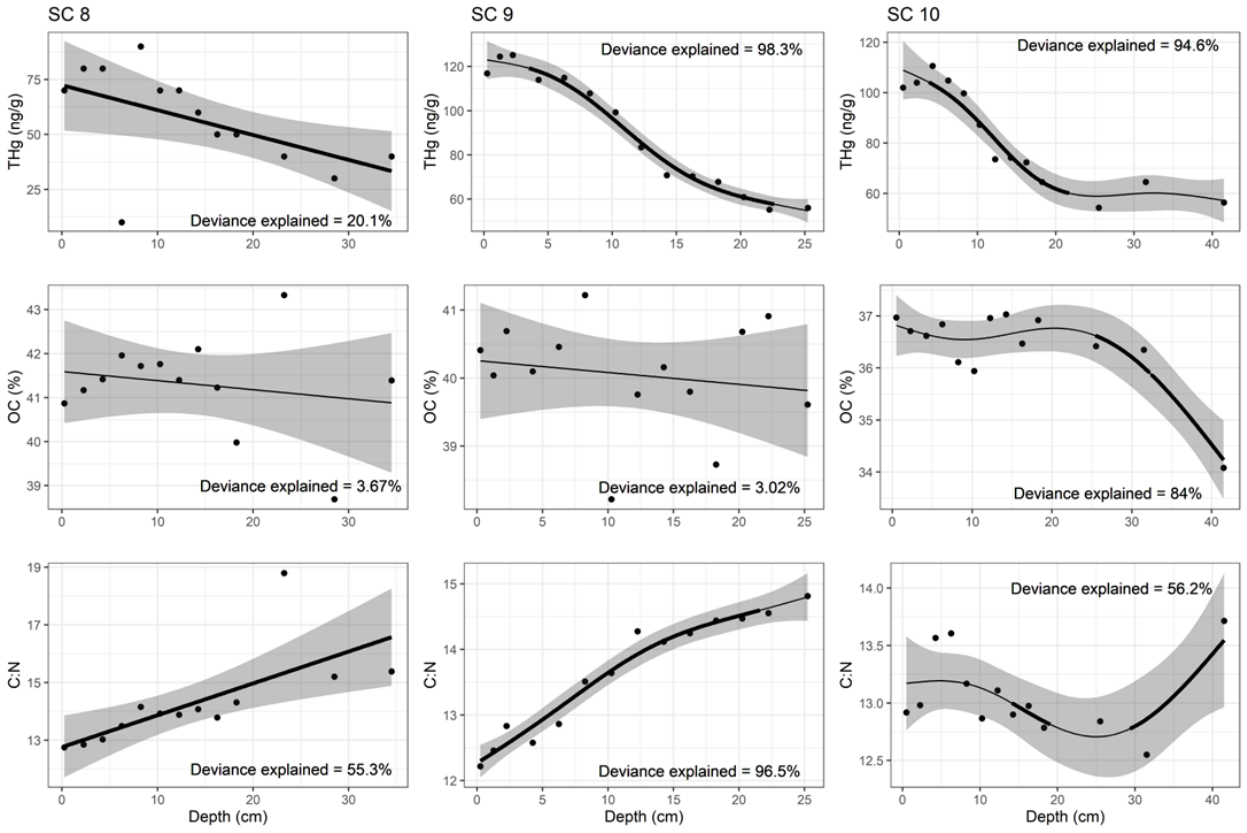

Figure 4.17: Results of the General Additive Models (GAMs) for SC8, SC9 and SC10, showing time series trends for total mercury (THg), the percent organic carbon content (%OC), and the atomic carbon to nitrogen ratio (C:N) plotted against sediment core depth (cm). The % of Deviance explained from the fitted

GAM model is shown. Bold portions represent areas of significant change, while grey shaded areas represent the 95% confidence intervals for the models.

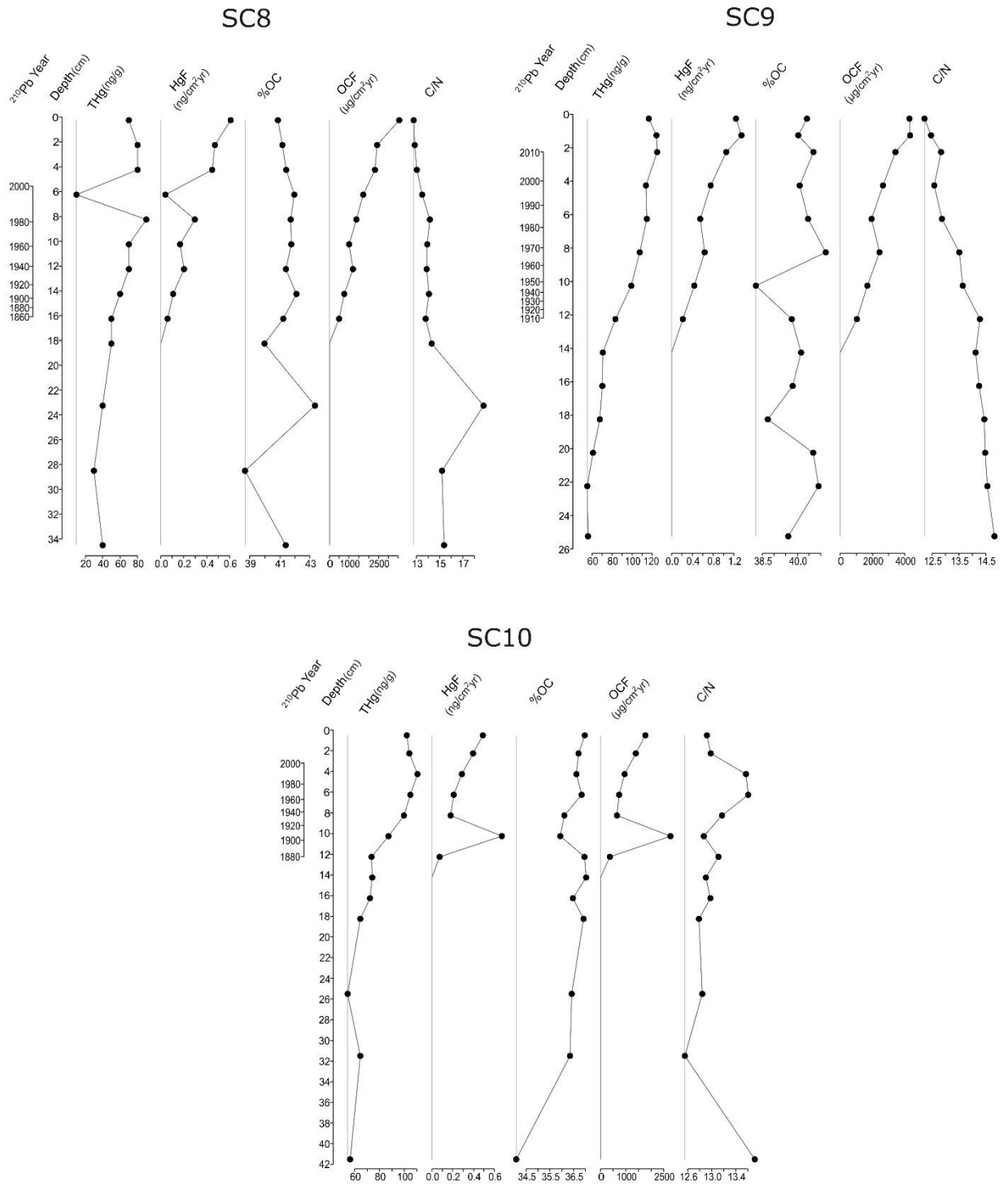

Figure 4.18: Stratigraphic profiles showing changes in total mercury (THg), mercury flux rate (HgF), % organic carbon (%OC), organic carbon flux rate (OCF), and atomic carbon to nitrogen ratio (C:N) with sediment core depth in SC10, SC9 and SC8. The inferred dates based on the ^{210}Pb constant rate of supply model are shown on the left.

4.11 SC-9

There was a steady decline in ^{210}Pb activity with increasing depth of the sediment profile and background was reached at 14.5 cm (Figure 4.19). No clear peak in ^{137}Cs was observed (Figure 4.19). The earliest date obtained from CRS chronology was ~1847 at 16.5 cm depth (Figure 4.19). Sediment rate generally increased from 12 cm to the surface of the core (Figure 4.19). The sediment focusing factor was 0.52 (Table 4.1).

A)

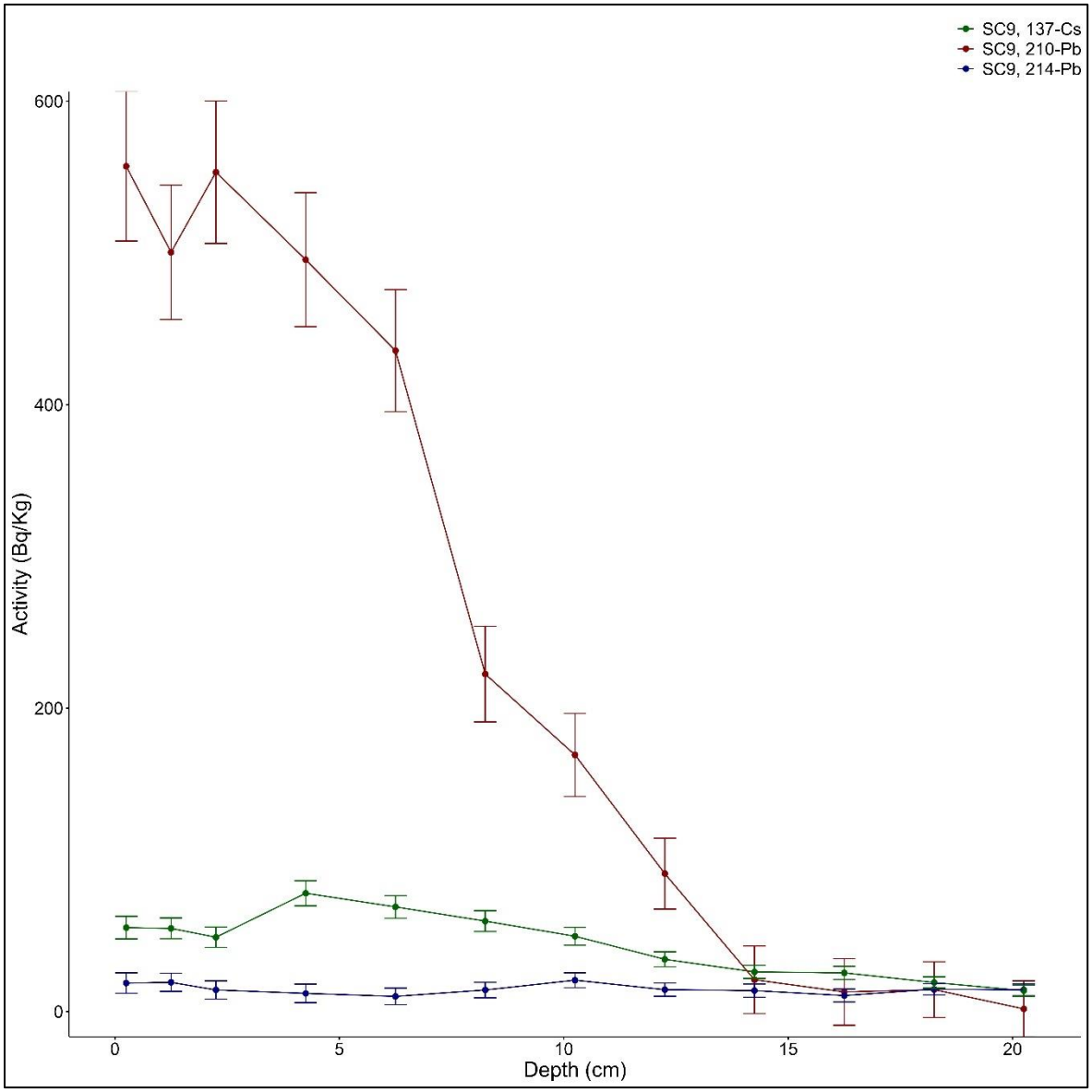

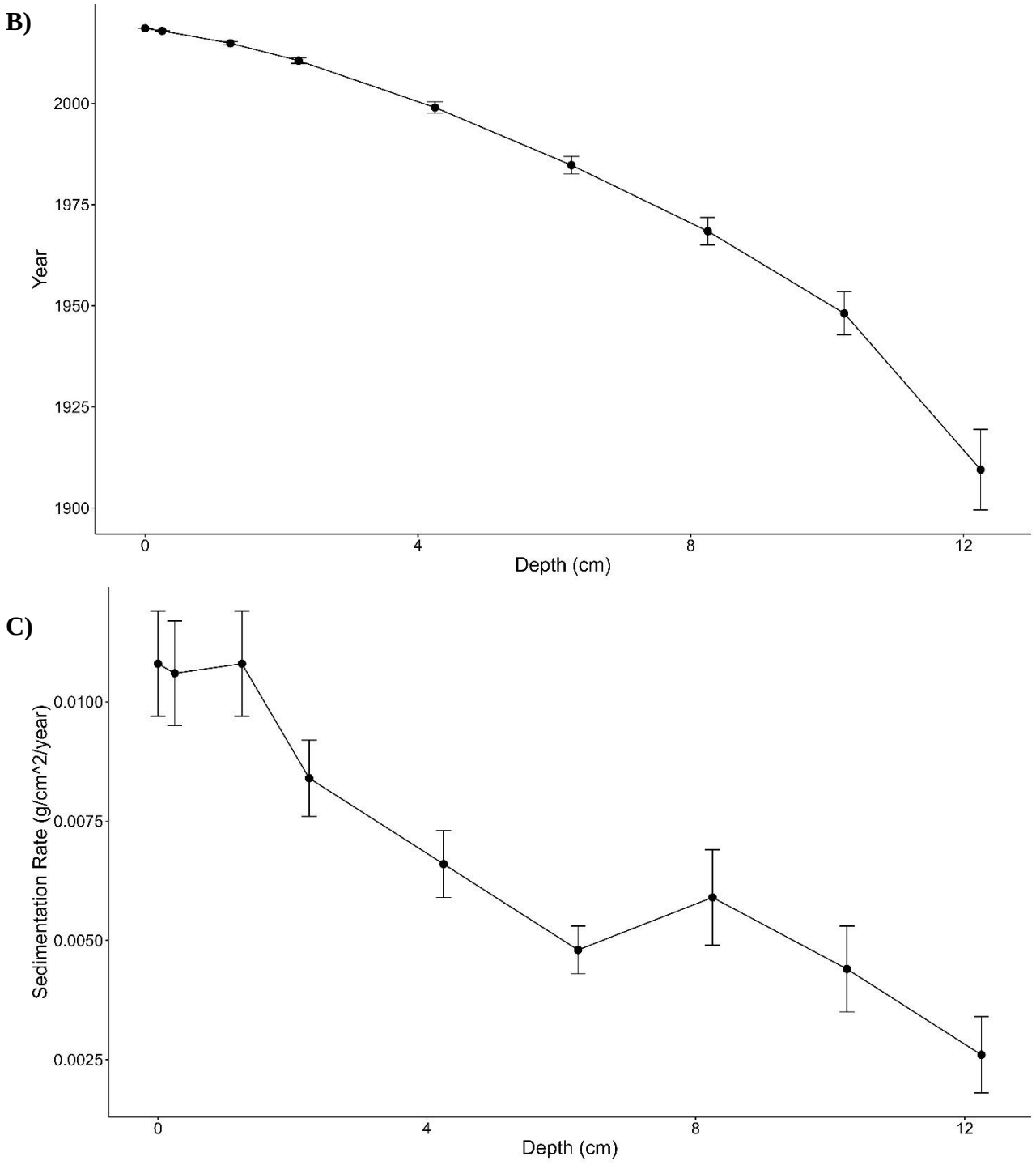

Figure 4.19: Results of ^{210}Pb dating for Lake SC-9: (A) sediment depth versus activities for radioisotopes ^{210}Pb, ^{214}Pb and ^{137}Cs, (B) sediment depth versus date based on the constant rate of supply (CRS) ^{210}Pb dating model, and (C) ^{210}Pb-inferred sedimentation rate versus depth based on the CRS model. Error bars are standard error.

There was a significant increase in THg concentration from ~70.32 ng/g to ~113.97 ng/g observed between 16 cm and 4 cm (Figure 4.17). HgF also increased steadily over time (Figure 4.18). The average HgF corrected for sediment focusing was 1.07 ± 0.132 ng/cm^{2}yr (Table 4.1). There was no significant change in %OC (Figure 4.17), but OCF increased steadily similar to HgF (Figure 4.18). The average OCF corrected for sediment focusing was 5231.2 ± 2311.5 µg/cm^{2}yr (Table 4.1). C:N decreased from 13.6 to 12.2 between 22.5 cm and the core surface (Figure 4.17).

4.12 SC-10

There was a steady decline in ^{210}Pb activity with increasing depth of the sediment profile and background was reached at 10 cm depth (Figure 4.20). A peak in ^{137}Cs activity was observed at 4-6 cm depth (Figure 4.20). The earliest date obtained from the chronology was ~1879 at 12 cm depth (Figure 4.20). Sedimentation rate decreased with increasing depth of the sediment profile, except for a peak in sedimentation rate (0.008 g/cm^2/yr) at 10 cm (Figure 4.20). The sediment focusing factor used to correct elemental flux values for sediment focusing was 0.74 (Table 4.1).

A)

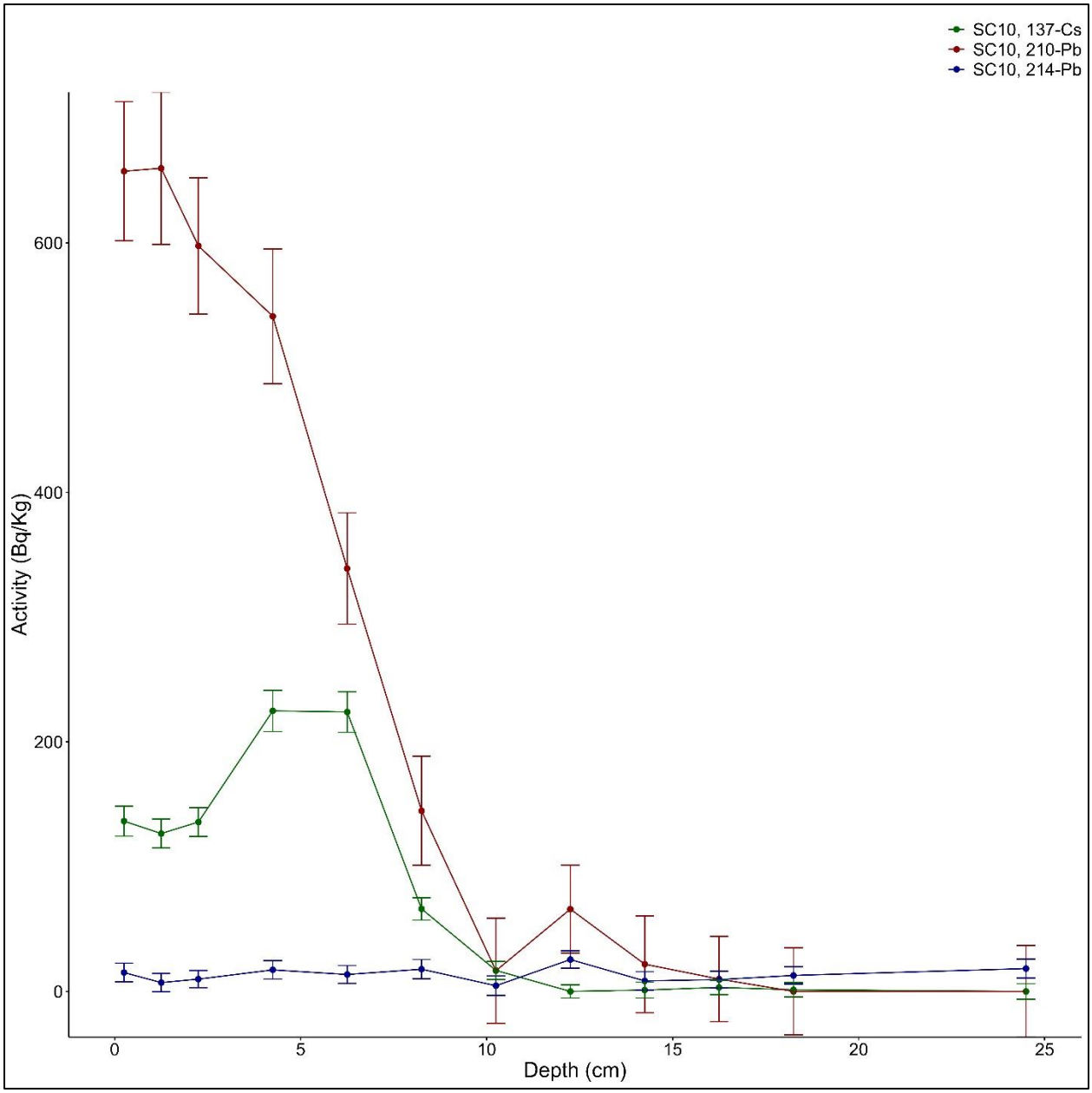
SC10, 137-Cs
SC10, 210-Pb
SC10, 214-Pb
Activity (Bq/Kg)
600
400
200
0
0
5
10
15
20
25
Depth (cm)

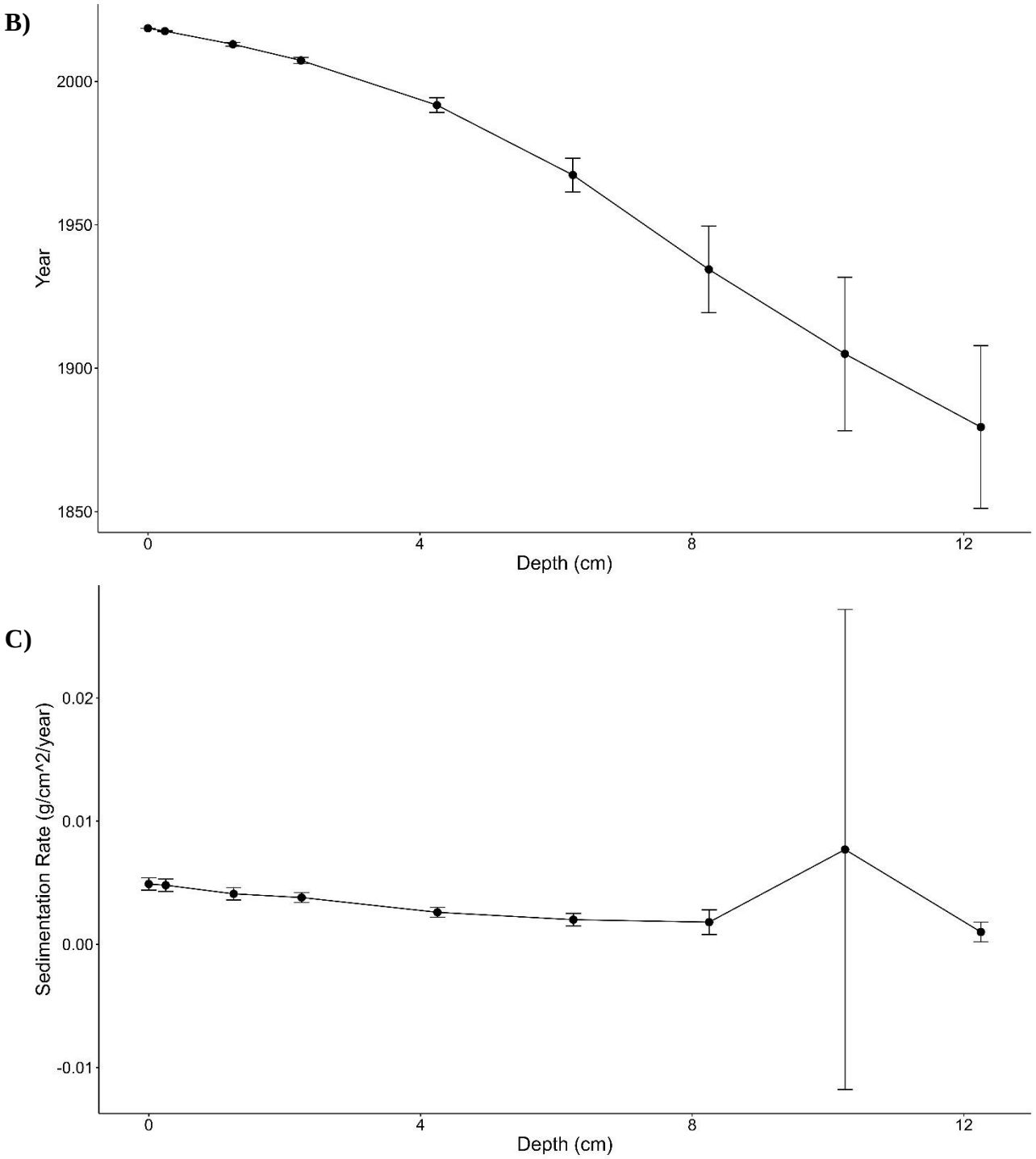

Figure 4.20: Results of ^{210}Pb dating for Lake SC-10: (A) sediment depth versus activities for radioisotopes ^{210}Pb, ^{214}Pb and ^{137}Cs, (B) sediment depth versus date based on the constant rate of supply (CRS) ^{210}Pb dating model, and (C) ^{210}Pb-inferred sedimentation rate versus depth based on the CRS model. Error bars are standard error.

A significant increase in THg concentration from ~60 ng/g to ~110 ng/g was observed between 21 cm and 4 cm depth (Figure 4.17). HgF generally increased over time, except for a subsurface peak recorded at ~10.25 cm depth that corresponds to the peak in sedimentation rate (Figure 4.18). The average HgF corrected for sediment focusing was 0.83 ± 0.74 ng/cm^{2}yr (Table 4.1). There was a significant increase in %OC from 34.1-36.4% between 41.5 and 25.5 cm (Figure 4.17). OCF followed the same trend as HgF, with highest flux rate (2767.4 µg/cm^{2}yr) recorded at 10 cm depth (Figure 4.18). The average OCF corrected for sediment focusing was 1669.0 ± 1114.9 µg/cm^{2}yr (Table 4.1). C:N significantly declined from 13.7 to 12.5 between 41.5 cm and 30 cm depth (Figure 4.17).

4.13 SC-11

A steady decline in ^{210}Pb activity was observed between 6 cm and 9 cm, when ^{210}Pb activity reached background, while ^{210}Pb activity was fairly consistent in the top 0-5 cm (Figure 4.21). ^{137}Cs activity increased at 6 cm but no clear peak was observed (Figure 4.21). The earliest date obtained from CRS chronology was ~1845, at 11.5 cm depth (Figure 4.21). Sedimentation rate was lowest at 5 cm, and then increased gradually from 5 cm to 0 cm (Figure 4.21). The sediment focusing factor used to correct elemental flux values for sediment focusing was 0.83 (Table 4.1).

A)

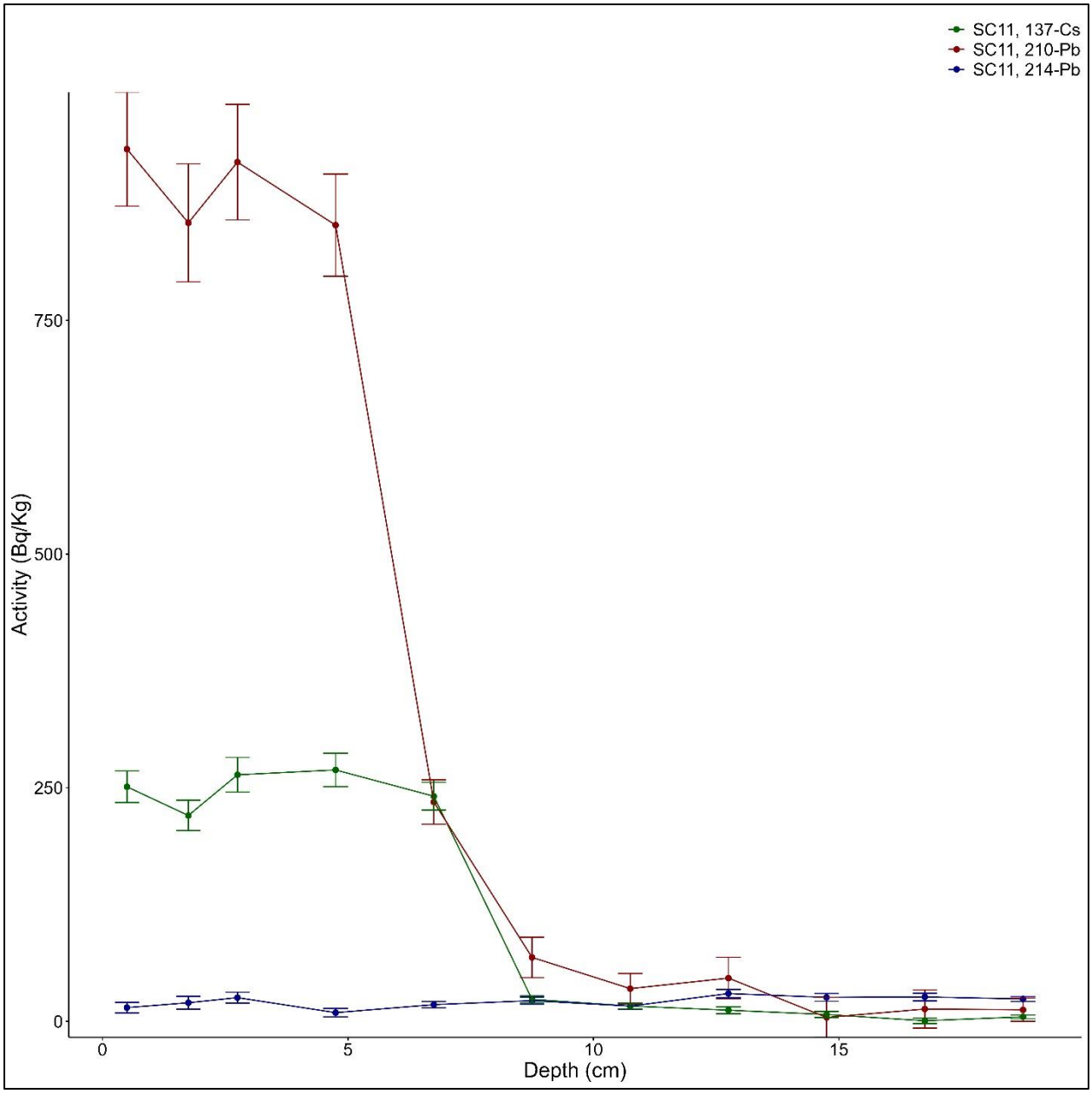
SC11, 137-Cs
SC11, 210-Pb
SC11, 214-Pb
Activity (Bq/Kg)
750
500
250
0
0
5
10
15
Depth (cm)

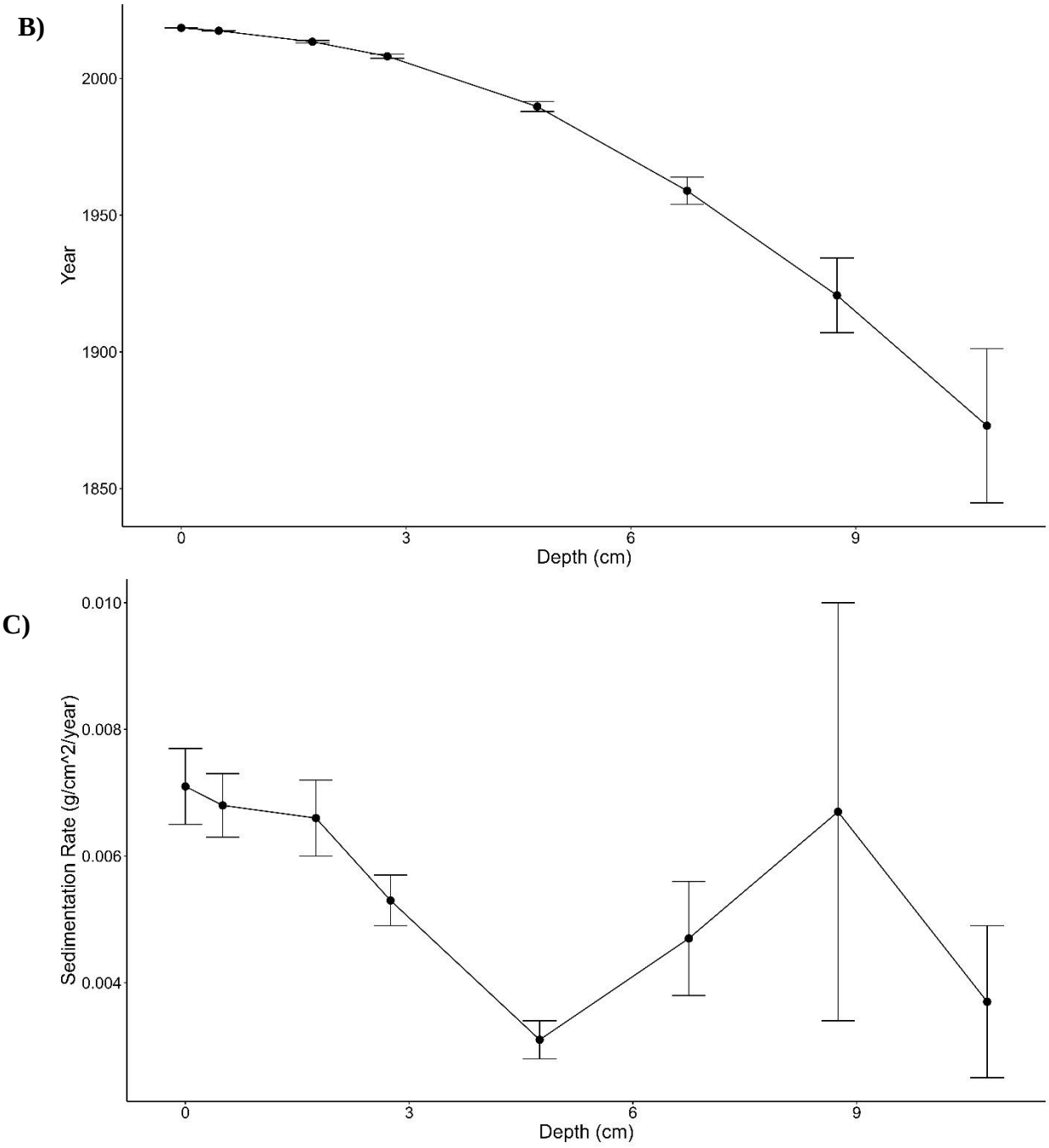

Figure 4.21: Results of ^{210}Pb dating for Lake SC-11: (A) sediment depth versus activities for radioisotopes ^{210}Pb, ^{214}Pb and ^{137}Cs, (B) sediment depth versus date based on the constant rate of supply (CRS) ^{210}Pb dating model, and (C) ^{210}Pb-inferred sedimentation rate versus depth based on the CRS model. Error bars are standard error.

THg increased significantly from 38.49 ng/g to 97.35 ng/g above 20.5 cm (Figure 4.22). HgF increased above 4 cm (Figure 4.15). The average HgF corrected for sediment focusing was 0.6 ± 0.1 ng/cm^{2}yr (Table 4.1). There was also a significant increase in %OC from 6.7% to 33.9% between 24.5 cm and the core surface (Figure 4.22). OCF followed a similar trend as HgF, increasing from 763.7 µg/cm^{2}yr to 2307.9 µg/cm^{2}yr above 4 cm (Figure 4.15). The average OCF corrected for sediment focusing was 1638.5 ± 870.2 µg/cm^{2}yr (Table 4.1). C:N exhibited a significant linear decrease from 13.7 to 12.7 between 24.5 cm and the surface, corresponding to the increase in %OC (Figure 4.22).

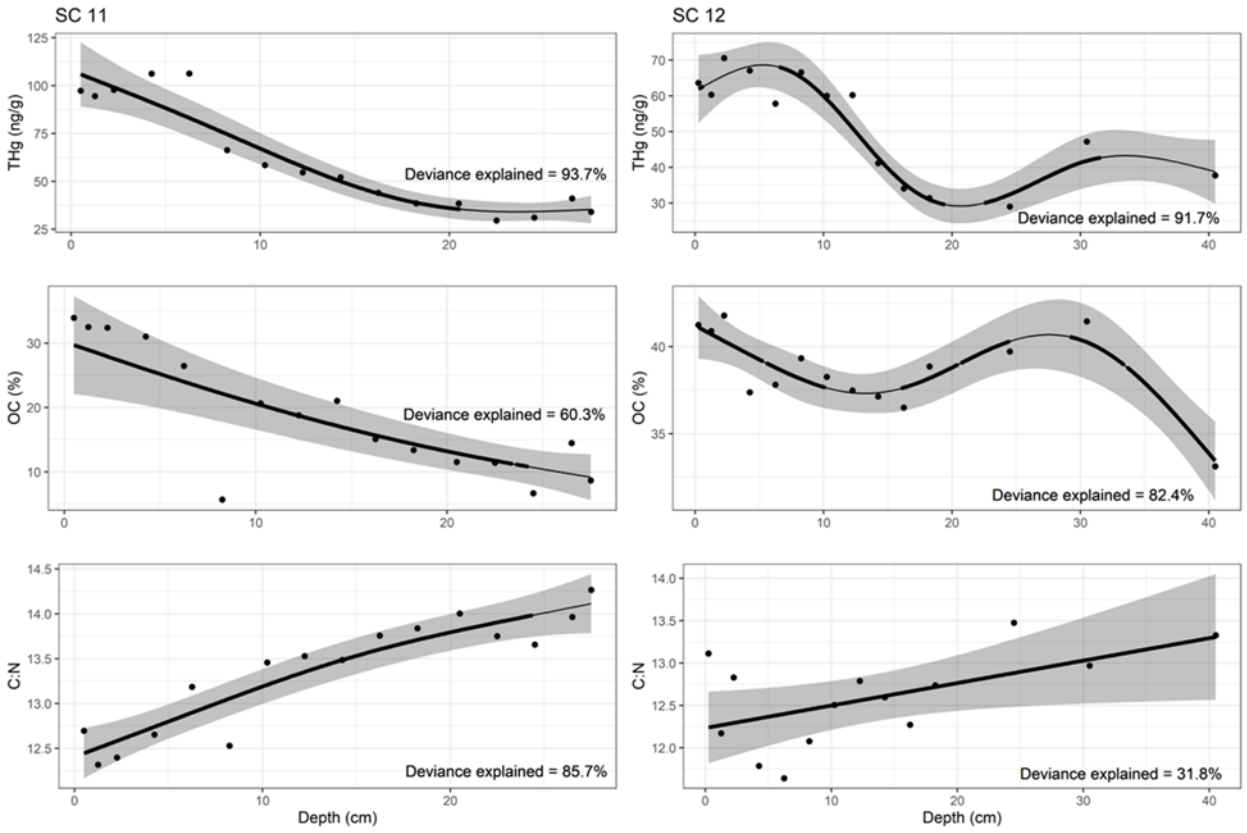

Figure 4.22: Results of the General Additive Models (GAMs) for SC11 and SC12, showing time series trends for total mercury (THg), the percent organic carbon content (%OC), and the atomic carbon to nitrogen ratio (C:N) plotted against sediment core depth (cm). The % of Deviance explained from the fitted GAM model is shown. Bold portions represent areas of significant change, while grey shaded areas represent the 95% confidence intervals for the models.

4.14 SC-12

There was a steady decline in ^{210}Pb activity from 4 cm to 16 cm, when background was reached (Figure 4.23). A peak in ^{137}Cs activity was observed at 10 cm depth (Figure 4.23). The earliest date obtained from the chronology was ~1851 at 29.5 cm. Sedimentation rate decreased from 14 cm to 10 cm, followed by a gradual increase above 10 cm (Figure 4.23). The sediment focusing factor used to correct elemental flux values for sediment focusing was 1.09 (Table 4.1).

A)

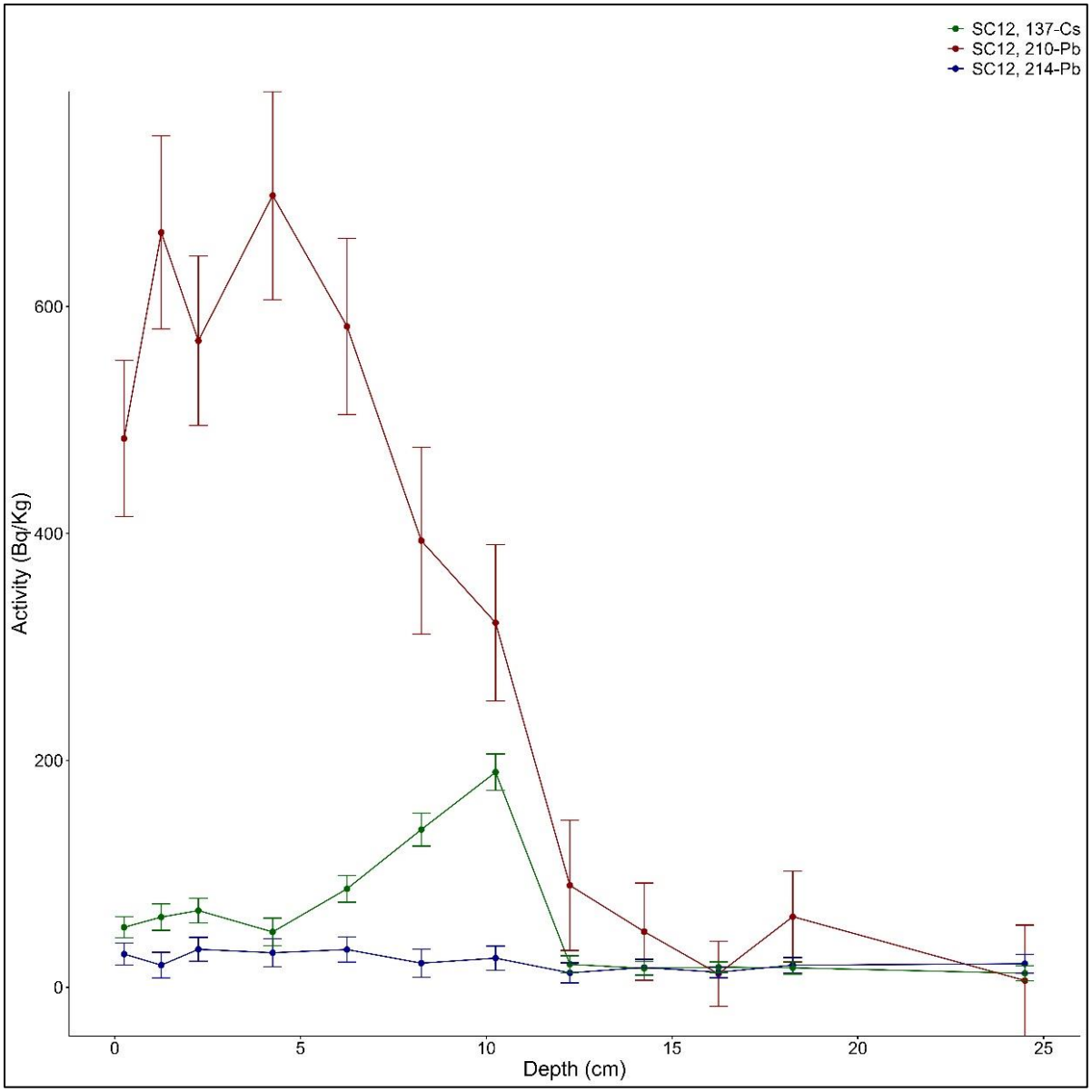

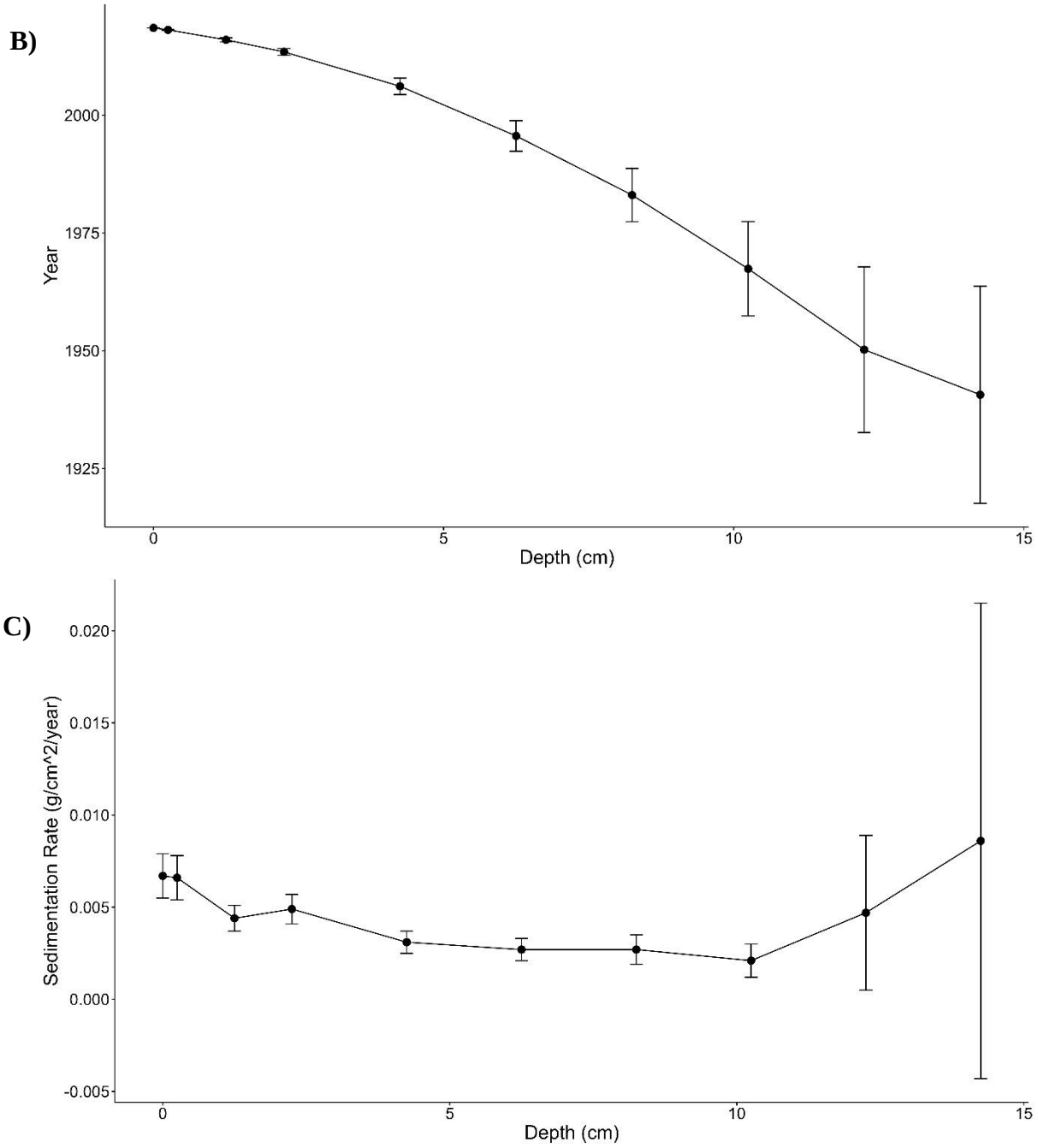

Figure 4.23: Results of ^{210}Pb dating for Lake SC-12: (A) sediment depth versus activities for radioisotopes ^{210}Pb, ^{214}Pb and ^{137}Cs, (B) sediment depth versus date based on the constant rate of supply (CRS) ^{210}Pb dating model, and (C) ^{210}Pb-inferred sedimentation rate versus depth based on the CRS model. Error bars are standard error.

There was a significant increase in mercury (THg) concentration from 31.4 ng/g to 57.8 ng/g between 18.5 cm to 6.5cm (Figure 4.22). HgF exhibited a subsurface peak of 0.3 ng/cm^{2}yr at

15 cm (Figure 4.15). The average HgF corrected for sediment focusing was 0.6 ± 0.3 ng/cm^{2}yr (Table 4.1). The %OC increased from 33.1% to 41.4% between 40 cm and 30 cm, declined from 39.7% to 36.5% between 24.5 cm and 16.0 cm, and increased again from 38.3% to 41.2% between 10 cm and the core surface (Figure 4.22). OCF exhibited a similar subsurface peak (3193.2 µg/cm^{2}yr) at 15 cm as HgF and increased steadily from 803.46 µg/cm^{2}yr to 2721.84 µg/cm^{2}yr above 10 cm (Figure 4.15) The average OCF corrected for sediment focusing was 1629.3 ± 693.7 µg/cm^{2}yr (Table 4.1). There was a significant decrease in C:N from ~13.5 to ~12 between 40.5 cm and the core surface (Figure 4.22).

Table 4.1: Mercury (HgF) and organic carbon (OCF) flux rates averaged since ~1850 (based on ^{210}Pb dates) for the 14 study lakes. The % Bog 250 and % Fen 250 represent the percentage of the shoreline within 250 m that is encompassed by bog (i.e. collapse scar) and fen vegetation, based on land classification presented in Coleman et al. (2023). Mercury and organic carbon fluxes have been corrected for sediment focusing factors. Depth = maximum lake depth. FF = sediment focusing factor. Area = lake surface area. Lakes are listed in order of descending HgF fluxes.

Lake	Average HgF ± Error (ng/cm^2/yr)	Depth (m)	FF Factor	Area (ha)	% Bog 250m	% Fen 250m	Average OCF ± Error (µg/cm^{2}yr)
SC2 (linked)	8.4 ± 2.9	1.7	0.52	11	13.4	30.9	3490.9 ± 1451.4
SC3 (linked)	1.4 ± 0.5	1.8	0.06	18	26.9	26.6	59678.0 ± 39496.5
SC9	1.1 ± 0.1	2.1	0.52	82	N/A	N/A	5231.2 ± 2311.5
SC10	0.8 ± 0.7	1.2	0.74	73	N/A	N/A	1669 ± 1114.9
SC1 (linked)	0.8 ± 0.6	1.3	0.05	21	21.3	19.5	58999.4 ± 48574.8
SC5 (isolated)	0.8 ± 0.2	1	0.67	21	31.6	9.6	2519.4 ± 1027.5
First Lake (linked)	0.7 ± 0.3	0.9	0.3	17	37.7	12.9	1576.3 ± 639.4
SC4	0.7 ± 0.3	1.1	0.74	22	N/A	N/A	2357.5 ± 1577.4
SC12	0.6 ± 0.3	0.9	1.09	116	N/A	N/A	1629.3 ± 693.7
SC11	0.6 ± 0.1	2	0.83	114	N/A	N/A	1638.5 ± 870.2
SC6 (linked)	0.5 ± 0.1	1.1	0.73	40	28.5	25.8	6032.2 ± 3865.2
Next Lake (linked)	0.4 ± 0.1	1.5	0.4	24	20.5	34	2311.8 ± 1147.7
SC8 (isolated)	0.3 ± 0.04	0.9	0.81	15	48.9	0	2037.9 ± 1196.8
Goose Lake (linked)	0.3 ± 0.05	1.1	0.38	244	22.9	34.1	3286.6 ± 1694.0

5.0 DISCUSSION

Recent research in the Dehcho has recorded drastic changes in the land cover as a result of climate change, with permafrost-underlain peat plateau forests converted into thermokarst wetlands and associated enhancement of watershed hydrological connectivity (Chasmer et al., 2014; Gordon et al., 2016; Olefeldt et al., 2016; Quinton et al., 2019; Turetsky et al., 2020; Connon et al., 2021; Coleman et al., 2023). This is expected to enhance the flux of organic carbon and associated mercury into downstream waterbodies, including lakes (Rydberg et al., 2010; Coleman et al., 2015; Korosi et al., 2015; Anderson et al., 2019). This study quantified the burial of carbon and mercury in the sediments of 14 shallow lakes located at or near the Scotty Creek Research Station (Northwest Territories, Canada). Using paleolimnological techniques, sediment cores were dated to evaluate spatiotemporal trends in carbon and mercury accumulation and flux rates, and carbon sources inferred from the elemental ratio of organic carbon to nitrogen (C/N), focusing on the influence of permafrost peatland thaw and the presence of wetland thermokarst features in the Scotty Creek basin's discontinuous permafrost zone. This study's outcomes provide valuable insights into the role that lakes play in the landscape cycling of organic carbon (OC) and mercury (Hg) in small, shallow discontinuous permafrost peatland lakes. I did not examine methyl mercury, only total mercury, as the paleolimnological methods employed in this study are not compatible with the assessment of methyl mercury that does not exhibit long-term preservation within sediment cores (Brazeau et al., 2013; Korosi et al., 2015).

5.1 Is mercury accumulation in Dehcho lake sediments linked to organic carbon?

Climate-induced permafrost thaw may influence mercury transport to lakes through changes in terrestrial carbon inputs (Korosi et al., 2015) and algal primary production (Michelutti et al., 2005). Mercury released from thawing permafrost is tightly bound to organic matter and thus, the role of terrestrial organic matter in the transport of mercury to aquatic ecosystems has been studied over the years, emphasizing that mercury transport from catchments to adjacent aquatic systems is strongly driven by terrestrial organic matter fluxes (Driscoll et al., 1995; Kolka et al., 1999; Ouellet et al., 2009; Teisserenc et al., 2010; Teisserenc et al., 2011). The 'algal scavenging' hypothesis suggests that climate warming may enhance mercury accumulation in Arctic lake sediments due to sorption to organic matter linked with heightened aquatic primary production (Outridge et al., 2007; Stern et al., 2009; Carrie et al., 2010; Sanei et al., 2012a; Grasby et al., 2013); however, the validity of this concept remains a subject of debate as some studies have identified significant correlations between total mercury (THg) and algal productivity in the sediments of one or more lakes (Sanei and Goodarzi, 2006; Stern et al., 2009; Carrie et al., 2010; Jiang et al., 2011; Deison et al., 2012; Sanei et al., 2012b; Brazeau et al., 2013; Biester et al., 2018; Burke et al., 2018), while others have found no relationship (Cooke et al., 2012; Hermanns et al., 2013) or only partial correlations between algal scavenging and THg concentration in a limited set of water bodies (Kirk et al., 2011; Korosi et al., 2018). Analyses of four Canadian high and subarctic lakes for mercury and algal-derived organic carbon have shown significant positive relationships between Hg and algal-derived organic carbon (Outridge et al., 2007; Stern et al., 2009; Carrie et al., 2010).

Sediment Hg concentrations ranged from 10-190 ng/g and were lower than those reported by others for the Canadian High Arctic and subarctic lakes (Muir et al., 2009; Stern et al., 2009; Carrie et al., 2010; Cooke et al., 2010; Kirk et al., 2011). This study only found positive associations between THg and %OC trends based on GAMs in SC11, where both THg and %OC increased, with a corresponding decrease in C/N, consistent with the algal scavenging hypothesis. A decreasing C:N ratio is an indication of greater in-lake produced algae over terrestrial organic matter (Meyers and Teranes, 2001), which may be the result of nutrients released through thawing permafrost (Coleman et al., 2015). Trends of increasing Hg corresponding to decreasing C/N, indicative of an algal scavenging effect, was also observed in lakes SC1, SC2, SC8, SC9, and SC12, but with no overall increase in %OC (SC8, SC9, SC12) or a decreasing trend in OC (SC1, SC2). This suggests that the source of organic carbon to these subarctic lake sediments was algal sources due to increased primary productivity in the lakes, similar to findings by Kirk et al. (2011).

However, other lakes showed contrasting results. THg increased in SC5 and SC10 without any corresponding changes to %OC or C/N. THg decreased in lakes SC3, SC4, and SC6, with no corresponding changes in %OC, and conflicting trends in C/N (C/N decreased in SC3, increased in SC4, and showed no change in SC6). This indicates that, overall, total mercury accumulation has generally increased across the 14 study lakes but was not primarily driven by organic carbon. This is consistent with findings by Kirk et al. (2011) which suggested that increased lake primary productivity does not appear to be driving changes in mercury (Hg) fluxes to Arctic and subartic lake sediments.

5.2 Rates of mercury and organic carbon burial in lake sediments

The results from this research suggest that Hg and OC fluxes are closely linked to sedimentation mass accumulation rate. Most of the lakes (12 out of 14) showed increasing THg and %OC fluxes since ~1850 (post-industrialization) corresponding to increases in sedimentation rate, consistent with study by Kirk et al. (2011) on mercury and algal-derived carbon from 14 Canadian arctic and subarctic lakes which reported a general increase in sedimentation rates and Hg fluxes in 11 out of the 14 lakes post-industrialization. Analysis of sediment cores from over 100 circumpolar Arctic lakes over the years has shown an increase in Hg fluxes since ~1850 (post-industrialization), with variation in the magnitude of increase between ~1.5- and 12-fold among lakes (Landers et al., 1998; Lockhart et al., 1998; Bindler et al., 2001; Fitzgerald et al., 2005; Lindeberg et al., 2006; Muir et al., 2009; Stern et al., 2009; Carrie e al., 2010; Cooke et al., 2010; Kirk et al., 2011).

Increased lake productivity (algal production) and corresponding increased sedimentation rate have also been observed in numerous Baffin Island (Nunavut) lakes (Michelutti et al., 2007). In this study, SC1, SC2, and SC10 both had notable sub-surface peaks in sedimentation rate that produced peaks in THg and %OC fluxes. This is similar to results from Sobek et al. (2009) where sedimentation rate was similarly identified as an important predictor of OC burial efficiency in lakes. This suggests that climate warming and/or accelerated permafrost thaw may lead to increases in carbon and mercury burial rates through increases in sedimentation rates (Kokfelt et al., 2010); however, diagenesis (post-depositional transformation of organic matter in sediments) is still occurring in the surface 5-10 cm (Sobek et al., 2014), and may influence the results.

The sediment focussing factor (FF) in the study lakes was low, ranging from 0.05 to 1.09. Focusing factor values <1 indicates that the sediment sampling area exports more sediment than it accumulates (Hermanson and Christensen, 1991b). Since the lake basins are relatively uniform, and cores were collected from the central, deepest location, low FF in many of the lakes may reflect the influence of flow moving through connected, shallow systems with flocculant sediments prone to resuspension and transport. SC8, which is a hydrologically disconnected lake, had one of the highest FF (0.81) of the lakes. Sediment focussing is the process responsible for contaminant burial in the lake bottom (Blais, 1995). The low FF would indicate that small lakes with high flow-through may not play a substantial role as sinks for mercury and organic carbon released from thawing permafrost, especially if thaw increases hydrological connectivity and flow.

Mercury and organic carbon flux rates are often corrected for FF to be able to compare values across different systems, especially for mercury where the goal is to infer atmospheric transport from industrial emissions (Lockhart et al., 1998; Muir et al., 2009). SC2 recorded the highest average corrected mercury flux rate of all 14 lakes, with a value of 8.4 ± 2.9 ng/cm^2/yr. Hg burial rates in lake sediment cores across the north are changing as a result of catchment transport processes, independent of anthropogenic emissions, especially in watersheds where permafrost thaw is causing significant change (Deison et al., 2012; Korosi et al., 2015). For organic carbon burial rates, SC3 exhibits the highest average corrected flux rate, recording 0.597 g/cm^2/yr (0.358 g/cm^2/yr uncorrected for FF). This rate is lower compared to average carbon burial rates in lakes reported by Dean and Gorham (1998), which typically fell within the range of 14 g/cm^2/yr. SC6 had the highest uncorrected average organic carbon flux rate (0.440 g/cm^2/yr), and a FF of 0.73.

5.3 Relationship between hydrological connectivity and OC & Hg burial

The research also qualitatively examined the role that channel fens and bogs might play in the transport, processing, and accumulation of organic carbon and mercury in these lakes and subsequent burial in lake sediments, focusing on 9 of the 14 study lakes where land classification data was available (Coleman et al., 2023). Permafrost degradation in the Taiga Plains has resulted in transformation of forested plateaus to permafrost-free bogs and fens (Quinton et al., 2011; Gibson et al., 2020). The prevalence of bogs and fens is known to have an impact on carbon and mercury export to aquatic systems (Schelker et al., 2011; Giesler et al., 2017). Thus, we can hypothesize that the proportion of bogs and fens on a lake's shoreline may regulate mercury and carbon transport and burial in lake sediments, and that changes in shoreline landscape characteristics will alter mercury and carbon dynamics in lakes. In particular, the presence of channel fens, which act as conveyors, may increase the downstream transport of organic carbon and mercury into lakes. The headwater lake, Goose Lake, which is the first in the fluvial hydrological chain in the Scotty Creek basin, was one of the few lakes to exhibit decreases in carbon and no change in THg. The lowest average HgF when corrected for sediment focusing was also recorded in Goose Lake. As mentioned above, SC8 is hydrologically isolated because of the lack of channel fens, and recorded higher FF compared to lakes with abundant channel fens. Lake SC5 had less than 10% coverage by channel fens within 250 m of the shoreline, and a FF of 0.67. In contrast, however, Lake SC6 had a higher FF of 0.73, despite 25% coverage of channel fens. The 5 lakes for which land classification data was unavailable all had higher FFs. Additional research is needed to continue to explore the relationship between sediment focussing and organic carbon and mercury burial in sediments, and the controls on sediment focussing in these lakes.

6.0 CONCLUSIONS AND FUTURE DIRECTIONS

6.1 General Conclusions

As the land cover at Scotty Creek is rapidly changing (Camill, 2005; Osterkamp and Romanovsky, 1999) due to accelerated permafrost thaw, there is need for more research to be conducted to understand the limnology of the landscape, including also the fate of carbon and mercury released from thawing permafrost in aquatic ecosystems (Dastoor et al., 2022; Dietz et al., 2022; Walvoord and Striegl, 2021).

This study found that total mercury concentrations increased in 9 of the 14 study lakes, independent of organic carbon, suggesting that the increase in mercury concentration wasn't driven by increasing total carbon. The increase in total mercury was, however, associated with a decrease in C/N in many of the lakes, suggesting that the lake sediments possibly received high proportion of autochthonous (i.e. algal) organic matter, partially supporting the algal scavenging hypothesis. Overall, the results indicate that total organic carbon concentrations have not experienced significant changes over time, but the proportion coming from increased algal production has increased for many lakes, which may be driving an increase in mercury concentrations in some (but not all) of the lakes. Increases in total mercury may have been further driven by anthropogenic mercury emissions, which are known to have increased mercury concentrations across the north (AMAP, 2009).

12 out of the 14 sampled lakes (First Lake, Goose Lake, SC1, SC2, SC3, SC5, SC6, SC8, SC9, SC10, SC11, and SC12) showed increasing trends in carbon and mercury flux rates since ~1850, linked to increased sediment mass accumulation rates. Calculated focussing factors were

<1 for all but one lake (SC12, FF=1.09), indicating that while sedimentation rates may be increasing, the coring areas are eroding more sediment than they are accumulating. This indicates that the lakes may not play a significant role as carbon and mercury sinks, instead acting similar to fens as conveyors of sediment downstream. Sub-surface peaks in sedimentation, and associated peaks in carbon and mercury fluxes, indicate that sedimentation patterns and sediment focussing can be highly variable in these lakes and prone to episodic increases in sedimentation. Overall, the research indicates that sediment accumulation rates are the greatest control on organic carbon and mercury burial, and that hydrological connectivity may be a key control on sediment accumulation in these small, shallow lakes.

6.2 Future Directions

Based on my research findings, I hypothesize that increased hydrological connectivity due to permafrost thaw can increase mercury and organic carbon export to downstream outlets, with small flow-through lakes playing only a minor role as carbon and mercury sinks. This is important to resolve because it suggests that mercury and other organically bound and stored contaminants might be released into Arctic and sub-arctic streams and rivers draining thawing discontinuous permafrost peatlands (AMAP, 2003; Braune et al., 2005; Macdonald et al., 2005; Schiedek et al., 2007; AMAP, 2009). Future research is needed to understand spatial and temporal controls on sediment focussing in these lakes, because sediment focussing will be the process that determines whether organic carbon and mercury are buried in lakes or transported downstream.

I also observed sub-surface peaks in sedimentation rates and organic carbon and mercury fluxes, as well as sub-surface anomalies in organic carbon and mercury concentrations. This indicates that episodic events may alter sedimentation and carbon and mercury dynamics in lakes.

I suggest that this might be related to forest fires, which is something that could be explored in future research. For example, macroscopic charcoal can be used to identify past fire events in sediment cores. The influence of forest fires on northern peatlands is a critical area for future research as there has been an increase in wildfire activity in the boreal environment has increased in the last few decades (Flannigan et al., 2009; Kelly et al., 2013) due to warmer summers (Masrur et al., 2018). Increased fire frequencies across the boreal forest due to warmer, drier climatic conditions will also likely cause more widespread permafrost thaw in peatlands. The Scotty Creek Research Station recently (October, 2022) burned down as a result of a wildfire. Recent increases in wildfire activity due to warmer summers have also been predicted to alter carbon dynamics in the coming century (Smith et al., 2005; Riordan et al., 2006; Hu et al., 2015; Coogan et al., 2019).

7.0 REFERENCES

AMAP. (2003). AMAP Assessment 2002: Human Health in the Arctic. Oslo, Norway: Arctic Monitoring and Assessment Programme.

AMAP. (2009). AMAP Assessment 2009: Human Health in the Arctic. Oslo, Norway: Arctic Monitoring and Assessment Programme.

AMAP. (2011). AMAP Assessment 2011: Mercury in the Arctic. Oslo, Norway: Arctic Monitoring and Assessment Programme.

AMAP. (2021). Arctic Climate Change Update 2021: Key Trends and Impacts. Summary for Policy-Makers. Oslo, Norway: Arctic Monitoring and Assessment Programme.

Anderson, L., Edwards, M., Shapley, M.D., Finney, B.P., & Langdon, C. (2019). Holocene thermokarst lake dynamics in northern interior Alaska: the interplay of climate, fire, and subsurface hydrology. *Frontiers in Earth Science, 7,* 53.

Anderson, N.J., Dietz, R.D., & Engstrom, D.R. (2013). Land-use change, not climate, controls organic carbon burial in lakes. *Proceedings of the Royal Society of London. Series B, Biological Sciences, 280*, 20131278.

Anderson, N.J., Heathcote, A. J., & Engstrom, D. R. (2020). Anthropogenic alteration of nutrient supply increases the global freshwater carbon sink. *Science Advances, 2145*.

Anthony, K.M., Zimov, S.A., Grosse, G., Jones, M.C., Anthony, P.M., FS III, C., Finlay, J.C., Mack, M.C., Davydov, S., Frenzel, P., & Frolking, S. (2014). A shift of thermokarst lakes from carbon sources to sinks during the Holocene epoch. *Nature*, ***511***(7510), 452- 456.

Appleby, P.G. (1997). Dating of sediments by ^{210}Pb: Problems and Solutions. In Proceedings of a seminar 'Dating of sediments and determination of sedimentation rate', Helsinki, STUK, A145:7.

Appleby, P.G. & Oldfield, F. (1978) The calculation of lead-210 dates assuming a constant rate of supply of unsupported ^{210}Pb to the sediment. *Catena*, *5*(1), 1–8.

Appleby P. G. & Oldfield F. (1992). Application of ^{210}Pb to sedimentation studies, [in:] Uranium-series disequilibrium: application to Earth, marine, and environmental sciences, M. Ivanovich & R. S. Harmon (eds.), Clarendon Press, Oxford, 731–778.

Ariya, P.A., Dastroor, A.P., Amyot, M., Schroeder, W.H., Barrie, L., Anlauf, K., Raofie, F., Ryzhkov, A., Davignon, D., Lalonde, J., & Steffen, A. (2004). The Arctic: a sink for mercury. *Tellus B: Chemical and Physical Meteorology, 56*(5), 397-403.

Baltzer, J.L., Veness, T., Chasmer, L.E., Sniderhan, A.E., & Quinton, W.L. (2014). Forests on thawing permafrost: Fragmentation, edge effects, and net forest loss. *Global Change Biology, 20*(3), 824-834.

Bastviken, D., Cole, J.J., Pace, M.L., & Van de Bogert, M.C. (2008). Fates of methane from different lake habitats: Connecting whole-lake budgets and CH_4 emissions. *Journal of Geophysical Research: Biogeosciences, 113*(G2).

Bastviken, D., Cole, J., Pace, M., & Tranvik, L. (2004). Methane emissions from lakes: Dependence of lake characteristics, two regional assessments, and a global estimate. *Global Biogeochemical Cycles, 18*(4).

Battin, T.J., Luyssaert, S., Kaplan, L.A., Aufdenkampe, A.K., Richter, A., & Tranvik, L. J. (2009). The boundless carbon cycle. *Nature Geoscience, 2*(9), 598–600. doi:10.1038/ngeo618.

Baud, A., Jenny, J.P., Francus, P., & Gregory-Eaves, I. (2021). Global acceleration of lake sediment accumulation rates associated with recent human population growth and land-use changes. *Journal of Paleolimnology, 66*(4), 453-467.

Beilman, D.W. & Robinson, S.D. (2003). Peatland permafrost thaw and landform type along a climate gradient. In: Phillips M., Springman S.M. & Arenson L.U. (eds.), *Proceedings of the Eighth International Conference on Permafrost, 1,* 61–65.

Benoit, J.M., Gilmour, C.C., Heyes, A., Mason, R.P., & Miller, C. (2003). Geochemical and biological controls over methylmercury production and degradation in aquatic ecosystems. *American Chemical Society,* 262-297.

Bierman, P.R., Albrecht, A., Bothner, M.H., Brown, E.T., Bullen, T.D., Gray, L.B., & Turpin L. (1998). Erosion, weathering and sedimentation, [in:] Isotope tracers on catchment hydrology, C. Kendall & J. J. McDonnell (eds.), Amsterdam, *Elsevier,* 839.

Biester, H., Bindler, R., Martinez-Cortizas, A., & Engstrom, D.R. (2007). Modeling the past atmospheric deposition of mercury using natural archives. *Environmental Science & Technology*, *41*(14), 4851-4860.

Biester, H., M. Pérez-Rodríguez, B. -S. Gilfedder, A. M. Cortizas, and Y. -M. Hermanns. 2018. Solar irradiance and primary productivity-controlled mercury accumulation in sediments of a remote lake in the Southern Hemisphere during the past 4000 years. *Limnology and Oceanography*, *63*, 540–549.

Biskaborn, B.K., Smith, S.L., Noetzli, J., Matthes, H., Vieira, G., Streletskiy, D.A., Schoeneich, P., Romanovsky, V.E., Lewkowicz, A.G., Abramov, A., Allard, M., Boike, J., Cable, W.L., Christiansen, H.H., Delaloye, R., Diekmann, B., Drozdov, D., Etzelmüller, B., Grosse, G., Guglielmin, M., Ingeman-Nielsen, T., Isaksen, K., Ishikawa, M., Johansson, M., Johannsson, H., Joo, A., Kaverin, D., Kholodov, A., Konstantinov, P., Kröger, T., Lambiel, C., Lanckman, J.P., Luo, D., Malkova, G., Meiklejohn, I., Moskalenko, N., Oliva, M., Phillips, M., Ramos, M., Sannel, A.B.K., Sergeev, D., Seybold, C., Skryabin, P., Vasiliev, A., Wu, Q., Yoshikawa, K., Zheleznyak, M., & Lantuit, H. (2019). Permafrost is warming at a global scale, *Nature Communications*, *10*, 264.

Blais, J.M., Kalff, J., Cornett, R.J., & Evans, R.D. (1995). Evaluation of ^{210}Pb dating in lake sediments using stable Pb, ambrosia pollen, and ^{137}Cs. *Journal of Paleolimnology*, *13*(2), 169–178. doi:10.1007/BF00678105.

Blattmann, T.M., Liu, Z., Zhang, Y., Zhao, Y., Haghipour, N., Montluçon, D.B., Plötze, M., & Eglinton, T.I. (2019). Mineralogical control on the fate of continentally derived organic matter in the ocean. *Science*, *366*, 742-745.

Bouchard, F., MacDonald, L.A., Turner, K.W., Thienpont, J.R., Medeiros, A.S., Biskaborn, B.K., Korosi, J.B., Hall, R.I., Pienitz, R., & Wolfe, B.B. (2016). Paleolimnology of thermokarst lakes: a window into permafrost landscape evolution. *Arctic Science*, *3*, 91-117.

Branfireun, B.A. & Roulet, N.T. (2002). Controls on the fate and transport of methylmercury in a boreal headwater catchment, northwestern Ontario, Canada. *Hydrology and Earth System Sciences*, *6*(4), 785-794.

Brännvall, M.L., Bindler, R., Emteryd, O., Nilsson, M., & Renberg, I. (1997). Stable isotope and concentration records of atmospheric lead pollution in peat and lake sediments in Sweden. *Water, Air, and Soil Pollution, 100,* 243-252.

Braune, B.M., Outridge, P.M., Fisk, A.T., Muir, D.C.G., Helm, P.A., Hobbs, K., Hoekstra, P.F., Kuzyk, Z.A., Kwan, M., Letcher, R.J., Lockhart, W.J., Norstrom, R.J., Stern, G.A., & Stirling, I. (2005). Persistent organic pollutants and mercury in marine biota of the Canadian Arctic: an overview of spatial and temporal trends. *Science of the Total Environment, 351,* 4-56.

Bravo, A.G. & Cosio, C. (2020). Biotic formation of methylmercury: A bio–physico–chemical conundrum. *Limnology and Oceanography, 65,* 1010–1027. doi:10.1002/lno.11366.

Brazeau, M.L., Poulain, A.J., Paterson, A.M., Keller, W.B., Sanei, H., & Blais, J.M. (2013). Recent changes in mercury deposition and primary productivity inferred from sediments of lakes from the Hudson Bay Lowlands, Ontario, Canada. *Environmental Pollution, 173,* 52-60. doi:10.1016/j.envpol.2012.09.017.

Brown, J., Ferrians Jr., O.J., Heginbottom, J.A., & Melnikov, E.S. (1997). Circum-Arctic Map of Permafrost and Ground-Ice Conditions, U.S. Geological Survey, Washington, D.C., Circum-Pacific Map Series CP–45.

Brown, R.J.E. (1970). *Proceedings of the 3rd International Peat Congress,* 174–181 (National Research Council of Canada, 1970).

Burke, E.J., Hartley, I.P., & Jones, C.D. (2012). Uncertainties in the global temperature change caused by carbon release from permafrost thawing. *The Cryosphere, 6*(5), 1063-1076.

Burke, S.M., Zimmerman, C.E., Branfireun, B.A., Koch, J.C., & Swanson, H.K. (2018). Patterns and controls of mercury accumulation in sediments from three thermokast lakes on the Arctic Coastal Plain of Alaska. *Aquatic Sciences, 80,* 1. doi:10.1007/s00027-017-0553-0.

Burn, C.R. & Smith C.A.S. (1988). Observations of the "thermal offset" in near-surface mean annual ground temperatures at several sites near Mayo, Yukon Territory, Canada. *Arctic, 41,* 99–104.

Camill, P. (2005). Permafrost thaw accelerates in boreal peatlands during late-20th century climate warming. *Climate Change, 68,* 135–152. doi:10.1007/s10584-005-4785-y.

Carpino, O., Haynes, K., Connon, R., Craig, J., Devoie, É., & Quinton, W. (2021). Long-term climate-influenced land cover change in discontinuous permafrost peatland complexes. *Hydrology and Earth System Sciences, 25*(6), 3301–3317.

Carrie, J., Wang, F., Sanei, H., Macdonald, R.W., Outridge, P.M., & Stern, G.A. (2010). Increasing contaminant burdens in an Arctic fish, burbot (Lota lota), in a warming climate. *Environmental Science & Technology, 44*, 316–322. doi:10.1021/es902582y.

Chasmer, L. & Hopkinson, C. (2017). Threshold loss of discontinuous permafrost and landscape evolution. *Global Change Biology, 23*(7), 2672–2686.

Chasmer, L., Hopkinson, C., Veness, T., Quinton, W., & Baltzer, J. (2014). A decision-tree classification for low-lying complex land cover types within the zone of discontinuous permafrost. *Remote Sensing of Environment, 143*, 73-84.

Chasmer, L., Quinton, W.L., Hopkinson, C., Petrone, R., & Whittington, P. (2011). Vegetation canopy and radiation controls on permafrost plateau evolution within the discontinuous permafrost zone, Northwest Territories, Canada. *Permafrost and Periglacial Processes, 22*, 199–213.

Chételat, J., McKinney, M.A., Amyot, M., Dastoor, A., Douglas, T.A., Heimbürger-Boavida, L., Kirk, J., Kahilainen, K.K., Outridge, P.M., Pelletier, N., Skov, H., St. Pierre, K., Vuorenmaa, J., & Wang, F. (2022). Climate change and mercury in the Arctic: Abiotic interactions. *Science of The Total Environment, 824*, 153715. doi:10.1016/j.scitotenv.2022.153715.

Chmiel, H.E., Niggemann, J., Kokic, J., Ferland, È., Dittmar, T., & Sobek, S. (2015). Uncoupled organic matter burial and quality in boreal lake sediments over the Holocene. *Journal of Geophysical Research: Biogeosciences, 120*(9), 1751-1763. doi:10.1002/2015JG002987.

Cole, J.J., Prairie, Y.T., Caraco, N.F., McDowell, W.H., Tranvik, L.J., Striegl, R.G., Duarte, C.M., Kortelainen, P., Downing, J.A., Middelburg, J.J., & Melack, J. (2007). Plumbing the Global Carbon Cycle: Integrating Inland Waters into the Terrestrial Carbon Budget. *Ecosystems, 10*(1), 172–185. doi:10.1007/s10021-006-9013-8.

Coleman, K.A., Hoskin, G.N., Chasmer, L., Thienpont, J.R., Quinton, W.L., & Korosi, J.B. (2023). Limnology and diatom ecology of shallow lakes in a rapidly thawing discontinuous permafrost peatland. *Inland Waters, 13*(1), 13-29.

Coleman, K.A., Palmer, M.J., Korosi, J.B., Kokelj, S.V., Jackson, K., Hargan, K.E., Courtney Mustaphi, C.J., Thienpont, J.R., Kimpe, L.E., Blais, J.M., Pisaric, M.F.J., & Smol, J.P. (2015). Tracking the impacts of recent warming and thaw of permafrost peatlands on aquatic ecosystems: a multi-proxy approach using remote sensing and lake sediments. *Boreal Environment Research, 20,* 363–377.

Connon, R.F., Chasmer, L., Haughton, E., Helbig, M., Hopkinson, C., Sonnentag, O., & Quinton, W.L. (2021). The implications of permafrost thaw and land cover change on snow water equivalent accumulation, melt and runoff in discontinuous permafrost peatlands. *Hydrological Processes, 35*(9), e14363.

Connon, R.F., Quinton, W.L., Craig, J.R., & Hayashi, M. (2014). Changing hydrologic connectivity due to permafrost thaw in the lower Liard River valley, NWT, Canada. *Hydrological Processes, 28*(14), 4163-4178.

Coogan, S.C., Robinne, F.N., Jain, P., & Flannigan, M.D. (2019). Scientists' warning on wildfire—a Canadian perspective. *Canadian Journal of Forest Research, 49*(9), 1015-1023.

Cooke, C.A., Hobbs, W.O., Neal, M., & Wolfe, A.P. (2010). Reliance on ^{210}Pb chronology can compromise the inference of preindustrial Hg flux to lake sediments. *Environmental Science & Technology, 44,* 1998–2003.

Cooke, C.A., Wolfe, A.P., Michelutti, N., Balcom, P.H., & Briner, J.P. (2012). A Holocene perspective on algal mercury scavenging to sediments of an Arctic Lake. *Environmental Science & Technology, 46,* 7135–7141. doi:10.1021/es3003124.

Couillard, Y., Cattaneo, A., Gallon, C., & Courcelles, M. (2008). Sources and chronology of fifteen elements in the sediments of lakes affected by metal deposition in a mining area. *Journal of Paleolimnology, 40*(1): 97-114.

Dastoor, A., Angot, H., Bieser, J., Christensen, J.H., Douglas, T.A., Heimbürger-Boavida, L.E., Jiskra, M., Mason, R.P., McLagan, D.S., Obrist, D., & Outridge, P.M. (2022). Arctic mercury cycling. *Nature Reviews Earth & Environment, 3*(4), 270-286.

Davis, R.B., Hess, C.T., Norton, S.A., Hanson, D.W., Hoagland, K.D., & Anderson, D.S. (1984). ^{137}Cs and ^{210}Pb dating of sediments from soft-water lakes in New England (USA) and Scandinavia, a failure of ^{137}Cs dating. *Chemical Geology, 44*(1-3), 151-185.

de Wit, H.A., Valinia, S., Weyhenmeyer, G.A., Futter, M.N., Kortelainen, P., Austnes, K., Hessen, D.O., Räike, A., Laudon, H., Vuorenmaa, J., 2016. Current browning of surface waters will be further promoted by wetter climate. *Environmental Science & Technology Letters, 12*(3), 430–435.

Dean, W. E. & Gorham, E. (1998). Magnitude and significance of carbon burial in lakes, reservoirs, and peatlands. *Geology, 26*, 535–538.

Deison, R., Smol, J.P., Kokelj, S.V., Pisaric, M.F.J., Kimpe, L.E., Poulain, A.J., Sanei, H., Thienpont, J.R., & Blais, J.M. (2012). Spatial and temporal assessment of mercury and organic matter in thermokarst affected lakes of the Mackenzie Delta Uplands, NT, Canada. *Environmental Science & Technology, 46,* 8748–8755. doi: 10.1021/es300798w.

Del Giorgio, P.A., Cole, J.J., Caraco, N.F., & Peters, R.H. (1999). Linking planktonic biomass and metabolism to net gas fluxes in northern temperate lakes. *Ecology, 80*(4), 1422-1431.

Delisle, G. (2007). Near-surface permafrost degradation: how severe during the 21st century*? Geophysical Research Letters, 34,* L09503. doi:10.1029/2003GL029323.

Devoie, É.G., Craig, J.R., Connon, R.F., & Quinton, W.L. (2019). Taliks: A tipping point in discontinuous permafrost degradation in peatlands. *Water Resources Research, 55*, 9838–9857. doi:10.1029/2018WR024488.

Dietz, R., Letcher, R.J., Aars, J., Andersen, M., Boltunov, A., Born, E.W., Ciesielski, T.M., Das, K., Dastnai, S., Derocher, A.E., & Desforges, J.P. (2022). A risk assessment review of mercury exposure in Arctic marine and terrestrial mammals. *Science of the Total Environment, 829,* 154445.

Downing, J.A., Cole, J.J., Middelburg, J.J., Striegl, R.G., Duarte, C.M., Kortelainen, P., Prairie, Y.T., & Laube, K.A. (2008). Sediment organic carbon burial in agriculturally eutrophic impoundments over the last century. *Global biogeochemical cycles*, *22*(1).

Downing, J.A., Prairie, Y.T., Cole, J.J., Duarte, C.M., Tranvik, L.J., Striegl, R.G., McDowell, W.H., Kortelainen, P., Caraco, N.F., Melack, J.M., & Middelburg, J.J (2006). The global abundance and size distribution of lakes, ponds, and impoundments. *Limnology and Oceanography, 51*(5), 2388-2397.

Driscoll, C.T., Blette, V., Yan, C., Schofield, C.L., Munson, R., & Holsapple, J. (1995). The role of dissolved organic carbon in the chemistry and bioavailability of mercury in remote Adirondack lakes. *Water, Air, and Soil Pollution, 80,* 499-508.

Durnford, D., Dastoor, A., Figueras-Nieto, D., & Ryjkov, A. (2010). Long range transport of mercury to the Arctic and across Canada. *Atmospheric Chemistry and Physics, 10*(13), 6063-6086.

Eckley, C.S. & Hintelmann, H. (2006). Determination of mercury methylation potentials in the water column of lakes across Canada. *Science of the Total Environment, 368*(1), 111-125.

Eckley, C.S., Watras, C.J., Hintelmann, H., Morrison, K., Kent, A.D., & Regnell, O. (2005). Mercury methylation in the hypolimnetic waters of lakes with and without connection to wetlands in northern Wisconsin. *Canadian Journal of Fisheries and Aquatic Sciences, 62*(2), 400-411.

Engstrom, D.R. & Rose, N.L. (2013). A whole-basin, mass-balance approach to paleolimnology. *Journal of Paleolimnology, 49*, 333-347.

Engstrom, D.R. (1984). Lake Development in the Boreal Peatlands of Southeastern Labrador, Canada. *Arctic, Antarctic, and Alpine Research, 16,* 447–452.

Fahnestock, M.F., Bryce, J.G., McCalley, C.K., Montesdeoca, M., Bai, S., Li, Y., Driscoll, C.T., Crill, P.M., Rich, V.I., & Varner, R.K. (2019). Mercury reallocation in thawing subarctic peatlands. *Geochemical Perspectives Letters, 11,* 33–38.

Ferland, M.E., del Giorgio, P.A., Teodoru, C.R., & Prairie, Y.T. (2012). Long-term C accumulation and total C stocks in boreal lakes in northern Québec. *Global Biogeochemical Cycles, 26*(4). doi:10.1029/2011GB004241.

Finger, R.A., Turetsky, M.R., Kielland, K., Ruess, R.W., Mack, M.C., & Euskirchen, E.S. (2016). Effects of permafrost thaw on nitrogen availability and plant–soil interactions in a boreal Alaskan lowland. *Journal of Ecology, 104*(6), 1542-1554. doi:10.1111/1365-2745.12639.

Fitzgerald, W.F., Engstrom, D.R., Lamborg, C.H., Tseng, C.M., Balcom, P.H., & Hammerschmidt, C.R. (2005). Modern and historic atmospheric mercury fluxes in northern Alaska: Global sources and Arctic depletion. *Environmental Science & Technology, 39*, 557–568.

Flannigan, M.D., Krawchuk, M.A., de Groot, W.J., Wotton, B.M., & Gowman, L.M. (2009). Implications of changing climate for global wildland fire. *International Journal of Wildland Fire, 18*(5), 483-507.

Fouché, J., Christiansen, C.T., Lafrenière, M.J., Grogan, P. & Lamoureux, S.F. (2020). Canadian permafrost stores large pools of ammonium and optically distinct dissolved organic matter. *Nature Communications,* 11: 4500.

Garmo, Ø.A., Skjelkvåle, B.L., de Wit, H.A., Colombo, L., Curtis, C., Fölster, J., Hoffmann, A., Hruška, J., Høgåsen, T., Jeffries, D.S., & Keller, W.B. (2014). Trends in surface water chemistry in acidified areas in Europe and North America from 1990 to 2008. *Water, Air, & Soil Pollution, 225*, 1-14.

Gibson, C.M., Chasmer, L.E., Thompson, D.K., Quinton, W.L., Flannigan, M.D., & Olefeldt, D. (2018). Wildfire as a major driver of recent permafrost thaw in boreal peatlands. *Nature Communications, 9*(1), 1-9. doi:10.1038/s41467-018-05457-1.

Gibson, C., Morse, P.D., Kelly, J.M., Turetsky, M.R., Baltzer, J.L., Gingras-Hill, T., & Kokelj, S.V. (2020). Thermokarst Mapping Collective: Protocol for organic permafrost terrain and preliminary inventory from the Taiga Plains test area. Northwest Territories, appendix, and digital data, NWT Open Report, 10.

Giesler, R., Clemmensen, K.E., Wardle, D.A., Klaminder, J., & Bindler, R. (2017). Boreal forests sequester large amounts of mercury over millennial time scales in the absence of wildfire. *Environmental science & technology, 51*(5), 2621-2627.

Gilmour, C.C., Henry, E.A., & Mitchell, R. (1992). Sulfate stimulation of mercury methylation in freshwater sediments. *Environmental Science & Technology, 26*(11), 2281-2287.

Gilmour, C.C., Riedel, G.S., Ederington, M.C., Bell, J.T., Gill, G.A., & Stordal, M.C. (1998). Methylmercury concentrations and production rates across a trophic gradient in the northern Everglades. *Biogeochemistry, 40*, 327-345.

Gilmour, C.C., Podar, M., Bullock, A.L., Graham, A.M., Brown, S.D., Somenahally, A.C., Johs, A., Hurt Jr, R.A., Bailey, K.L., & Elias, D.A. (2013). Mercury methylation by novel microorganisms from new environments. *Environmental Science & Technology, 47*(20), 11810-11820.

Glew, J.R. (1988). A portable extruding device for close interval sectioning of unconsolidated core samples. *Journal of Paleolimnology*, *1*(3), 235–239.

Gopikrishna, V.G., Kannan, V., Binish, M.B., Abdul Shukkur, M., Krishnan, K.P., & Mohan, M. (2020). Mercury in the sediments of freshwater lakes in Ny-Ålesund, Arctic. *Environmental Monitoring and Assessment, 192*. doi:10.1007/s10661-020- 08511-y.

Gordon, J., Quinton, W., Branfireun, B.A., Olefeldt, D. (2016). Mercury and methylmercury biogeochemistry in a thawing permafrost wetland complex, Northwest Territories, Canada. *Hydrological Processes, 30*, 3627–3638.

Graneli, W., Lindell, M.J., & Tranvik, L.J. (1996). Photo-oxidative production of dissolved inorganic carbon in lakes of different humic content. *Limnology and Oceanography, 41*, 698-706.

Grasby, S.E., Sanei, H., Beauchamp, B., & Chen, Z. (2013). Mercury deposition through the Permo-Triassic biotic crisis. *Chemical Geology, 351*, 209–216.

Grigal, D.F. (2003). Mercury sequestration in forests and peatlands: a review. *Journal of Environmental Quality, 32*(2), 393-405.

Grosse, G., Jones, B., & Arp, C. (2013). Thermokarst lakes, drainage, and drained basins. *In Treatise on Geomorphology*. Edited by J.F. Shroder. Academic Press, San Diego, California, 325–353.

Gudasz, C., Bastviken, D., Premke, K., Steger, K., & Tranvik, L.J. (2012). Constrained microbial processing of allochthonous organic carbon in boreal lake sediments. *Limnology and Oceanography*, *57*, 163–175. doi:10.4319/lo.2012.57.1.0163.

Guillemette, F., von Wachenfeldt, E., Kothawala, D.N., Bastviken, D., & Tranvik, L.J. (2017). Preferential sequestration of terrestrial organic matter in boreal lake sediments: Preferential Terrestrial C Sequestration. *Journal of Geophysical Research: Biogeosciences, 122*(4), 863–874. doi:10.1002/2016JG003735.

Guo, L., Semiletov, I., Gustafsson, O., Ingri, J., Anderson, P., Dudarev, O., & White, D. (2004). Characterization of Siberian Arctic coastal sediments: Implications for terrestrial organic carbon export. *Global Biogeochemical Cycles, 18*, GB1036. doi:10.1029/2003GB002087.

Gustafsson, O., van Dongen, B. E., Vonk, J. E., Dudarev, O. V., & Semiletov, I. P. (2011). Widespread release of old carbon across the Siberian Arctic echoed by its large rivers. *Biogeosciences, 8*(6), 1737–1743.

Haitzer, M., Aiken, G.R., & Ryan, J.N. (2003). Binding of mercury (II) to aquatic humic substances: Influence of pH and source of humic substances. *Environmental Science & Technology, 37*(11), 2436-2441.

Harris, D., Horwáth, W.R., & Van Kessel, C. (2001). Acid fumigation of soils to remove carbonates prior to total organic carbon or carbon-13 isotopic analysis. *Soil Science Society of America Journal, 65*(6), 1853-1856.

Haynes, K.M., Connon, R.F., & Quinton, W.L. (2018). Permafrost thaw induced drying of wetlands at Scotty Creek, NWT, Canada. *Environmental Research Letters, 13*(11), 114001.

Heathcote, A.J., Anderson, N.J., Prairie, Y.T., Engstrom, D.R., & Del Giorgio, P.A. (2015). Large increases in carbon burial in northern lakes during the Anthropocene. *Nature Communications, 6,* 10016.

Hegginbottom, A. J., Dubreil, M. A., & Harker, P. T. (1995). Canada, permafrost. *National Atlas of Canada* (5th Ed.) (Natural Resources Canada, MCR 4177).

Hemingway, J.D., Schefuß, E., Spencer, R.G.M., Dinga, B.J., Eglinton, T.I., McIntyre, C., & Galy, V.V. (2017). Hydrologic controls on seasonal and inter-annual variability of Congo River particulate organic matter source and reservoir age. *Chemical Geology, 466*, 454–465. doi:10.1016/j.chemgeo.2017.06.034.

Hermanns, Y.M. & Biester, H. (2013). A 17,300-year record of mercury accumulation in a pristine lake in southern Chile. *Journal of Paleolimnology, 49*, 547–561.

Hermanns, Y.M., Cortizas, A., Arz, H., Stein, R., & Biester, H. (2013). Untangling the influence of in-lake productivity and terrestrial organic matter flux on 4,250 years of mercury accumulation in Lake Hambre, southern Chile. *Journal of Paleolimnology, 49,* 563–573. doi:10.1007/s10933-012-9657-7.

Hermanson, M.H. & Christensen, E.R. (1991b). Recent sedimentation in Lake Michigan. *Journal of Great Lakes Research, 17*(1), 33-50.

Heslop, J.K., Walter Anthony, K.M., Winkel, M., Sepulveda-Jauregui, A., Martinez-Cruz, K., Bondurant, A., Grosse, G., & Liebner, S. (2020). A synthesis of methane dynamics in thermokarst lake environments. *Earth-Science Reviews, 210*. doi:10.1016/j.earscirev.2020.103365.

Hill, J.R., O'Driscoll, N.J., & Lean, D.R.S. (2009). Size distribution of methylmercury associated with particulate and dissolved organic matter in freshwaters. *Science of the Total Environment, 408,* 408– 414.

Hintelmann, H., Harris, R., Heyes, A., Hurley, J.P., Kelly, C.A., Krabbenhoft, D.P., Lindberg, S., Rudd, J.W., Scott, K.J., & St. Louis, V.L. (2002). Reactivity and mobility of new and old mercury deposition in a boreal forest ecosystem during the first year of the METAALICUS study. *Environmental Science & Technology, 36*(23), 5034-5040.

Hobbs, W.O., Engstrom, D.R., Scottler, S.P., Zimmer, K.D., & Cotner, J.B. (2013). Estimating modern carbon burial rates in lakes using a single sediment sample. *Limnology and Oceanography: Methods, 11*(6), 316-326.

Holmes, R.M., McClelland, J.W., Peterson, B.J., Tank, S.E., Bulygina, E., Eglinton, T.I., Gordeev, V.V., Gurtovaya, T.Y., Raymond, P.A., Repeta, D.J., & Staples, R. (2012). Seasonal and annual fluxes of nutrients and organic matter from large rivers to the Arctic Ocean and surrounding seas. *Estuaries and Coasts, 35*, 369-382.

Houghton, R.A., (2003). Revised estimates of the annual net flux of carbon to the atmosphere from changes in land use and land management 1850–2000. *Tellus B: Chemical and Physical Meteorology, 55*(2), 378–390. doi:10.3402/tellusb.v55i2.16764.

Hu, F.S., Higuera, P.E., Duffy, P., Chipman, M.L., Rocha, A.V., Young, A.M., Kelly, R., & Dietze, M.C. (2015). Arctic tundra fires: natural variability and responses to climate change. *Frontiers in Ecology and the Environment, 13*(7), 369-377.

Jackson, T.A. (1986). Methyl mercury levels in a polluted prairie river–lake system: seasonal and site-specific variations, and the dominant influence of trophic conditions. *Canadian Journal of Fisheries and Aquatic Sciences, 43*(10), 1873-1887.

Jansson, M., Bergstrom, A.K., Blomqvist, P., & Drakare, S. (2000). Allochthonous organic carbon and phytoplankton/ bacterioplankton production relationship in lakes. *Ecology, 81*, 3250–3255.

Jiang, S., Liu, X., & Chen, Q. (2011). Distribution of total mercury and methylmercury in lake sediments in Arctic Ny-Ålesund. *Chemosphere, 83*(8), 1108–1116.

Johannessen, O.M., Bengtsson, L., Miles, M.W., Kuzmina, S.I., Semenov, V.A., Alekseev, G.V., Nagurnyi, A.P., Zakharov, V.F., Bobylev, L.P., Pettersson, L.H., Hasselmann, K., & Cattle, H.P. (2004). Arctic climate change: observed and modelled temperature and sea-ice variability. *Tellus A: Dynamic Meteorology and Oceanography, 56*(4), 328-341.

Jones, M. C. & Yu, Z. (2010). Rapid deglacial and early Holocene expansion of peatlands in Alaska. *Proceedings of the National Academy of Sciences, 107*(16), 7347-7352.

Jorgenson, M.Y., Shur, Y.L., & Osterkamp, T.E. (2008). Thermokarst in Alaska. In Kane D.L., and Hinkel K.M. (eds). *Proceedings of the Ninth International Conference on Permafrost*, 29 June – 3 July 2008, Fairbanks, Alaska. Institute of Northern Engineering, University of Alaska, Fairbanks, Alaska, 869-876.

Jorgenson, M.T., Romanovsky, V., Harden, J., Shur, Y., O'Donnell, J., Schuur, E. A. G., Kanevskiy, M., & Marchenko, S. (2010). Resilience and vulnerability of permafrost to climate change. *Canadian Journal of Forest Research, 40*(7), 1219–1236. doi:10.1139/X10-060.

Kainz, M., Lucotte, M., & Parrish, C.C. (2003). Relationships between organic matter composition and methyl mercury content of offshore and carbon-rich littoral sediments in an oligotrophic lake. *Canadian Journal of Fisheries and Aquatic Sciences, 60*(7), 888-896.

Keil, R.G., Mayer, L.M., Quay, P.D., Richey, J.E., & Hedges, J.I. (1997). Loss of organic matter from riverine particles in deltas. *Geochimica et Cosmochimica Acta, 61*(7), 1507-1511.

Kelly, R., Chipman, M.L., Higuera, P.E., Stefanova, I., Brubaker, L.B., & Hu, F.S. (2013). Recent burning of boreal forests exceeds fire regime limits of the past 10,000 years. *Proceedings of the National Academy of Sciences, 110*(32), 13055-13060.

Kerin, E.J., Gilmour, C.C., Roden, E., Suzuki, M.T., Coates, J.D., & Mason, R. (2006). Mercury methylation by dissimilatory iron-reducing bacteria. *Applied and Environmental Microbiology, 72*(12), 7919-7921.

Kirk, J.L., Muir, D.C., Antoniades, D., Douglas, M.S., Evans, M.S., Jackson, T.A., Kling, H., Lamoureux, S., Lim, D.S.S., Pienitz, R., Smol, J.P., Stewart, K., Wang, X., & Yang, F. (2011). Climate change

and mercury accumulation in Canadian high and subarctic lakes. *Environmental Science & Technology, 45*(3), 964-970.

Klaminder, J., Appleby, P., Crook, P., & Renberg, I. (2012). Post-deposition diffusion of 137Cs in lake sediment: Implications for radiocaesium dating. *Sedimentology, 59*(7), 2259-2267.

Kling, G.W., Kipphut, G.W., & Miller, M.C. (1991). Arctic lakes and streams as gas conduits to the atmosphere: implications for tundra carbon budgets. *Science, 251*(4991), 298-301.

Kokelj, S.V. & Jorgenson, M.T. (2013). Advances in thermokarst research. *Permafrost and Periglacial Processes, 24*(2), 108-119.

Kokfelt, U., Reuss, N., Struyf, E., Sonesson, M., Rundgren, M., Skog, G., Rosen, P., & Hammarlund, D. (2010) Wetland development, permafrost history and nutrient cycling inferred from late Holocene peat and lake sediment records in subarctic Sweden. *Journal of Paleolimnology, 44*, 327-342.

Kolka, R.K., Grigal, D.F., Verry, E.S., & Nater, E.A. (1999) Mercury and organic carbon relationships in streams draining forested upland/peatland watersheds. *Journal of Environmental Quality, 28*, 766–775.

Korosi, J.B., Griffiths, K., Smol, J.P., & Blais, J.M. (2018). Trends in historical mercury deposition inferred from lake sediment cores across a climate gradient in the Canadian High Arctic. *Environmental Pollution, 241*, 459-467.

Korosi, J.B., Coleman, K.A., Hoskin, G., Little, A.J., Stewart, E.M., & Thienpont, J.R. (2022). Paleolimnological perspectives on the shifting geographic template of permafrost landscapes and its implications for Arctic freshwater biodiversity. *Canadian Journal of Fisheries and Aquatic Sciences, 79*(7): 1162-1172. doi:10.1139/cjfas-2021-0280.

Korosi, J.B., McDonald, J., Coleman, K.A., Palmer, M.J., Smol, J.P, Simpson, M.J., & Blais, J.M. (2015). Long-term changes in organic matter and mercury transport to lakes in the sporadic discontinuous permafrost zone related to peat subsidence. *Limnology and Oceanography, 60*, 1550-1561.

Kortelainen, P., Pajunen, H., Rantakari, M., & Saarnisto, M. (2004). A large carbon pool and small sink in boreal Holocene Lake sediments. *Global Change Biology, 10*(10), 1648-1653.

Kremenetski, K., Velichko, A., Borisova, O., MacDonald, G., Smith, L., Frey, K., & Orlova, L. (2003). Peatlands of the Western Siberian lowlands: Current knowledge on zonation, carbon content and Late Quaternary history. *Quaternary Science Reviews, 22*(5-7), 703-723. doi:10.1016/S0277-3791(02)00196-8.

Krishnaswamy, S., Lal, D., Martin, J.M., & Meybeck, M. (1971). Geochronology of lake sediments. *Earth and Planetary Science Letters, 11*(1-5), 407-414.

Kurylyk, B., Hayashi, M., Quinton, W., McKenzie, J., & Voss, C. (2016). Influence of vertical and lateral heat transfer on permafrost thaw, peatland landscape transition, and groundwater flow. *Water Resources Research, 52*, 1286–1305. doi:10.1002/2015WR018057.

Lalonde, K., Mucci, A., Ouellet, A., & Gélinas, Y. (2012). Preservation of organic matter in sediments promoted by iron. *Nature, 483*(7388), 198-200.

Landers, D.H., Gubala, C., Verta, M., Lucotte, M., Johansson, K., Vlasova, T., & Lockhart, W.L. (1998). Using lake sediment mercury flux ratios to evaluate the regional and continental dimensions of mercury deposition in arctic and boreal ecosystems. *Atmospheric Environment, 32*(5), 919–928. doi:10.1016/S1352- 2310(97)00116-7.

Lattaud, J., Bröder, L., Haghipour, N., Rickli, J., Giosan, L., & Eglinton, T.I. (2021). Influence of Hydraulic Connectivity on Carbon Burial Efficiency in Mackenzie Delta Lake Sediments. *Journal of Geophysical Research: Biogeosciences, 126*(3). doi:10.1029/2020JG006054.

Lawrence, D.M., Slater, A.G., & Swenson, S.C. (2012). Simulation of present-day and future permafrost and seasonally frozen ground conditions in CCSM4. *Journal of Climate, 25*(7), 2207–2225.

Lehnherr, I. (2014). Methylmercury biogeochemistry: a review with special reference to Arctic aquatic ecosystems. *Environmental Reviews, 22*(3), 229-243.

Lehnherr, I., St. Louis, V.L., Sharp, M., Gardner, A.S., Smol, J.P., Schiff, S.L., Muir, D.C., Mortimer, C.A., Michelutti, N., Tarnocai, C., & St. Pierre, K.A. (2018). The world's largest High Arctic lake responds rapidly to climate warming. *Nature Communications, 9*(1), 1290.

Leitch, D.R. (2006). Mercury distribution in water and permafrost of the lower Mackenzie Basin, their contribution to the mercury contamination in the Beaufort Sea marine ecosystem, and potential effects of climate variation.

Leitch, D.R, Carrie, J., Lean, D., Macdonald, R.W., Stern, G.A., & Wang, F. (2007). The delivery of mercury to the Beaufort Sea of the Arctic Ocean by the Mackenzie River. *Science of the Total Environment, 373,* 178–195.

Lim, A.G., Sonke, J.E., Krickov, I.V., Manasypov, R.M., Loiko, S.V., & Pokrovsky, O.S. (2019). Enhanced particulate Hg export at the permafrost boundary, Western Siberia. *Environmental Pollution, 254,* 113083. doi:10.1016/j.envpol.2019.113083.

Lim, A.G., Jiskra, M., Sonke, J.E., Loiko, S.V., Kosykh, N., & Pokrovsky, O.S. (2020). A revised pan-Arctic permafrost soil Hg pool based on Western Siberian peat Hg and carbon observations. *Biogeosciences, 17,* 3083–3097. doi:10. 5194/bg-17-3083-2020.

Lindeberg, C., Bindler, R., Renberg, I., Emteryd, O., Karlsson, E., & Anderson, N.J. (2006). Natural fluctuations of mercury and lead in Greenland lake sediments. *Environmental Science & Technology, 40,* 90–95.

Lockhart, W.L., Stern, G.A., Low, G., Hendzel, M., Boila, G., Roach, P., Evans, M.S., Billeck, B.N., DeLaronde, J., Friesen, S., Kidd, K., Atkins, S., Muir, D.C.G., Stoddart, M., Stephens, G., Stephenson, S., Harbicht, S., Snowshoe, N., Grey, B., Thompson, S., & DeGraff, N. (2005). A history of total mercury in edible muscle of fish from lakes in northern Canada. *Science of The Total Environment, 351,* 427–463.

Lockhart, W.L., Macdonald, R.W., Outridge, P.M., Wilkinson, P., DeLaronde, J.B., Rudd, J.W.M. (2000). Tests of the fidelity of lake sediment core records of mercury deposition to known histories of mercury contamination. *Science of the Total Environment, 260,* 171– 180.

Lockhart, W.L., Wilkinson, P., Billeck, B.N., Danell, R.A., Hunt, R.V., Brunskill, G.J., Delaronde, J., & St Louis, V. (1998). Fluxes of mercury to lake sediments in central and northern Canada inferred from dated sediment cores. *Biogeochemistry, 40,* 163–173.

MacMillan, G.A., Girard, C., Chételat, J., Laurion, I., & Amyot, M. (2015). High methylmercury in Arctic and subarctic ponds is related to nutrient levels in the warming eastern Canadian Arctic. *Environmental Science & Technology, 49*(13), 7743-7753.

Manasypov, R.M., Lim, A.G., Krickov, I.V., Shirokova, L.S., Shevchenko, V.P., Aliev, R.A., Karlsson, J., & Pokrovsky, O.S. (2022). Carbon storage and burial in thermokarst lakes of permafrost peatlands. *Biogeochemistry*, *159*(1), 69–86. doi:10.1007/s10533- 022-00914-y.

Mann, P.J., Davydova, A., Zimov, N., Spencer, R.G.M., Davydov, S., Bulygina, E., Zimov, S., & Holmes, R.M. (2012). Controls on the composition and lability of dissolved organic matter in Siberia's Kolyma River basin. *Journal of Geophysical Research: Biogeosciences, 117*(G1). doi:10.1029/2011JG001798.

Mason, R.P., Reinfelder, J.R., & Morel, F.M.M. (1995). Bioaccumulation of mercury and methylmercury. *Water, Air and Soil Pollution, 80*, 915-921.

Masrur, A., Petrov, A.N., & DeGroote, J. (2018). Circumpolar spatio-temporal patterns and contributing climatic factors of wildfire activity in the Arctic tundra from 2001–2015. *Environmental Research Letters, 13*(1), 014019.

McGuire, A.D., Anderson, L.G., Christensen, T.R., Dallimore, S., Guo, L., Hayes, D.J., Heimann, M., Lorenson, T.D., Macdonald, R.W., & Roulet, N. (2009). Sensitivity of the carbon cycle in the Arctic to climate change. *Ecological Monographs, 79*(4), 523-555.

Meerhoff, M., Clemente, J.M., De Mello, F.T., Iglesias, C., Pedersen, A.R., & Jeppesen, E. (2007). Can warm climate-related structure of littoral predator assemblies weaken the clear water state in shallow lakes? *Global Change Biology, 13*(9), 1888-1897. doi:10.1111/j.1365-2486.2007.01408.x.

Meyers, P.A. & Teranes, J. L. (2001). Sediment organic matter, in Tracking Environmental Change Using Lake Sediments, *Physical Geochemical Methods*, edited by W. M. Last and J. P. Smol, 239–270, Kluwer Acad, Dordrecht, Netherlands.

Michelutti, N., Wolfe, A.P., Vinebrooke, R.D., Rivard, B., & Briner, J.P. (2005). Recent primary production increases in Arctic lakes. *Geophysical Research Letters, 32*(19).

Michelutti, N., Wolfe, A.P., Briner, J.P., Miller, G.H. (2007). Climatically controlled chemical and biological development in Arctic lakes. *Journal of Geophysical Research: Biogeosciences, 112*, G03002.

Mitchell, C.P., Branfireun, B.A., & Kolka, R.K. (2008). Total mercury and methylmercury dynamics in upland–peatland watersheds during snowmelt. *Biogeochemistry, 90*, 225-241.

Monteith, D.T., Stoddard, J.L., Evans, C.D., De Wit, H.A., Forsius, M., Høgåsen, T., Wilander, A., Skjelkvåle, B.L., Jeffries, D.S., Vuorenmaa, J., Keller, B., Kopácek, J., & Vesely, J. (2007). Dissolved organic carbon trends resulting from changes in atmospheric deposition chemistry. *Nature, 450*(7169), 537-540. doi:10.1038/nature06316.

Moore, D.R.J., Pawlisz, A., & Teed, R.S. (2003). Developing Ambient Water Quality Criteria for Mercury: A Probabilistic Site-specific Approach. UK: IWA Publishing.

Muir, D.C.G., Wang, X., Yang, F., Nguyen, N., Jackson, T.A., Evans, M.S., Douglas, M., Kock, G., Lamoureux, S., Pienitz, R., Smol, J.P., Vincent, W.F., & Dastoor, A. (2009). Spatial trends and historical deposition of mercury in eastern and northern Canada inferred from lake sediment cores. *Environmental Science & Technology, 43*(13), 4802-4809.

Mulholland, P.J. & Elwood, J.W. (1982). The role of lake and reservoir sediments as sinks in the perturbed global carbon cycle. *Tellus, 34*(5), 490-499.

Musielak, S. (1985). Sediments of Seas and Oceans. Wydawnictwo Uniwersytetu Gdanskiego, Gdansk, 179.

O'Driscoll, N.J., Covelli, S., Petranich, E., Floreani, F., Klapstein, S., & Acquavita, A. (2019). Dissolved gaseous mercury production at a marine aquaculture site in the mercury-contaminated Marano and Grado Lagoon, Italy. *Bulletin of Environmental Contamination and Toxicology, 103*, 218-224.

O'Driscoll, N.J., Siciliano, S.D., Lean, D.R.S., & Amyot, M. (2006). Gross photoreduction kinetics of mercury in temperate freshwater lakes and rivers: application to a general model of DGM dynamics. *Environmental Science & Technology, 40*, 837–843. doi:10.1021/es051062y.

O'Neill, H.B., Wolfe, S.A., & Duchesne, C. (2019). New ground ice maps for Canada using a paleogeographic modelling approach. *Cryosphere, 13*, 753–773.

Obrist, D., Agnan, Y., Jiskra, M., Olson, C.L., Colegrove, D.P., Hueber, J., Moore, C.W., Sonke, J.E., & Helmig, D. (2017). Tundra uptake of atmospheric elemental mercury drives Arctic mercury pollution. *Nature, 547*(7662), 201-204. doi:10.1038/nature22997.

Obrist, D., Johnson, D. W., Lindberg, S.E., Luo, Y., Hararuk, O., Bracho, R., Battles, J.J., Dail, D.B., Edmonds, R.L., Monson, R.K., Ollinger, S.V., Pallardy, S.G., Pregitzer, K.S., & Todd, D.E. (2011). Mercury distribution across 14 US forests. Part I: Spatial patterns of concentrations in biomass, litter, and soils. *Environmental Science & Technology, 45*(9), 3974-3981.

Ojala, A., Bellido, J.L., Tulonen, T., Kankaala, P., & Huotari, J. (2011). Carbon gas fluxes from a brown-water and a clear-water lake in the boreal zone during a summer with extreme rain events. *Limnology and Oceanography, 56*(1), 61-76.

Olefeldt, D. & Roulet, N. T. (2012). Effects of permafrost and hydrology on the composition and transport of dissolved organic carbon in a subarctic peatland complex. *Journal of Geophysical Research, 117*, G01005. doi:10.1029/2011JG001819.

Olefeldt, D., Goswami, S., Grosse, G., Hayes, D., Hugelius, G., Kuhry, P., McGuire, A.D., Romanovsky, V.E., Sannel, A.B.K., Schuur, E.A.G., & Turetsky, M.R. (2016). Circumpolar distribution and carbon storage of thermokarst landscapes. *Nature Communications, 7*(1), 13043, doi:10.1038/ncomms13043.

Olefeldt, D., Hovemyr, M., Kuhn, M.A., Bastviken, D., Bohn, T.J., Connolly, J., Crill, P., Euskirchen, E.S., Finkelstein, S.A., Genet, H., & Grosse, G. (2021). The Boreal–Arctic wetland and lake dataset (BAWLD). *Earth System Science Data, 13*(11), 5127-5149.

Olefeldt, D., Persson, A., & Turetsky, M.R. (2014). Influence of the permafrost boundary on dissolved organic matter characteristics in rivers within the Boreal and Taiga plains of western Canada. *Environmental Research Letters, 9,* 035005. doi:10.1088/1748-9326/9/3/035005.

Osterkamp, T.E. & Romanovsky, V.E. (1999). Evidence for warming and thawing of discontinuous permafrost in Alaska. *Permafrost and Periglacial Processes, 10*(1), 17-37.

Osterkamp, T.E., Viereck, L., Shur, Y., Jorgenson, M.T., Racine, C., Doyle, A., & Boone, R.D. (2000). Observations of Thermokarst and Its Impact on Boreal Forests in Alaska, U.S.A. *Arctic, Antarctic, and Alpine Research, 32*(3), 303-315. doi:10.1080/15230430.2000.12003368.

Ouellet, J., Lucotte, M., Teisserenc, R., Paquet, S., & Canuel, R. (2009). Lignin biomarkers as tracers of mercury sources in lakes water column. *Biogeochemistry, 94*, 123–140.

Outridge, P.M., Sanei, H., Stern, G.A., Hamilton, P.B., & Goodarzi, F. (2007). Evidence for control of mercury accumulation rates in canadian high arctic lake sediments by variations of aquatic primary productivity. *Environmental Science & Technology, 41,* 5259– 5265.

Paterson, M.J., Muir, D.C.G., Rosenberg, B., Fee, E.J., Anema, C., & Franzlin, W. (1998). Does lake size affect concentrations of atmospherically derived polychlorinated biphenyls in water, sediment, zooplankton and fish. *Canadian Journal of Fisheries and Aquatic Sciences, 55*(3), 544–553.

Pelletier, N., Chételat, J., Sinon, S., & Vermaire, J.C. (2022). Wildfires trigger multi-decadal increases in sedimentation rate and metal loading to subarctic montane lakes. *Science of The Total Environment, 824*, 153738.

Peterson, B.J., Holmes, R.M., McClelland, J.W., Vorosmarty, C.J., Lammers, R.B., Shiklomanov, A.I., Shiklomanov, I.A. and Rahmstorf, S. (2002). Increasing river discharge to the Arctic Ocean. *Science, 298*(5601), 2171-2173.

Petrova, M.V., Krisch, S., Lodeiro, P., Valk, O., Dufour, A., Rijkenberg, M.J., Achterberg, E.P., Rabe, B., Rutgers van der Loeff, M., Hamelin, B., Sonke, J.E., Garnier, C., & Heimbürger-Boavida, L. (2020). Mercury species export from the Arctic to the Atlantic Ocean. *Marine Chemistry, 225,* 103855. doi:10.1016/j.marchem.2020.103855.

Porcal, P., Koprivnjak, J.F., Molot, L.A., & Dillon, P.J. (2009). Humic substances-part 7: The biogeochemistry of dissolved organic carbon and its interactions with climate change. *Environmental Science and Pollution Research, 16*, 714– 726.

Post, E., Alley, R.B., Christensen, T.R., Macias-Fauria, M., Forbes, B.C., Gooseff, M.N., Iler, A., Kerby, J.T., Laidre, K.L., Mann, M.E., Olofsson, J., Stroeve, J.C., Ulmer, F., Virginia, R.A., & Wang, M. (2019). The polar regions in a 2°C warmer world. *Science Advances*, 9883.

Quinton, W.L., Hayashi, M., & Chasmer, L.E. (2009). Peatland hydrology of discontinuous permafrost in the Northwest Territories: overview and synthesis. *Canadian Water Resources Journal, 34*(4), 311-328.

Quinton, W.L., Hayashi, M., & Chasmer, L.E. (2011). Permafrost-thaw-induced land-cover change in the Canadian subarctic: Implications for water resources. *Hydrological Processes, 25*(1), 152–158. doi:10.1002/hyp.7894.

Quinton, W., Berg A., Braverman, M., Carpino, O., Chasmer, L., Connon, R., Craig, J., Devoie, É., Hayashi, M., Haynes, K., & Olefeldt, D. (2019). A synthesis of three decades of hydrological research at Scotty Creek, NWT, Canada. *Hydrology and Earth System Sciences*, *23*(4), 2015–2039.

Qureshi, A., O'Driscoll, N.J., MacLeod, M., Neuhold Y.M., & Hungerbühler, K. (2010). Photoreactions of Mercury in Surface Ocean Water: Gross Reaction Kinetics and Possible Pathways. *Environmental Science & Technology, 44*, 644-649.

R Core Team, (2023). R: A language and environment for statistical computing. R Foundation for Statistical Computing, Vienna, Austria.

Räike, A., Kortelainen, P., Mattsson, T., & Thomas, D.N. (2016). Long-term trends (1975-2014) in the concentrations and export of carbon from Finnish rivers to the Baltic Sea: organic and inorganic components compared. *Aquatic Sciences, 78*(3), 505–523.

Rantakari, M. & Kortelainen, P. (2005). Interannual variation and climatic regulation of the CO_2 emission from large boreal lakes. *Global Change Biology, 11*(8), 1368-1380.

Rantanen, M., Karpechko, A. Y., Lipponen, A., Nordling, K., Hyvärinen, O., Ruosteenoja, K., Vihma, T., & Laaksonen, A. (2022). The Arctic has warmed nearly four times faster than the globe since 1979. *Communications Earth & Environment, 3*(1), 168.

Riordan, B., Verbyla, D., & McGuire, A.D. (2006). Shrinking ponds in subarctic Alaska based on 1950–2002 remotely sensed images. *Journal of Geophysical Research: Biogeosciences*, *111*(G4).

Robbins, J. A. (1978). Geochemical and geophysical applications of radioactive lead. In Nriagu, J. O. (ed.). Biogeochemistry of Lead in the Environment, *Elsevier Scientific*, 285–393.

Robinson, S.D. & Moore, T.R. (2000). The influence of permafrost and fire upon carbon accumulation in high boreal peatlands, Northwest Territories, Canada. *Arctic, Antarctic, and Alpine Research, 32*(2), 155-166.

Romanovsky, V., Grosse, G., & Marchenko, S. (2008). Past, present and future of permafrost in a changing world. *Geological Society of America, 40*(6), 397.

Rose, N.L., Morley, D., Appleby, P.G., Battarbee, R.W., Alliksaar, T., Guilizzoni, P., Jeppesen, E., Korhola, A., & Punning, J.M. (2011). Sediment accumulation rates in European lakes since AD 1850: trends, reference conditions and exceedence. *Journal of Paleolimnology, 45*, 447-468.

Rudd, J. W. (1995). Sources of methyl mercury to freshwater ecosystems: A review. *Water, Air, and Soil Pollution, 80*, 697-713.

Rydberg, J., Klaminder, J., Rosén, P., & Bindler, R. (2010). Climate driven release of carbon and mercury from permafrost mires increases mercury loading to sub-arctic lakes. *Science of The Total Environment, 408*(20), 4778-4783. doi:10.1016/j.scitotenv.2010.06.056.

Salonen, K. & Vahatalo, A. (1994). Photochemical mineralization of dissolved organic-matter in Lake Skjervatjern. *Environment International, 20*, 307-312.

Sanei, H. & Goodarzi, F. (2006). Relationship between organic matter and mercury in recent lake sediment: The physical–geochemical aspects. *Applied Geochemistry, 21*(11), 1900-1912.

Sanei, H., Outridge, P.M., Dallimore, A., & Hamilton, P.B. (2012b). Mercury—organic matter relationships in the pre-pollution sediments of thermokast and tundra lakes from the Mackenzie River Delta, Canada: The role of depositional environment. *Biogeochemistry, 107*, 149–164. doi:10.1007/s10533-010-9543-1.

Sanei, H., Grasby, S. E., & Beauchamp, B. (2012a). Latest Permian mercury anomalies. *Geology, 40*, 63–66, doi:10.1130/G32596.1.

Sannel, A.B.K. & Kuhry, P. (2008) Long-term stability of permafrost in subarctic peat plateaus, west central Canada. *Holocene, 18*, 589–601. doi:10.1177/0959683608089658.

Savelieva, N.I., Semiletov, I.P., Vasilevskaya, L.N., & Pugach, S.P. (2000). A climate shift in seasonal values of meteorological and hydrological parameters for Northeastern Asia. *Progress in Oceanography, 47*(2-4), 279-297.

Schädel, C., Bader, M.K.F., Schuur, E.A., Biasi, C., Bracho, R., Čapek, P., De Baets, S., Diáková, K., Ernakovich, J., Estop-Aragones, C., & Graham, D.E. (2016). Potential carbon emissions dominated by carbon dioxide from thawed permafrost soils. *Nature Climate Change, 6*(10), 950-953.

Schädel, C., Schuur, E.A., Bracho, R., Elberling, B.O., Knoblauch, C., Lee, H., Luo, Y., Shaver, G.R. & Turetsky, M.R. (2014). Circumpolar assessment of permafrost C quality and its vulnerability over time using long-term incubation data. *Global Change Biology, 20*(2), 641-652.

Schaefer, K., Zhang, T., Bruhwiler, L., Barrett, A.P. (2011). Amount and timing of permafrost carbon release in response to climate warming. *Tellus Series B: Chemical Physical Meteorology, 63*(2), 165–180.

Schaphoff, S., Heyder, U., Ostberg, S., Gerten, D., Heinke, J., & Lucht, W. (2013). Contribution of permafrost soils to the global carbon budget. *Environmental Research Letters, 8*(1), 014026.

Schelker, J., Burns, D.A., Weiler, M., & Laudon, H. (2011). Hydrological mobilization of mercury and dissolved organic carbon in a snow-dominated, forested watershed: Conceptualization and modeling. *Journal of Geophysical Research: Biogeosciences*, *116*(G1).

Schiedek, D., Sundelin, B., Readman, J.W., & Macdonald, R.W. (2007). Interactions between climate change and contaminants. *Marine Pollution Bulletin, 54*(12), 1845-1856.

Schlüter, K. (2000). Evaporation of mercury from soils: An integration and synthesis of current knowledge. *Environmental Geology, 39*(3-4), 249-271.

Schuster, P.F., Striegl, R.G., Aiken, G.R., Krabbenhoft, D.P., Dewild, J.F., Butler, K., Kamark, B., & Dornblaser, M. (2011). Mercury export from the Yukon River Basin and potential response to a changing climate. *Environmental Science & Technology*, *45*(21), 9262–9267.

Schuster, P.F., Schaefer, K.M., Aiken, G.R., Antweiler, R.C., Dewild, J.F., Gryziec, J.D., Gusmeroli, A., Hugelius, G., Jafarov, E., Krabbenhoft, D.P., Liu, L., Herman-Mercer, N., Mu, C., Roth, D.A., Schaefer, T., Striegl, R.G., Wickland, K.P., & Zhang, T. (2018). Permafrost Stores a Globally Significant Amount of Mercury. *Geophysical Research Letters*, *45*(3), 1463-1471. doi:10.1002/2017GL075571.

Schuster, P.F, Striegl, R.G., Aiken, G.R., Krabbenhoft, D.P., Dewild, J.F., Butler, K., Kamark, B., & Dornblaser, M. (2011). Mercury export from the Yukon River Basin and potential response to a changing climate. *Environmental Science & Technology*, *45*(21), 9262–9267.

Schuur, E.A., McGuire, A.D., Schädel, C., Grosse, G., Harden, J.W., Hayes, D.J., Hugelius, G., Koven, C.D., Kuhry, P., Lawrence, D.M., Natali, S.M., Olefeldt, D., Romanovsky, V.E., Schaefer, K.,

Turetsky, M.R., Treat, C.C., & Vonk, J.E. (2015). Climate change and the permafrost carbon feedback. *Nature, 520*(7546), 171-179. doi:10.1038/nature14338.

Schuur, E.A., Vogel, J.G., Crummer, K.G., Lee, H., Sickman, J. O., & Osterkamp, T. E. (2009). The effect of permafrost thaw on old carbon release and net carbon exchange from tundra. *Nature, 459*(7246), 556-559. doi:10.1038/nature08031.

Selin, N.E. (2009). Global Biogeochemical Cycling of Mercury: A Review. doi:10.1146/annurev.environ.051308.084314.

Semiletov, I.P., Savelieva, N.I., Weller, G.E., Pipko, I.I., Pugach, S.P., Gukov, A.Y., & Vasilevskaya, L.N. (2000). The dispersion of Siberian River flows into coastal waters: Meteorological, hydrological and hydrochemical aspects. In *The Freshwater Budget of the Arctic Ocean*, 323-366. Dordrecht: Springer Netherlands.

Smith, S. L., O'Neill, H. B., Isaksen, K., Noetzli, J. & Romanovsky, V. E. (2022). The changing thermal state of permafrost. *Nature Reviews Earth & Environment, 3*, 10–23.

Smith, S., Sleezer, R., & Renwick, W. (2005). Fates of eroded soil organic carbon: Mississippi Basin case study. *Ecological Applications, 15*(6): 1929–1940.

Smol, J.P. (2008). Pollution of lakes and rivers: A Paleoenvironmental perspective. John Wiley & Sons, Inc., 42–43.

Sobek, S., Algesten, G., Bergström, A.K., Jansson, M., & Tranvik, L.J. (2003). The catchment and climate regulation of CO_2 in boreal lakes. *Global Change Biology, 9*(4), 630-641.

Sobek, S., Anderson, N.J., Bernasconi, S.M., & Del Sontro, T. (2014). Low organic carbon burial efficiency in arctic lake sediments. *Journal of Geophysical Research: Biogeosciences, 119*(6), 1231-1243.

Sobek, S., Durisch-Kaiser, E., Zurbrügg, R., Wongfun, N., Wessels, M., Pasche, N., & Wehrli, B. (2009). Organic carbon burial efficiency in lake sediments controlled by oxygen exposure time and sediment source. *Limnology and Oceanography, 54*, 2243–2254. doi:10.4319/lo.2009.54.6.2243.

Sobek, S., Tranvik, L.J., & Cole, J. J. (2005). Temperature independence of carbon dioxide supersaturation in global lakes. *Global Biogeochemical Cycles, 19*(2).

St. Louis, V.L., Rudd, J.W., Kelly, C.A., Beaty, K.G., Flett, R.J., & Roulet, N.T. (1996). Production and loss of methylmercury and loss of total mercury from boreal forest catchments containing different types of wetlands. *Environmental Science & Technology, 30*(9), 2719-2729.

St. Pierre, K.A., Zolkos, S., Shakil, S., Tank, S.E., St. Louis, V.L., & Kokelj, S.V. (2018). Unprecedented increases in total and methyl mercury concentrations downstream of retrogressive thaw slumps in the western Canadian Arctic. *Environmental Science & Technology, 52*(24), 14099-14109.

Stern, G.A., Sanei, H., Roach, P., Delaronde, J., & Outridge, P.M. (2009). Historical interrelated variations of mercury and aquatic organic matter in lake sediment cores from a subarctic lake in Yukon, Canada: further evidence toward the algal-mercury scavenging hypothesis. *Environmental Science & Technology, 43*(20), 7684-7690.

Stopford, W. & Goldwater, L. J. (1975). Methylmercury in the environment: a review of current understanding. *Environmental Health Perspectives, 12*, 115-118.

Szmytkiewicz, A. & Zalewska, T. (2014). Sediment deposition and accumulation rates determined by sediment trap and ^{210}Pb isotope methods in the Outer Puck Bay (Baltic Sea). *Oceanologia, 56*(1), 85-106.

Tank, S.E., Vonk, J.E., Walvoord, M.A., McClelland, J.W., Laurion, I., & Abbott, B.W. (2020). Landscape matters: predicting the biogeochemical effects of permafrost thaw on aquatic networks with a state factor approach. *Permafrost and Periglacial Processes, 31*, 358–370.

Tarnocai C., Canadell C.J.G., Schuur E.A.G., Kuhry P., Mazhitova G., & Zimov S. (2009). Soil organic carbon pools in the northern circumpolar permafrost region. *Global Biogeochemical Cycles, 23*, GB2023.

Teisserenc, R., Lucotte, M., & Houel, S. (2011). Terrestrial organic matter biomarkers as tracers of Hg sources in lake sediments. *Biogeochemistry, 103*, 235–244. doi:10.1007/s10533-010-9458-x.

Thompson, L.M., Kuhn, M.A., Winder, J.C., Braga, L.P., Hutchins, R.H., Tanentzap, A.J., St. Louis, V.L., & Olefeldt, D. (2023). Controls on methylmercury concentrations in lakes and streams of peatland-rich catchments along a 1700 km permafrost gradient. *Limnology and Oceanography, 68*(3), 583-597. doi:10.1002/lno.12296.

Tranvik, L.J., Cole, J.J., & Prairie, Y.T. (2018). The study of carbon in inland waters—From isolated ecosystems to players in the global carbon cycle. *Limnology and Oceanography Letters, 3*(3), 41–48. doi:10.1002/lol2.10068.

Tranvik, L.J., Downing, J.A., Cotner, J.B., Loiselle, S.A., Striegl, R.G., Ballatore, T.J., Dillon, P., Finlay, K., Fortino, K., Knoll, L.B., Kortelainen, P.L., Kutser, T., Larsen, Soren., Laurion, I., Leech, D. M., McCallister, S. L., McKnight, D. M., Melack, J. M., Overholt, E., … Weyhenmeyer, G. A. (2009). Lakes and reservoirs as regulators of carbon cycling and climate. *Limnology and Oceanography, 54*(2), 2298–2314.

Turetsky, M.R., Abbott, B.W., Jones, M.C., Anthony, K.W., Olefeldt, D., Schuur, E.A., Grosse, G., Kuhry, P., Hugelius, G., Koven, C., Lawrence, D.M., Gibson, C., Sannel, A.B., & McGuire, A.D. (2020). Carbon release through abrupt permafrost thaw. *Nature Geoscience, 13*(2), 138-143. doi:10.1038/s41561-019-0526-0.

Vachon, D. & Del Giorgio, P.A. (2014). Whole-lake CO_2 dynamics in response to storm events in two morphologically different lakes. *Ecosystems, 17,* 1338-1353.

van Dongen, B.E., Semiletov, I., Weijers, J.W., & Gustafsson, Ö. (2008). Contrasting lipid biomarker composition of terrestrial organic matter exported from across the Eurasian Arctic by the five great Russian Arctic rivers. *Global Biogeochemical Cycles, 22*(1).

Villar, E., Cabrol, L., & Heimbürger-Boavida, L.E. (2020). Widespread microbial mercury methylation genes in the global ocean. *Environmental Microbiology Reports, 12*(3), 277-287.

Vincent, L.A., Zhang, X., Brown, R.D., Feng, Y., Mekis, E., Milewska, E.J., Wan, H., & Wang, X.L. (2015). Observed trends in Canada's climate and influence of low-frequency variability modes. *Journal of Climate, 28*(11), 4545-4560.

Voigt, C., Marushchak, M.E., Abbott, B.W., Biasi, C., Elberling, B., Siciliano, S.D., Sonnentag, O., Stewart, K.J., Yang, Y., & Martikainen, P.J. (2020). Nitrous oxide emissions from permafrost-affected soils. *Nature Reviews Earth & Environment, 1*, 420 - 434.

Vonk, J.E., Tank, S.E., & Walvoord, M.A. (2019). Integrating hydrology and biogeochemistry across frozen landscapes. *Nature Communications, 10*, 5377.

Vonk, J.E., Tank, S.E., Bowden, W.B., Laurion, I., Vincent, W.F., Alekseychik, P., Amyot, M., Billet, M.F., Canário, J., Cory, R.M., Deshpande, B.N., Helbig, M., Jammet, M., Karlsson, J., Larouche, J., MacMillan, G., Rautio, M., Walter Anthony, K.M., & Wickland, K.P. (2015) Reviews and syntheses: effects of permafrost thaw on Arctic aquatic ecosystems. *Biogeosciences*, *12*, 7129–7167. doi:10.5194/bg-12-7129-2015.

Vonk, J.E., van Dongen, B.E., & Gustafsson, O. (2010a). Selective preservation of old organic carbon fluvially released from sub-Arctic soils. *Geophysical Research Letters, 37*, L11605. doi:10.1029/2010GL042909.

Vonk, J.E., Mann, P.J., Davydov, S., Davydova, A., Spencer, R.G., Schade, J., Sobczak, W.V., Zimov, N., Zimov, S., Bulygina, E., & Eglinton, T.I. (2013). High biolability of ancient permafrost carbon upon thaw. *Geophysical Research Letters*, *40*(11), 2689-2693.

Walvoord, M.A. & Striegl, R.G. (2021). Complex vulnerabilities of the water and aquatic carbon cycles to permafrost thaw. *Frontiers in Climate*, *3*, 730402.

Wauthy, M., Rautio, M., Christoffersen, K.S., Forsström, L., Laurion, I., Mariash, H.L., Peura, S. & Vincent, W.F. (2018). Increasing dominance of terrigenous organic matter in circumpolar freshwaters due to permafrost thaw: increasing allochthony in arctic freshwaters. *Limnology and Oceanography Letters, 3*, 186–198.

Wickland, K.P., Aiken, G.R., Butler, K., Dornblaser, M.M., Spencer, R.G.M., & Striegl, R.G. (2012). Biodegradability of dissolved organic carbon in the Yukon River and its tributaries: Seasonality and importance of inorganic nitrogen. *Global Biogeochemical Cycles, 26*(4).

Williamson, C.E., Saros, J.E., Vincent, W.F., & Smol, J.P. (2009). Lakes and reservoirs as sentinels, integrators, and regulators of climate change. *Limnology and Oceanography*, *54*(6:2), 2273-2282.

Wood, S.N. (2017). Generalized Additive Models: An Introduction with R, Second Edition (2nd ed.). Chapman and Hall/CRC. doi:10.1201/9781315370279.

Yang, H., Turner, S., & Rose, N. L. (2016). Mercury pollution in the lake sediments and catchment soils of anthropogenically-disturbed sites across England. *Environmental Pollution*, *219*, 1092-1101.

Yang, Y.K., Zhang, C., Shi, X.J., Tao, L.I.N., & Wang, D.Y. (2007). Effect of organic matter and pH on mercury release from soils. *Journal of Environmental Sciences, **19***(11), 1349-1354.

Zhang, T., Barry, R.G., Knowles, K., Heginbottom, J.A. & Brown, J. (1999). Statistics and characteristic of permafrost and ground-ice distribution in the Northern Hemisphere. *Polar Geography*, *23*, 132-154.

Zhuang, Q., Melillo, J.M., Sarofim, M.C., Kicklighter, D.W., McGuire, A.D., Felzer, B.S., Sokolov, A., Prinn, R.G., Steudler, P.A., & Hu, S. (2006). CO_2 and CH_4 exchanges between land ecosystems and the atmosphere in northern high latitudes over the 21st century. *Geophysical Research Letters, 33*(17). doi:10.1029/2006GL026972.

Zolkos, S., Krabbenhoft, D.P., Suslova, A., Tank, S.E., McClelland, J.W., Spencer, R.G., Shiklomanov, A., Zhulidov, A.V., Gurtovaya, T., Zimov, N., & Zimov, S. (2020). Mercury export from Arctic great rivers. *Environmental Science & Technology*, *54*(7), 4140-4148.

Zoltai, S.C. (1993). Cyclic development of permafrost in the peatlands of northwestern Alberta, Canada. *Arctic, Antarctic and Alpine Research*, *25*, 240-246.

Zoltai, S.C. & Tarnocai, C. (1975). Perennially frozen peatlands in the Western Arctic and Subarctic of Canada. *Canadian Journal of Earth Sciences*, *12*, 28–43.

Zoltai, S.C. (2011). Palsas and Peat Plateaus in Central Manitoba and Saskatchewan. *Canadian Journal of Forest Research*, *2*(3), 291-302. doi:10.1139/x72-046.